Ollscoil na hÉireann, Corcaigh

National University of Ireland, Cork

University College Cork, Ireland
Coláiste na hOllscoile Corcaigh

Development of a Low-power, Battery-less Near Field Communication Sensor Transponder for Wireless Sensing Applications

Thesis presented by

Dinesh R. Gawade

Bachelor of Technology (Electronics & Communication)

ORCID: 0000-0001-9355-2821

for the degree of

Masters in Electrical and Electronic Engineering Science (MEngSc) by Research

School of Engineering and Architecture

University College Cork

Electrical & Electronic Engineering

Head of School: Prof. Jorge Oliveira

Supervisor(s): Dr. John L. Buckley

Dr. Brendan O'Flynn

December 2022

Table of Contents

List of Figures

List of Tables

Glossary of Terms

AC	Alternating Current
APB	Advanced Peripheral Bus
ASK	Amplitude Shift Keying
BLE	Bluetooth Low-Energy
BW	- 3dB bandwidth
CAGR	Compound annual growth rate
CC	Capability Container
CDC	Capacitance to Digital Converter
CH	Cultural Heritage
CMOS	Complementary Metal Oxide Semiconductor
COTS	Commercial-off-the-shelf
CPM	Cork Public Museum
CPU	Centre Processing Unit
CR	Coding Rate
DC	Direct Current
DIW	Deionized Water
EEPROM	Electrically Erasable Programmable Read-Only Memory
EH	Energy Harvesting
FFP2	Filtering Face Piece
FR4	Glass-reinforced Epoxy Laminate Material
FSR	Force Sensing Resistor
FST	Fondazione Scienza e Tecnica Museum
GO	Graphene Oxide
GPIO	General Purpose Input/output
GPO	General Purpose Output
HCLK	Clock Source for CPU of microcontroller
HF-RFID	High Frequency Radio Frequency Identification
HIS	High Speed Internal

HSE	High Speed External
HVAC	Heating, ventilation, and air conditioning
I2C/I2C	Inter-Integrated Circuit
IC	Integrated Circuit
IEC	International Electro technical Commission
IoT	Internet of Things
ISO	International Organization for Standardization
LDO	Low Dropout Voltage Regulator
LF-RFID	Low Frequency Radio Frequency Identification
LIG	Laser-Induced Graphene
Li-SOCL2	Lithium-Thionyl Chloride
LLCP	Logical Link Control Protocol
LoRaWAN	Long-Range Wide-Area Network
LPD	Low Power Down
MCU	Microcontroller
MSI	Multi Speed Internal
NCI	NFC Controller Interface
NDEF	NFC Data Exchange Format
NFC	Near Field Communication
P2P	Peer to Peer
PCB	Printed Circuit Board
PDR	Packet Delivery Ratio
PLL	Phase Locked Loop
RF	Radio Frequency
RFID	Radio Frequency Identification
RH	Relative Humidity
RTD	Record Type Definition
Rx	Receive
SCL	Serial Clock
SDA	Serial Data
SNEP	Simple NDEF Exchange Protocol

SWF	Skin Wittedness Factor
SYSCLK	System Clock
Temp	Temperature
TEWL	Transepidermal Water Loss
TNF	Type Name Format
TPMS	Tire Pressure Monitoring System
TTN	The Things Network
Tx	Transmit
UHF-RFID	Ultra High Frequency Radio Frequency Identification
UI	User Interface
URI	Universal Resource Identifier
URL	Uniform Resource Locator
vCard	Visiting Card
VCORE	MCU Core Supply Voltage
VEH	Vibration Energy Harvester
WLC	Wireless Charging
WPT	Wireless Power Transfer

List of Symbols (with SI units)

C	Capacitance (F)
C_{IC}	Internal Capacitance of NFC Radio Transceiver that Connects in Shunt with the NFC Loop Antenna Terminals (F)
C_P	Parasitic Capacitance (F)
C_T	External Tuning Capacitance that Connects in Shunt with the NFC Loop Antenna Terminals (F)
f_C	Centre Frequency (Hz)
f_C'	Centre Frequency After Integration (Hz)
f_{CLK}	CPU Clock (Hz)
f_{I2C_IN}	I2C Core Input Clock (Hz)
f_R	Resonant Frequency (Hz)
H	Magnetic Field Strength (A/m)
H_{AVG}	Average Magnetic Field Strength (A/m)
H_{MIN}	Minimum Magnetic Field Strength (A/m)
I	Current (A)
L	Inductance (H)
M	Mutual inductance (H)
Q	Quality factor
RH	Relative Humidity (%)
$Temp$	Temperature (°C)
T_S	Turns Spacing (m)
T_W	Trace Width (m)
V_{CORE}	MCU Core Supply Voltage (V)
V_{DD}	Supply voltage to integrated circuit (V)

Declaration

This is to certify that the work I am submitting is my own and has not been submitted for another degree, either at University College Cork or elsewhere. All external references and sources are clearly acknowledged and identified within the contents. I have read and understood the regulations of University College Cork concerning plagiarism.

Signed: Date: 06 December 2022

Acknowledgements

The work described in this thesis is based on the results of several sponsored programs on which I have had the opportunity to work during MEngSc studies. I would like to acknowledge the funding support of the European Union's Horizon 2020 research and innovation program for the APACHE project under grant agreement number 814496. I would also like to acknowledge support from Science Foundation Ireland under grant numbers 13/RC/2077 (CONNECT), 16/RC/3918 (CONFIRM) and 16/RC/3835 (Vistamilk), which contributed to aspects of this research.

I am incredibly grateful to my supervisors, Dr. John L. Buckley and Dr. Brendan O'Flynn, for allowing me to work on this exciting topic. My sincerest gratitude goes out to John in particular for all the guidance and motivation he has given to me. As a result of John's willingness, I have always been motivated to work hard and excel in my endeavours. It has been a pleasure to have Brendan's support and motivation throughout my research work and thesis writing. The continuous support and encouragement of my supervisors helped me achieve the outcome of this research work, and there are no words to adequately express my gratitude to my supervisors for all their hard work behind every critical step of my Master's research work. For valuable suggestions and support with this research, I would like to thank my thesis adviser Dr. Ray Duffy as well as the APACHE project work package leader Dr. Daniela Iacopino. Likewise, I am grateful for the teachings of Dr Kevin McCarthy of University College Cork regarding Radio Frequency Integrated Circuit design (RFIC).

I would like to acknowledge the support of all the members of the Antenna and RF team and WSN Group, especially Dr. Sanjeev Kumar, John Barton, Dr. Roy B V B Simorangkir, Marco Belcastro, Davide Alfieri, Adhurim Hajzeraj, Nadeem Rather, Dr. Su Zhen, Dr. Matteo Menolotto, Dr. Salvatore Tedesco, Javier Torres, Marco Sica, Dr. Gholamhosein Moloudian, Omid Talebi, Brendan O'Callaghan, Masoud Emam, Dr. Mariusz Wilk and all my postgraduate colleagues.

I would also like to thank APACHE project partners and co-authors of the research articles emanated from this research for their support: Dr. Steffen Ziemann and Dr. Manfred Anders from ZFB Zentrum für Bucherhaltung GmbH, Germany, George Paterakis and Dr. George Gorgolis from the University of Patras, Greece, Dr. Dimitrios Zorbas from Nazarbayev University, Kazakhstan, Daniel Breen and Mera Qamar from Cork public museum, Ireland, Luciano Pensabene from Guggenheim museum, Italy, Balazs Lencz and Matyas Eszter from Hungarian National Museum, Hungary, Antonio Mirabile, Art restoration service, France and Eoghan Vaughan, Richard Murray, Kankana Paul, Dr. Aidan J Quinn from Tyndall National Institute, Ireland.

I would also like to acknowledge all departments and members of Tyndall National Institute for their direct and indirect support with my Master's research, specifically the Graduate Studies, IT, HR and Finance.

Throughout my career at Tyndall National Institute, I have been surrounded by incredible colleagues and friends: Dr. Swatchith Lal, Amit Tanwar, Arindam Samanta, Dr. Rahul Jaiswal, Mohammed Nasser, Cian O'Donnell and Vaishnavi Belur Jairam, who have always supported, motivated and believed in me.

My sincere gratitude goes out to my thesis examiners, Dr. Marco Crepaldi from Istituto Italiano di Tecnologia, Genoa, Italy and Dr. Pádraig Cantillon-Murphy from University College Cork, Ireland, for their time and expertise.

As a final note, I would like to thank my parents, Raosaheb M. Gawade and Chandrakala R. Gawade, along with my brother, Nitin R. Gawade, for all their love, support, and sacrifices over the years and for standing by my side all through despite the geographical boundaries. It would not have been possible to accomplish this research work without their inspiration and support.

To my parents, brother, academic mentors and to the memory of my beloved grandfather *Mayanji S. Gawade*.

Abstract

Cultural heritage objects and artefacts are precious objects owned by museums and archives, which are generally old and fragile. Often, such objects are stored in climatically uncontrolled storage areas, particularly inside sealed archive boxes and storage crates. Such storage practices can lead to significant degradation of valuable artefacts. Implementing air conditioning and heating, ventilation, and air conditioning (HVAC) systems constitutes a highly technical conservation challenge that often cannot be financially justified, especially for small and medium-sized museums. Commercially available environmental sensors, such as hygrometers and wireless data loggers are known for monitoring microenvironments in museums. However, these devices are unsuitable for integration within museum storage boxes because these sensors are either too large or expensive. For example, the Testo series 160TH data logger can be used for monitoring temperature and humidity in museum environments but the cost is significant at approximately €245. Another critical disadvantage associated with monitoring the inside microenvironments of an archive box using a hygrometer is the necessity to open the box for the analysis. A key disadvantage of existing methods is the interference caused to the internal microclimate.

This thesis presents the development of both short-range and long-range wireless sensor platforms that monitor the microclimatic environment inside museum artefact storage boxes. The short-range wireless communication platform focuses on developing a battery-less near-field communication (NFC) sensor transponder with a wireless communication range of several centimetres. On the other hand, the long-range communication platform development involves the selection and implementation of optimum wireless communication technology to yield a wireless communications range of 100 metres to several kilometres and which is scalable according to the large number of artefacts that may need to be monitored.

In the first contribution, for the first time, a smart museum archive box that features fully integrated wirelessly powered temperature and humidity sensing capabilities is developed and demonstrated.

The developed NFC sensor transponder has been optimized for low power operation using voltage and frequency scaling techniques with a measured peak DC power consumption of 597 μW while yielding a 5 cm wireless communication range. The achieved power consumption is 33.6 % lower in comparison with the current state-of-the-art in this area. In addition, the developed battery-less NFC sensor transponder can wirelessly measure temperature and relative humidity with a mean error of ± 0.37 $^{\circ}$C and ± 2 %, respectively, over a maximum distance of 5 cm.

In addition, a battery-less NFC humidity sensor prototype is developed and demonstrated using laser-induced graphene (LIG) electrodes and a graphene oxide (GO)-based humidity sensor. Furthermore, the feasibility of enhancing the wireless communication range of the NFC sensor transponder is explored. This is achieved by powering the transponder electronics using energy harvested from a vibrational energy harvester. A maximum wireless communication range of 11 cm is achieved in free space, which is 120 % beyond the state-of-the-art reported in the literature. Finally, the developed battery-less NFC sensor transponders were deployed in Cork Public Museum, Cork, Ireland and Fondazione Scienza e Tecnica (FST) in Florence, Italy to monitor artefacts in these museums. In addition, the transponder was also deployed in the world-famous Guggenheim museum in Venice, Italy, to monitor the interior temperature and humidity of *Andy Warhol's painting* entitled flowers.

In the second contribution, the optimum wireless communication technology for museum artefact monitoring applications in warehouses and exhibition cabinets was identified. For the identified technology (LoRaWAN), a testbed network was developed and deployed (7 sensor nodes) as proof of concept at Cork Public Museum, Cork, Ireland, to monitor the interior temperature and humidity of artefact display cases and storage cabinets. The wireless communication performance of LoRaWAN is shown to offer the optimal solution for wireless communication for this long-range application with a measured packet delivery ratio of 0.994 and an estimated battery lifetime of 10 years, considering a duty cycle of 1 data packet per day.

The outcomes of this thesis contribute to the advancement of museum artefact monitoring, battery-less NFC sensing state-of-the-art for short-range storage analytics and a LoRaWAN solution for long-range analysis of warehouse cabinets and exhibitions.

List of Publications

The following peer-reviewed publications have emanated from this Master's thesis research work in this thesis:

Peer Reviewed Journals:

[1] **Dinesh R. Gawade**, Steffen Ziemann, Sanjeev Kumar, Daniela Iacopino, Marco Belcastro, Davide Alfieri, Katharina Schuhmann, Manfred Anders, Melusine Pigeon, John Barton, Brendan O'Flynn and John L. Buckley, "A Smart Archive Box for Museum Artefact Monitoring Using Battery-Less Temperature and Humidity Sensing," *MDPI Sensors Journal 21, no. 14 (2021): 4903,* DOI: https://doi.org/10.3390/s21144903, **(Impact Factor = 3.847)**

[2] Kankana Paul, **Dinesh R. Gawade,** Roy B. V. B. Simorangkir, Brendan O'Flynn, John L. Buckley, Andreas Amann and Saibal Roy, "A Concertina–Shaped Vibration Energy Harvester–Assisted NFC Sensor With Improved Wireless Communication Range," in *IEEE Internet of Things Journal*, 2022, *Early Assess*, DOI: 10.1109/JIOT.2022.3197233, **(Impact Factor = 10.238).**

[3] Paterakis George, Vaughan Eoghan, **Dinesh R. Gawade**, Murray Richard, Gorgolis George, Matsalis Stefanos, Anagnostopoulos George, John L. Buckley, Brendan O'Flynn, Quinn Aidan and Iacopino Daniela and Galiotis Costas. Highly Sensitive and Ultra-Responsive Humidity Sensors Based on Graphene Oxide Active Layers and High Surface Area Laser-Induced Graphene Electrodes. *MDPI Nanomaterials Journal* 12, no. 15 (2022): 2684, DOI: https://doi.org/10.3390/nano12152684, **(Impact Factor = 5.719).**

Peer Reviewed International Conference:

[4] **Dinesh R. Gawade,** Roy B. V. B. Simorangkir, Dimitrios Zorbas, Sanjeev Kumar, Steffen Ziemann, Daniela Iacopino, John Barton, Katharina Schuhmann, Manfred Anders, Brendan O'Flynn, John L. Buckley, "A Museum Artefact Monitoring Testbed using LoRaWAN," *26th IEEE Symposium on Computers and Communications (ISCC 2021), Athens, Greece,* 5-8 September 2021.

Chapter 1: Introduction

The last few years have witnessed a significant advancement in battery-less, wireless sensing devices due to the increasing number of Internet of Things (IoT) applications. Many of these applications require low or no maintenance cost and not create an adverse environmental impact [5]. In addition, the advancement in low to ultra-low power electronics and sensors has steered the rapid growth of battery-less, wireless sensing devices, particularly those based on radio-frequency identification (RFID) and near field communication (NFC) technology. Recently for instance, the market for NFC technology has increased significantly due to the incorporation of NFC reader capability within smartphones [5]. At present, NFC technology not only enables consumers to carry out payments, but also enables the passive wireless measurement of multiple disparate parameters, including soil moisture monitoring [6-8], fruit quality measurement [9, 10], long-term building structural health monitoring [11, 12], gas monitoring (ammonia, CO_2, oxygen) [13], and environmental parameter monitoring [14, 15] to name a few.

The inclusion of NFC technology in smartphones enables not only wirelessly power sensing devices but also allows on-call sensor data acquisition and frictionless data migration from the edge to the cloud. NFC integration in smartphone results in a cost reduction for the NFC sensor transponders, which paves the way for a number of low-cost, battery-less and short-range applications such as museum artefact monitoring, which is the key focus of this research.

1.1 Motivation for this Work

The degradation rate of stored museum artefacts, such as cultural heritage (CH) objects and artefacts can speed up considerably due to exposure to unstable climatic conditions and environmental pollutants [16]. For example, historic papers and documents containing iron gall ink are prone to deterioration when exposed to temperature fluctuation of ± 5 °C and relative humidity fluctuations of ± 10 % [17-19]. The majority of precious documents and artefacts owned by museums and archives are often stored in *climatically uncontrolled* storage areas and in museum building basements for example.

The implementation of modern air conditioning systems and heating, ventilation and air conditioning (HVAC) systems constitutes a highly technical conservation challenge in itself that often cannot be financially justified, especially for small and medium-size institutions.

The ability to monitor the microclimatic environmental conditions in a museum setting is a key enabler and an important tool for preventive conservation, even in climatically controlled areas. However, the microclimatic environmental parameters such as temperature and relative humidity for artefacts stored in archive boxes (also referred to as an artefact storage box) can differ significantly from that of the external environment due to the intrinsic water content of stored materials within the archive box. A common and legitimate concern of conservators therefore is the often-unknown temperature and relative humidity levels within the enclosures themselves that are used to house valuable artefacts [1]. Therefore, there is a need to monitor the effective interior microclimates in sealed archive boxes. The ability to record real-time measurement of these local temperature and humidity parameters can provide museum owners with the opportunity to act quickly and prevent degradation of valuable artefacts due to shrinkage or mould growth for example.

Commercially available hygrometers or data loggers and other environmental monitoring devices are well known for monitoring microenvironments in museums, during transport of artefacts, or inside storage or display rooms [16, 20]. However, these commercially available solutions are not always suitable for integration into a large number of museum archive boxes because they are either too large or too expensive [21]. Additionally, the storage box needs to be physically opened to enable the reading of sensor data and any required maintenance, such as the changing of batteries. This in itself may cause artefact degradation by introducing contaminants when opening the box.

To the best of the author’s knowledge, there are no convenient cost-effective (< €5 per sensor device), battery-less wireless solutions available to solve the above problem in this application domain at the present time [1].

The challenges with current state-of-the-art low-cost, battery-less NFC sensor transponder for museum artefact monitoring are summarized below:

- The harvested DC power consumption of the NFC sensor is defined as the DC power consumption of the sensor while operating with harvested RF power from the reader. For battery-less NFC sensor transponders reported in the literature, the harvested DC power consumption for these sensors is mostly greater than 1.5 mW [7, 9, 10, 22-27]. The wireless communication range for the battery-less NFC sensor transponder also depends on factors such as reader RF transmit power, NFC antenna size and coupling coefficient between the NFC reader and transponder antennas. However, these additional parameters are not investigated in this research work.
- The wireless communication range of NFC sensor transponders, specifically those including a microcontroller as a data processing unit, has been reported to be less than 3 cm with NFC-enabled smartphone as a reader [7, 9, 10, 22-31]. However, as discussed in Chapter 3, the wireless communication range requirement for the intended application is 4 cm. Therefore, there was a need to develop a new battery-less NFC sensor transponder with greater wireless communication range.
- Commercial NFC sensor transponders have a limited operational life of approximately 3 years because of the limited battery lifetime [32], which does not meet the requirement of the intended application (discussed in Chapter 3). In addition, only a limited number of the reported solutions support battery-less operation [33, 34] and are not optimized for low-cost applications [32-36].
- NFC sensor transponder integration within archive boxes without using any adhesive is also one of the key design challenges.

The above-discussed challenges signify the need to develop a new battery-less NFC sensor transponder and integrate it within an artefact archive box to sense interior temperature and relative humidity without opening the box.

1.2 Aim and Objectives

The aim of this thesis is to address the aforementioned research challenges and develop a novel low power, battery-less NFC sensor transponder with improved wireless communication range when compared with the literature.

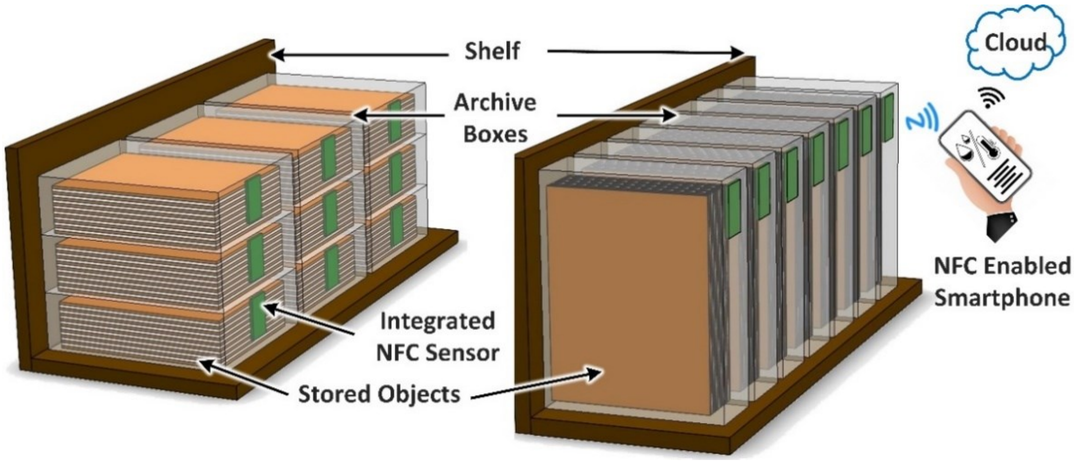

Figure 1.1: Illustration of artefact monitoring using an NFC sensor (Fig.1 of [1]).

In addition, this research also aims to integrate an NFC sensor transponder within an archive box that features fully-integrated wireless powered temperature and humidity sensing capabilities. The archive box featuring all the above-mentioned features is referred to as a *smart archive box*.

Figure 1.1 illustrates the proposed solution for artefact storage monitoring using a novel, battery-less temperature and humidity sensor that is NFC-powered using a standard smartphone. The NFC sensor is integrated directly within the archive box itself as shown in Figure 1.1. In addition, the smartphone is used to wirelessly transfer the measured data to the cloud for further analysis and processing, using a dedicated smartphone application.

This proposed solution enables conservators to monitor microenvironments within the enclosure to help protect the contents. For example, monitoring at regular intervals via the proposed approach makes it possible to identify increased interior humidity levels at an early stage. This can facilitate the timely de-humidification of the enclosure or even the simple movement of the enclosure to an alternative location in the storage area that has improved air circulation.

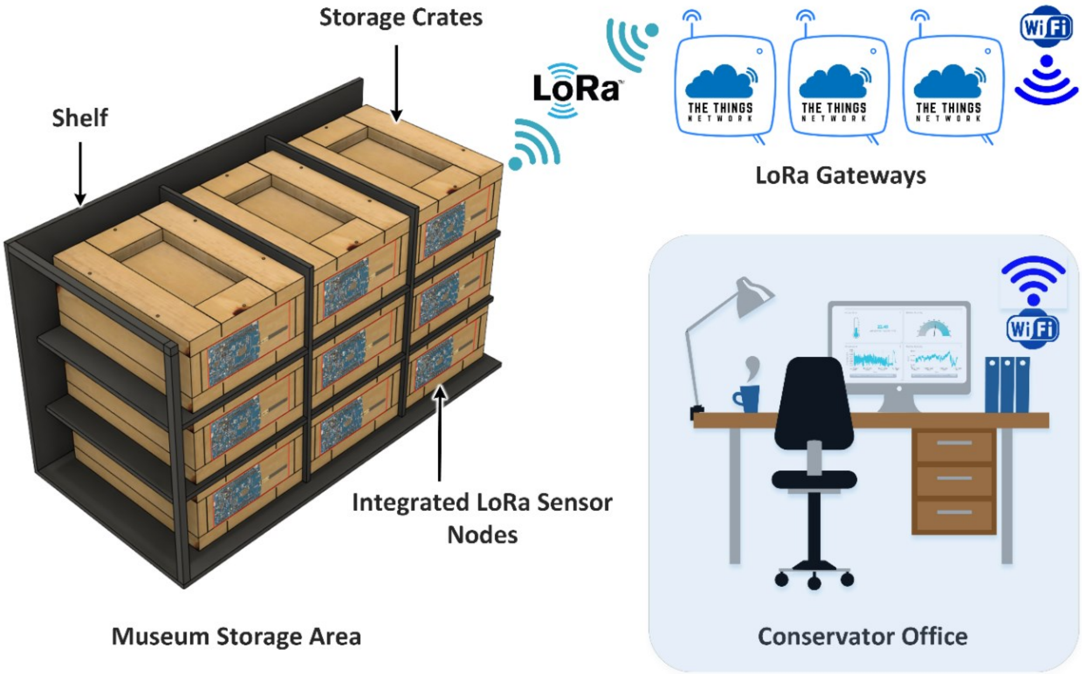

Figure 1.2: Illustration of stored artefact monitoring using LoRaWAN (Fig. 1 of [4]).

The proposed "smart" archive box leads to additional advantages such as low maintenance cost, long-term, and intelligent sensing solutions for museum artefact preservation, storage and monitoring. In addition, this thesis also aims to select a suitable wireless communication technology for museum artefact monitoring in case where the implementation of battery-less NFC sensor technology is *not* viable; for example, monitoring of museum artefacts that are stored in wooden storage crates (see Figure 1.2) which feature a wall thickness of greater than 5 cm. In this case, the wooden storage crate wall thickness is greater than the wireless communication range of the battery-less NFC sensor transponder, so making use of the NFC sensor transponder is not possible in this instance. The wireless monitoring of museum artefacts that are stored in museum storage facilities using long-range wide-area network (LoRaWAN) is shown in Figure 1.2 and is also discussed in Chapter 5.

The main objectives of this thesis work are as follows:

- Develop embedded hardware and firmware for a battery-less NFC sensor transponder with the aim of reducing the harvested DC power consumption and improving the wireless communication range of the transponder to at least 4 cm.

- Characterizing the performance of the proposed NFC sensor transponder through measurement and experiments.
- Integrating the developed NFC sensor transponder into archive boxes using adhesive-less packaging solutions to avoid contamination of the atmosphere inside the box.
- Achieving the minimum required wireless communication range of 4 cm as defined in the user requirements by stakeholders including museum conservation scientists, conservators and museum archive box manufacturers (discussed in Chapter 3).
- In addition, this thesis also explores the feasibility of wireless communication range enhancement of the NFC sensor transponder by assisting the transponder with a vibrational energy harvester (VEH) to power the sensor electronics for IoT applications.
- This thesis also explores the feasibility of integrating a custom, highly sensitive humidity sensor [based on Laser-induced graphene (LIG) electrodes] with an NFC sensor transponder for IoT applications.
- Furthermore, selecting a suitable wireless technology for museum artefact monitoring where the implementation of battery-less NFC sensor technology is not viable and developing and deploying a long-range wireless communication testbed network is also one of the objectives of this thesis.
- A final goal is to contribute to the advancement of next-generation NFC sensor transponder technology and museum artefact monitoring in general.

1.3 Organization of the Thesis

The reminder of the thesis is organized as follows:

Chapter 2: This chapter discusses the background of RFID and NFC technologies and provides a comprehensive overview of state-of-the-art NFC sensor transponder. In this chapter, the performance of several NFC sensor transponders is presented, mainly focusing on the ISO/IEC 15693 air-interface standard-based transponder. Furthermore, several limitations, design challenges and technology gaps in state-of-the-art NFC sensor transponders are identified, and a research hypothesis is then formulated.

Chapter 3: With the aim of increasing the wireless communication range, the battery-less NFC sensor transponder is designed with a view to optimizing DC power consumption and is described in this chapter. In addition, the feasibility of wireless communication range enhancement of the NFC sensor transponder by assisting the transponder with a vibration energy harvester (VEH) is also explored in this chapter. Furthermore, this chapter presents the integration of a custom humidity sensor with the NFC sensor transponder. Finally, integration of the NFC sensor transponder within an artefact storage box is demonstrated using an adhesive-less packaging solution.

Chapter 4: This chapter describes the performance characterization of the developed battery-less NFC sensor transponders described in Chapter 3. The key performance measurement parameters include RF receiver sensitivity, DC power consumption, wireless communication range, temperature, and humidity sensing accuracy. In addition, this chapter also discusses the demonstration of the developed NFC sensor transponder technology to the project stakeholders during three public training events held in Paris (France), Turin (Italy) and Budapest (Hungary). Finally, this chapter also explains the deployment of the NFC sensor transponder in the Cork Public Museum, Cork, Ireland and Guggenheim Museum, Venice, Italy.

Chapter 5: This chapter discusses selecting suitable wireless communication technologies for museum artefact monitoring applications, where employing battery-less NFC sensing is not feasible. For instance, in museum storage facilities where artefacts are stored inside wooden storage crates that have wall thickness of greater than 5 cm. In addition, this chapter also explains the development of a LoRaWAN testbed network using a commercial LoRaWAN gateway and an open-source hardware platform for sensor nodes for museum artefact monitoring. Finally, this chapter also explains the deployment of the developed LoRaWAN testbed network in the Cork Public Museum, Cork, Ireland, as a proof of concept.

Chapter 6: This chapter presents the key conclusions and findings of this thesis, and suggestions for future research work are outlined.

The following *four peer-reviewed publications* describe the battery-less NFC sensor transponder that was designed and demonstrated in this thesis. These publications report on the development and characterization of the NFC sensor transponder and the integration of the transponder within archive boxes for museum artefact monitoring applications. In addition, these publications also report on the integration of the vibrational energy harvester to improve the wireless communication range of the NFC sensor transponder and as well as the integration of a custom humidity sensor. Finally, a peer-reviewed conference publication also reported the selection of suitable wireless communication technologies for use in museum artefact monitoring applications.

1. **Dinesh R. Gawade,** Steffen Ziemann, Sanjeev Kumar, Daniela Iacopino, Marco Belcastro, Davide Alfieri, Katharina Schuhmann, Manfred Anders, Melusine Pigeon, John Barton, Brendan O'Flynn and John L. Buckley, "A Smart Archive Box for Museum Artefact Monitoring Using Battery-Less Temperature and Humidity Sensing," *MDPI Sensors Journal* 21, no. 14 (2021): 4903, DOI: https://doi.org/10.3390/s21144903 **(Impact Factor = 3.847).**
2. Kankana Paul, **Dinesh R. Gawade**, Roy B. V. B. Simorangkir, Brendan O'Flynn, John L. Buckley, Andreas Amann and Saibal Roy, "A Concertina–Shaped Vibration Energy Harvester–Assisted NFC Sensor With Improved Wireless Communication Range," in IEEE Internet of Things Journal, 2022, DOI: 10.1109/JIOT.2022.3197233 **(Impact Factor = 10.238).**
3. Paterakis George, Vaughan Eoghan, **Dinesh R. Gawade**, Murray Richard, Gorgolis George, Matsalis Stefanos, Anagnostopoulos George, John L. Buckley, Brendan O'Flynn, Quinn Aidan and Iacopino Daniela and Galiotis Costas. Highly Sensitive and Ultra-Responsive Humidity Sensors Based on Graphene Oxide Active Layers and High Surface Area Laser-Induced Graphene Electrodes. *MDPI Nanomaterials Journal* 12, no. 15 (2022): 2684 DOI: https://doi.org/10.3390/nano12152684 **(Impact Factor = 5.719).**

4. **Dinesh R. Gawade**, Simorangkir Roy BVB, Zorbas Dimitrios, Kumar Sanjeev, Ziemann Steffe, Iacopino Daniela, Barton John, Schuhmann Katharina, Anders Manfred, O'Flynn Brendan and John L. Buckley, A museum artefact monitoring testbed using LoRaWAN. In Proceedings of the 2021 *IEEE Symposium on Computers and Communications (ISCC)*, 2021; pp. 1-3, DOI: 10.1109/ISCC53001.2021.9631253.

Chapter 2: Literature Review and State of the Art Summary

2.1 Background

As discussed in Chapter 1, the degradation rate of valuable cultural heritage objects and artefacts can considerably increase due to exposure to unstable climatic conditions, light and environmental pollutants during transport and storage [16]. Monitoring microenvironments is an important technique for preventive conservation of such artefacts, even in climatically controlled areas and enclosures. The microclimatic environmental conditions, such as temperature and humidity for artefacts stored in archive boxes can differ significantly from that of the external environment due to the intrinsic moisture content of stored materials within the archive box. Therefore, a common and legitimate interest and concern for conservators is the status of the (often-unknown) microclimate within the enclosures themselves that are used to house valuable artefacts. Consequently, there is a need to monitor the effective interior microclimates in sealed storage enclosures. This is ideally accomplished without the need to open the enclosure or interfere with the sealed internal environmental. The focus of this research is to design a novel, wirelessly powered wireless sensor device (NFC sensor transponder) for microenvironment monitoring and to integrate it within an artefact storage box.

This chapter first briefly explains the background on near field communication (NFC) technology. Secondly, this chapter also provides a comprehensive review of the state-of-the-art in battery-less NFC sensor transponders. A detailed review of battery-less sensor transponders is presented, focusing on those that operate at 13.56 MHz using the ISO/IEC 14443 and ISO/IEC 15693 air interface and initialization standards. A performance comparison of the reported solutions in the literature is conducted to help identify areas for improvement for a new battery-less sensor transponder design particularly for museum artefacts monitoring application. Finally, several gaps in the state-of-the-art for NFC sensor transponder technology are identified.

In particular, for museum artefact monitoring applications, the need for developing a new battery-less sensing solution is highlighted to fill the identified gaps in the current state of the art in this area.

2.2 Background Information

This section briefly describes the background information for Radio-Frequency Identification (RFID) and NFC technology, which includes a technology overview, operating principle, a simplified circuit model and system architecture for an NFC system which is described in Chapters 3 and 4.

2.2.1 Overview of radio frequency identification (RFID) technology

In 1973, Mario W. Cardullo and William L. Parks patented a RFID transponder that comprises of writable memory [37]. Table 2.1 summarizes classifications of RFID transponders based on the operation frequency and type of coupling between the RFID transponder and reader antenna. RFID transponders are generally classified according to operating frequency and include Low frequency (LF), High frequency (HF) and ultra-high frequency (UHF) type devices [38].

Table 2.1: Classification of RFID transponder [38].

Parameter	Low Frequency (LF) RFID	High Frequency (HF) RFID	Ultra High Frequency (UHF) RFID
Frequency of operation (MHz)	0.125 to 0.135	13.56	860 (Europe), 915 (USA)
Air interface Standard	ISO/IEC 14223, ISO/IEC 18000-2	ISO/IEC 14443 A/B, ISO/IEC 15693,	EPC Class 1 Gen 2, ISO/IEC 18000-6 B/C
Frequency band regulation	Worldwide	Worldwide	Various with countries
Coupling method	Inductive	Inductive	Electro-magnetic backscattered

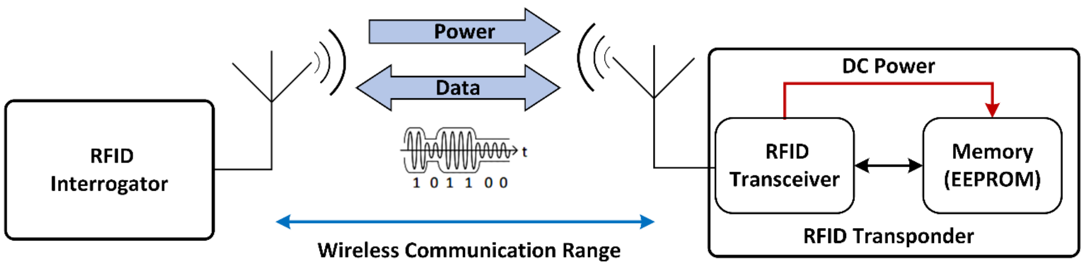

Figure 2.1: High-level overview of an RFID system.

A block diagram of a typical RFID system is depicted in Figure 2.1. As shown in the figure, a RFID system comprises an RFID interrogator (also referred to as a reader) and an RFID tag (also referred to as a transponder). The main function of the RFID transponder is to transmit and receive data, store data or in some cases, measure ambient parameters, such temperature and humidity [38-41]. Likewise, the primary function of an RFID reader is to transmit wireless power, read, and write data wirelessly to and from the RFID transponder.

As shown in Figure 2.1, a simplified view of a standard RFID transponder comprises an antenna that uses a backscatter technique (described shortly) for wireless data transmission and reception. The antenna interfaces with an RFID radio transceiver for wireless communication. The transponder also features a non-volatile memory, for instance, an electrically erasable programmable read-only memory (EEPROM) for data storage. In some cases, the transponder may feature a low-power microcontroller (MCU) and sensor to measure various environmental parameters such as temperature [40]. The reader typically features the following elements: antennas, a control unit, and an RFID reader transceiver [42].

As summarised in Table 2.1 the HF-RFID and LF-RFID uses inductive coupling to enable wireless power and data transfer between two loop antenna [43, 44]. LF-RFID and HF-RFID systems operate in the 0.120 to 0.135 MHz and 13.56 MHz Industrial, Scientific, and Medical (ISM) bands, respectively [38]. LF-RFID follows the ISO/IEC 18000-2 air-interface protocol, and HF-RFID is based on the ISO/IEC 18000-3 standard together with additional smart cards ISO/IEC 15693, ISO/IEC 14443A and 14443B air-interface [1].

The UHF RFID transponders harvest DC power from the reader's carrier signal and use a backscattering technique for wireless communication between the reader and transponder which is typically located within a distance of less than 5 meters of the reader [45]. UHF-RFID complies with the EPC Class 1 Gen 2, ISO18000-6 B/C standard and operates in the unlicensed ISM band at 860 MHz and 915 MHz [46].

2.2.2 Overview of near-field communication (NFC) technology

NFC technology has evolved from traditional HF-RFID technologies, and uses near-field inductive coupling between two NFC loop antennas located closely in each other's vicinity [43] (described shortly in Sub-section 2.2.4). In particular, NFC technology is a short-range, contactless wireless communication technology that operates within the worldwide available unlicensed radio frequency band of 13.56 MHz [43]. In passive communication mode, NFC technology offers a data rate of between 106 kbps and 848 kbps with a maximum wireless communication range of less than 10 cm using the ISO/IEC 14443 standard air interface. NFC also offers a lower data rate of between 6 kbps and 26.48 kbps using the ISO/IEC 15693 standard air interface and has a range of less than 100 cm [47-51].

An additional NFC standard is also available (ISO/IEC 18092 and ECMA-340) that supports data frame format, modulation, interoperability, and data exchange between based NFC-enabled devices [42, 43, 52-54]. In addition, the NFC forum[1] has developed technical specifications to ensure interoperability between NFC devices and Radio Frequency (RF) and also NFC test and characterization methods [55]. NFC technology is also backward compatible with proximity and vicinity smartcard standards, such as ISO/IEC 14443A, ISO/IEC 14443B, and ISO/IEC 15693 [43]. A benefit of backward compatibility is that an NFC radio transceiver based on the ISO/IEC 15693 standard can transmit data up to 1 m with a 13.56 MHz reader as well as up to 7 cm with an NFC type 5 enabled smartphone [56].

[1] NFC Forum is an industry association that was established in 2004 and formed by community-led organizations to advance the use of NFC based wireless interaction with mobile devices and consumer electronics.

As defined by the NFC forum technical specification, NFC transponders operate within one of the following operating modes [38, 55].

Card emulation: In card emulation mode, the NFC transponder operates as a contactless card that enables wireless communication with an NFC enabled reader. A typical use case for card emulation mode is in contactless payment using a bankcard, i.e., debit and credit card.

Peer-to-Peer (P2P): In P2P mode, two NFC-enabled devices come in contact for the exchange of data. A typical use is the transfer of data for music applications.

Read/write: In read/write mode, an NFC-enabled reader operates like a contactless reader to facilitate wireless communication with the NFC transponder. The read/write mode also allows the reader to read and write data to and from the transponder. This data can includes text data, i.e., measured sensor data, uniform resource locator (URL) information, smart poster and contact info. Typical use cases using read mode are NFC labelling and NFC sensing. The *NFC sensor transponder design presented in this thesis* fully complies with ISO/IEC 15693 standard with the read/write mode.

Wireless charging mode (WLC): Wireless charging mode is dedicated to wireless power transfer (WPT) over an NFC connection and wireless communications is used to manage wireless power transfer between the charging device and target device. A typical use case of the WLC mode is for charging small devices, for instance, headsets, fitness trackers, smartwatches, and other consumer products. NFC Forum approved the technical specification of the WLC mode in October 2021 [57]. However, commercial device based on this mode are not yet available in the market but will emerge in the near future.

2.2.3 Choosing a suitable RFID technology

This subsection describes the rationale for the selection of the optimum RFID technology for museum artefacts monitoring applications. The design choices were informed by the user requirements for the application as defined by the project stakeholders (including museum conservation scientists and artefact storage box manufacturers). The user requirements are discussed in detail in Chapter 3.

As discussed in section 2.2.1, LF-RFID technology operates in the low-frequency band from 0.125 to 0.135 MHz and can wirelessly transmit data with a bit rate of 12 bits per second as reported in [39]. LF-RFID technology can wirelessly transmit data with a bit rate of 12 bits per second. However, because a low data rate of 12 bits per second, LF-RFID would require more than 10 seconds to transmit 50 bytes of data.

Table 2.2: Comparison of RFID technologies.

Parameter	**HF-RFID (ISO/IEC 14443A)**	**HF-RFID (ISO/IEC 15693)**	**UHF-RFID (ECP global Gen2)**	**Ref**
Interoperability	NFC Type 1, 2 and 4[2]	NFC Type 5	ECP global Gen 2	[58-61]
Wireless communication Range (cm)	< 10 with Reader < 3 with smartphone	< 150 with Reader < 7 with smartphone	<500 with Reader	[62-64]
Coupling method	Inductive (Proximity)	Inductive (Vicinity)	Backscattered (Far-field)	[59, 65, 66]
Modulation (Reader to Tag)	ASK 100 % depth of modulation	ASK 10 % or 100 % depth of modulation	ASK	[61, 67]
Modulation (Tag to Reader)	Load Modulation	Load Modulation	ASK or PSK	[59, 61, 67]
Data Rate (kbit/s)	106 and 424	26.48	26.7-128	[59, 61, 67]
Memory (kB)	2	64	< 64	[59, 68]
Reader	Smartphone	Smartphone	UHF RFID Reader	[1, 51]

[2] The NFC forum defined technical specifications for five transponder types, i.e., Type - 1 to Type - 5, to ensure interoperability between NFC transponder and reader.

Therefore, LF-RFID technology is difficult to employ for the museum artefact monitoring application. A comparison of HF-RFID and UHF-RFID is summarized in Table 2.2. It is evident from Table 2.2 that HF-RFID technology based on ISO/IEC 14443 A and B air interface can wirelessly transmit data with a data rate of 424 kbps. However, NFC transponder based on ISO/IEC 14443 air-interface can provide a maximum wireless communication range of less than 3 cm with an NFC enabled smartphone when used as a reader [1, 40]. Ultra-high frequency radio-frequency identification (UHF-RFID) technology can be used to provide a maximum wireless communication range of approximately 5 m in battery-less mode [45]. However, the cost of an UHF RFID reader can be prohibitively expensive (approximately €1600 [69]) whereas for HF-RFID, only a smartphone is required with no additional cost. Thus, UHF RFID technology may be unsuitable for monitoring low-cost museum artefacts [40] due to budgetary reasons.

As summarized in Table 2.2, an NFC sensor transponder uses ISO/IEC 15693 air interface can transmit data with the data rate of 26.48 kbps with a wireless communication range of 7 cm with an NFC enabled smartphone used as a reader [1] (See Section 2.2.2). Therefore, HF-RFID technology that uses ISO/IEC 15693 air interface was chosen for the museum artefact monitoring application. Detailed reviews of state-of-the-art NFC sensor transponders are presented in sub-section 2.3.2.

2.2.4 Physical principles of operation for an NFC system

This subsection describes the physical principles of operation for an HF-RFID and NFC system.

2.2.4.1 NFC system wireless power transfer and communication model

This subsection describes the wireless power transfer and communication between the reader and the tag from circuit point of view. Figure 2.2 shows the simplified equivalent circuit model of the NFC system. This model of the NFC reader consists of the equivalent circuit of the reader integrated circuit (IC) connected to a loop antenna (L_1) with ohmic losses (R_1) and tuning capacitor (C_1).

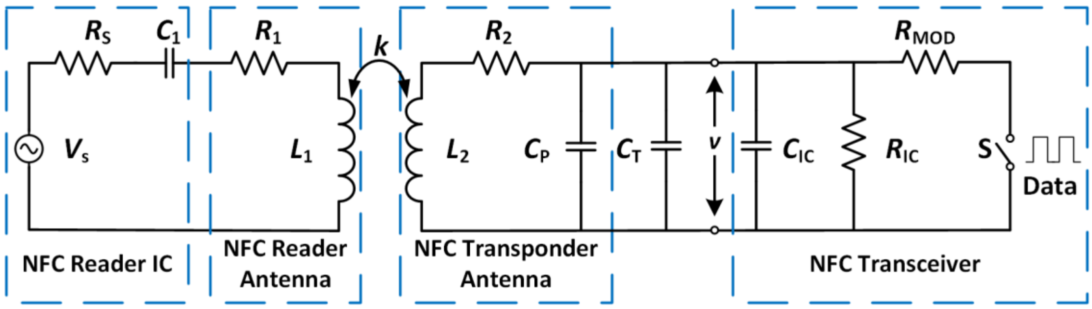

Figure 2.2: Simplified equivalent circuit model of NFC system.

The reader also includes an impedance matching network and perfect impedance match at resonant frequency has been assumed (R_1 = R_S). Likewise, the simplified NFC transponder model comprises an equivalent circuit model of NFC transceiver, NFC loop antenna (L_2) and external tuning capacitor (C_T). As shown in Figure 2.2 the NFC reader and transponder are inductively coupled, and the coupling coefficient is denoted by parameter k. The value of k can vary between $0 \leq k \leq 1$ [51]. An NFC reader loop antenna (L_1) is connected to the reader integrated circuit (IC) and generates an alternating magnetic field (H).

Resistance R_1 represents the ohmic losses in the reader antenna L_1. In order to achieve maximum current (I) in the conductor loop L_1, capacitance C_1 and inductance (L_1) form a series resonant LC circuit that has a nominal resonant frequency (f_R) of 13.56 MHz. The mutual inductive coupling between L_1 and L_2 induces an alternating voltage (v) on terminals of the transponder loop antenna, L_2.

The ohmic losses in the transponder loop antenna L_2 are represented by the series resistance R_2, as shown in Figure 2.2. In addition, the NFC radio transceiver features an internal capacitance (C_{IC}). This internal capacitance (C_{IC}), along with parasitic capacitance (C_P) and external tuning capacitor (C_T) connects in shunt with the transponder loop antenna L_2 to form a parallel LC circuit with a nominal resonant frequency (f_R) of 13.56 MHz. The induced voltage (v) on the terminal of the transponder antenna (L_2) is then used to power the NFC transponder.

In order to transmit data from the transponder to the reader, NFC system use a load modulation technique where load modulation resistance (R_{MOD}) and switch (S), are modelled as shown in Figure 2.2. Resistance R_{MOD} is toggled between the ON and OFF states using switch (S) and is driven by the data stream.

Toggling the state of R_{MOD}, i.e., turning it ON and OFF generates an amplitude modulated (AM) voltage at the terminals of the reader loop antenna (L_1). From Figure 2.2, it can be seen that $R_{MOD} \parallel R_{IC}$ reduces the total resistance and thus will affect the transformed impedance (Z_T') of the transponder. Through the load modulator, Z_T' of the transponder switches between $Z_T' = R_{IC}$ and $Z_T' = R_{IC} \parallel R_{MOD}$. This results in a voltage change (v_{RX}) at the reader's antenna (L_1), i.e. amplitude modulation occurs. The data transmitted by the transponder is not available in the baseband at L_1. Instead, the transmitted data is found in modulated subcarrier signals, i.e., sidebands centred at $-f_H$ and $+f_H$ subcarrier frequencies of the load-modulated voltage [51].

2.2.5 Architecture of NFC system

As discussed in Section 2.2.2, NFC has evolved from HF-RFID technologies [43]. Figure 2.3 shows the structured stack of the hardware and software layers upon which NFC is built [38].

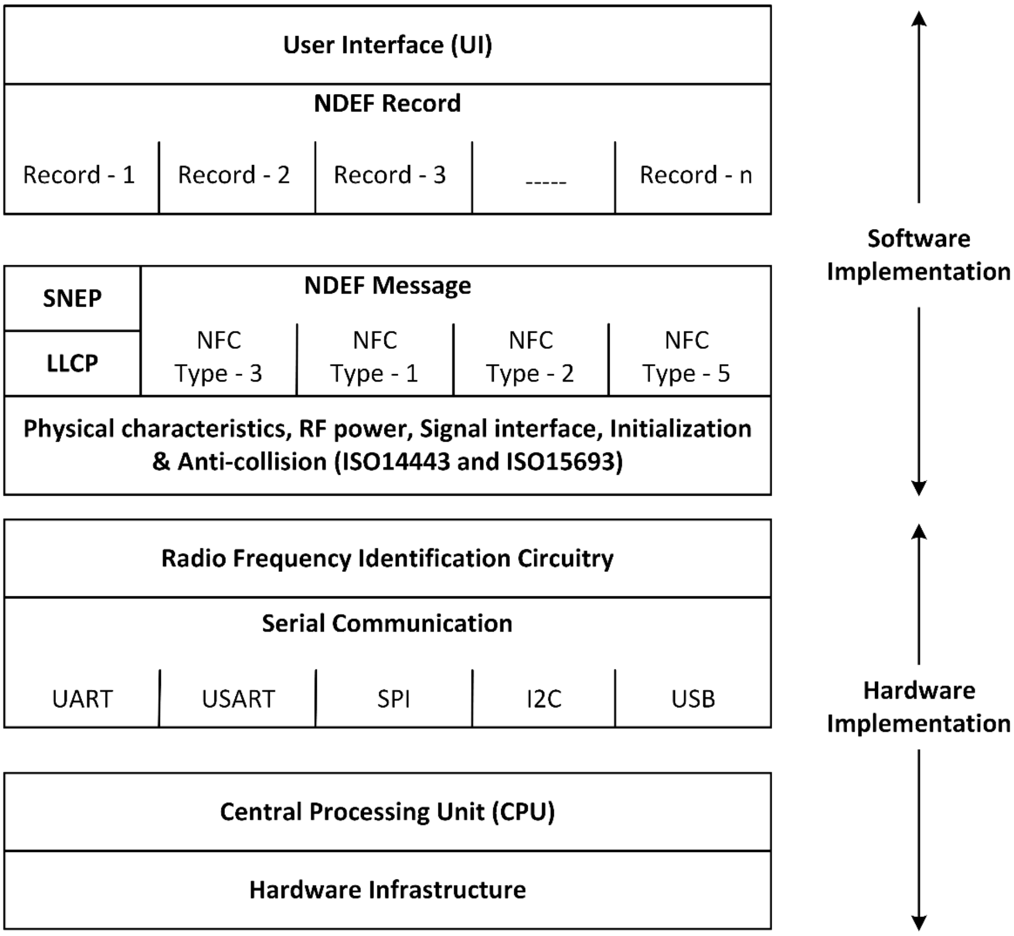

Figure 2.3: High-level architecture of the NFC system.

From Figure 2.3, it can be seen that the NFC system uses several parameters that standardized for an RFID system including physical characteristics, signal interface, initialization and the anti-collision mechanism. In order to ensure interoperability between NFC enabled devices, the NFC forum has developed and implemented technical specifications for the software layer, including protocols, specific data exchange formats with differentiated record types, and tag types [55]. The technical specification for the software layer includes the following dedicated parameters:

A. Data exchange frame
    I. NFC data exchange format (NDEF)
B. Record type definition (RTD)
    I. Text
    II. Uniform Resource Identifier (URI), i.e., website link
    III. Smart poster
C. Protocols
    I. Logical link control protocol (LLCP)
    II. Simple NDEF exchange protocol (SNEP)
    III. NFC controller interface (NCI)

In order to ensure interoperability between NFC-enabled device in the NFC system architecture, a new data exchange format, i.e., NFC data exchange format (NDEF), is implemented in the upper software layer, as shown in Figure 2.3. The NDEF is a lightweight binary message format used to create an application-defined payload of various types of data into a single message. The structure of the NDEF is shown in Figure 2.4. The NDEF may consist of one or more record types with header and payload.

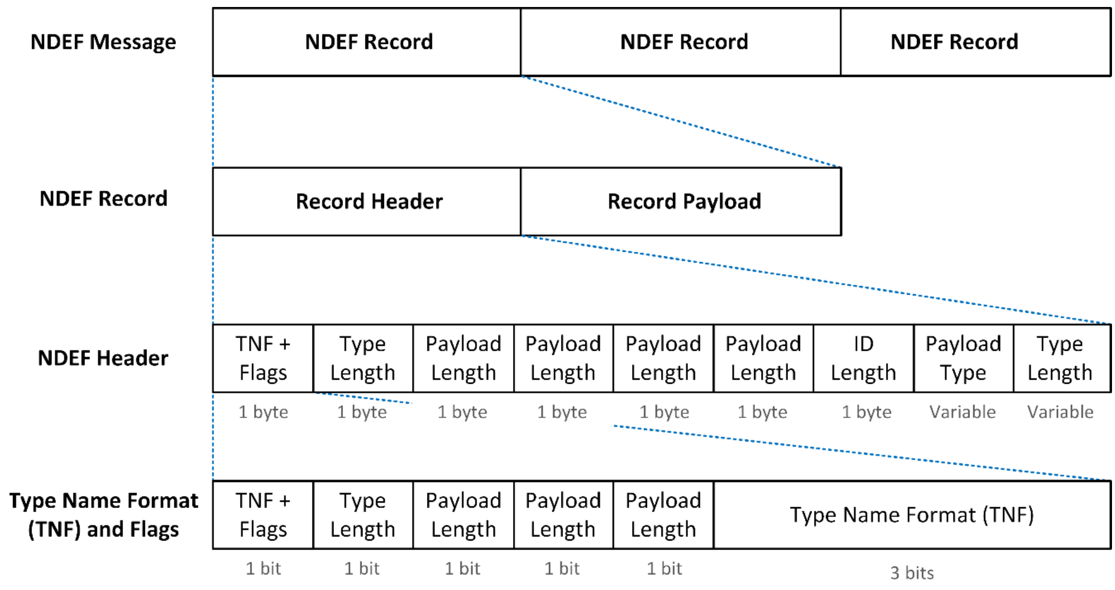

Figure 2.4: NFC Data Exchange Format (NDEF) structure.

The header contains flags that indicate the start and end of the NDEF message with the message type and length of the payload. As discussed earlier in this section, the NDEF also comprises various standardized record type definition (RTD) to construct payload, including URI, text, vCard, i.e., visiting card, smart poster, and pairing Bluetooth or Wi-Fi. The NFC sensor transponder design presented in this thesis uses "*Text*" as a RTD to create a payload.

2.3 State of the Art and Literature Review

This section thoroughly reviews the prior academic and commercial works in the area of battery-less NFC and RFID sensor technology.

2.3.1 State-of-the-art battery-less RFID and NFC transponders

Recently, the demand for RFID and NFC enabled sensor transponders has been growing due to the increasing number of IoT applications using battery-less transponders for applications in soil moisture monitoring [6-8], fruit quality measurement [9, 10], long-term building structural health monitoring [11, 12], gas monitoring [13], museum artefact monitoring [1, 40] and environmental parameter monitoring [14, 15]. Figure 2.5 shows the global market trend for battery-less sensor device from 2018 to 2030. It is observed that in 2022, the market for battery-less sensor devices was valued at approximately $35 million and is projected to reach roughly $284.69 million by the year 2030, which will represent a compound annual growth rate (CAGR) of 28 % from 2022 through 2030 [70].

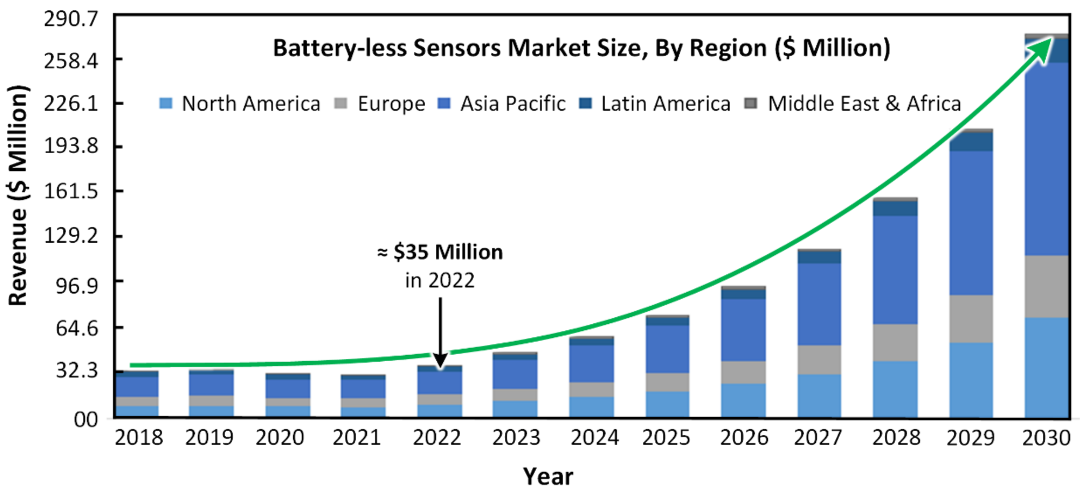

Figure 2.5: Market trend for battery-less sensor from 2018 to 2030 (Fig.9 of [70]).

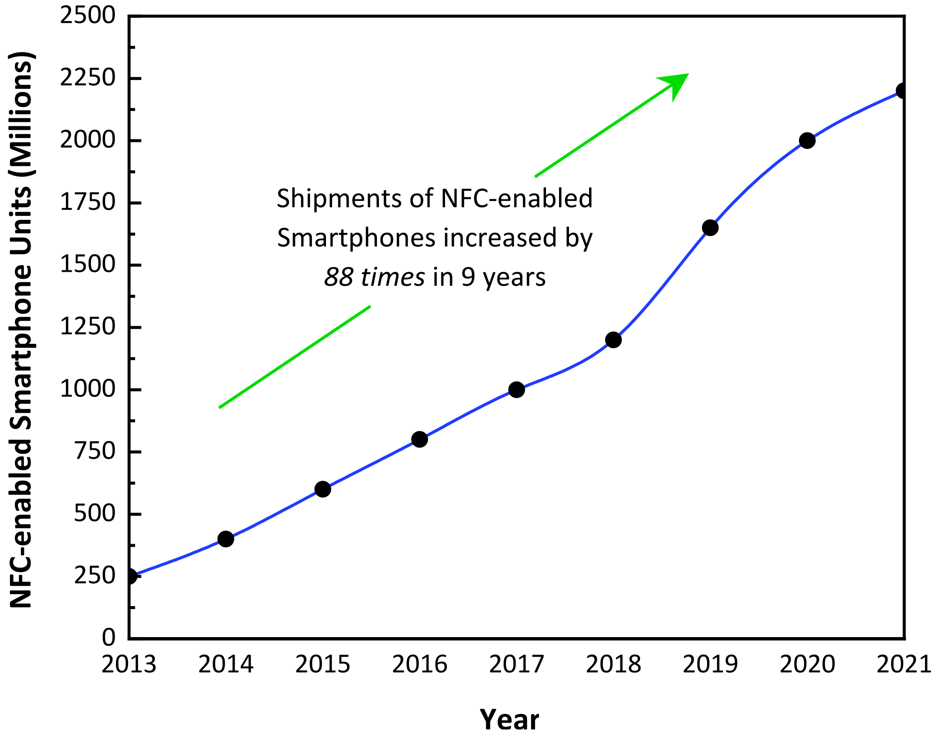

Figure 2.6: Shipped NFC-enabled smartphone units from 2013 to 2021 (Fig. 7 [71]).

As reported in [70], the miniaturization of sensing devices and the increased adoption of automated condition monitoring systems in smart factories is influencing the positive market growth for these devices. In addition, recently, the market for NFC technology has increased significantly due to the incorporation of an NFC reader capability within smartphones [5]. It is evident from Figure 2.6 that shipment of NFC-enabled smartphones is increased by 88 times from 2013 to 2021 [71]. At the present time, NFC technology not only enables consumers to perform payments for example, but also passively measures and wirelessly transmits data sets of various parameters such as temperature and humidity for a wide range of IoT application [47, 68].

NFC enabled sensor transponder with *battery-less* or *battery-assisted operation* along with sensing and wireless communication capabilities are more recently becoming available as commercial products in a variety of configurations.

Examples of such commercial NFC sensor products that are available at the present time include Monarch Instrument- Track-It [35], Microsensys - TELID 232 and TELID 332-th [32, 34], GoSense – Wireless NFC sensors [33], Intellilog – Temperature logger [36], Avery Dennison - TT Sensor Plus [72] and Identiv - *u*Trust Sense Temperature Tracker [73].

Table 2.3 summarizes some of the available battery-less and battery-assisted NFC and RFID-enabled commercial sensor transponders that are available in the market at present for various IoT applications such as cold supply chain or temperature-sensitive product monitoring. Table 2.3 indicates that two of the sensor transponder listed [32, 35] have a limited shelf life of a maximum of 3 years. In addition, only a limited number of the reported solutions support battery-less operation [33, 34] and are not optimized for low-cost applications [32-36, 72, 73]. Therefore, commercially available solutions cannot be easily adapted for low-cost museum artefact monitoring applications. This represents a challenge but also an opportunity.

Table 2.3: Commercial NFC sensor transponders.

Manufacturer	Unit Cost (€)	Shelf Life (Years)	Battery-less operation	Sensor	Ref
Monarch Instrument, USA	71	3	No	Temperature Humidity	[35]
Microsensys, Germany	48	3	No	Temperature Humidity	[32]
	24	Not reported	Yes	Humidity	[34]
GoSense, UK	23	Not reported	Yes	Temperature Humidity	[33]
Intellilog, Germany	17	1	No	Temperature	[36]
Avery Dennison, USA	15	1	No	Temperature	[72]
Identiv, USA	8	1	No	Temperature	[73]

2.3.2 NFC enabled battery-less sensor transponder

As discussed in sub-section 2.3.1, the research area associated with NFC enabled battery-less sensor transponders has received increased significant interest due to the incorporation of NFC reader capability within smartphones. In addition, the significant technology advancement in the development of low to ultra-low power electronics has enabled the rapid growth of IoT platforms, expanding into several application fields as described in the previous section. In this section a detailed review of the state-of-the-art battery-less NFC sensor is presented.

In 2007, one of the first NFC sensor transponder was reported in the literature and was referred to as an NFC interface module [74]. The reported NFC interface module comprised an inbuilt temperature sensor (LM20) and had the ability to communicate with an NFC-enabled smartphone. However, the reported NFC module was *battery-augmented (semi-passive)* and did *not* support battery-less operation [74]. In [75], a practical implementation of a battery-less NFC-enabled sensor was reported. This sensor was capable of measuring temperature and was wirelessly powered wirelessly using an NFC reader. However, the reported NFC temperature sensor was *not* compatible with standards based NFC-enabled smartphones. Likewise, in [76], a battery-less NFC sensor transponder that was wirelessly powered using NFC enabled by a smartphone (*Google Nexus S*) has been reported. The reported NFC sensor was designed to measure various health-related parameters, including temperature and urine content in a diaper monitoring application using a resistive moisture sensor. In addition, the reported NFC sensor could also detect blood level under wound bandages.

Figure 2.7 depicts the number of research papers that report the use of battery-less NFC sensors from 2015 in this active research domain. It can be seen from Figure 2.7 that the last five years have witnessed a growing interest in developing battery-less NFC sensor transponders for various applications due to the availability of NFC-enabled smartphones in the market. As discussed in Section 2.3.1, the shipment of NFC-enabled smartphones has increased by a factor 88 times from the year 2013 to 2021.

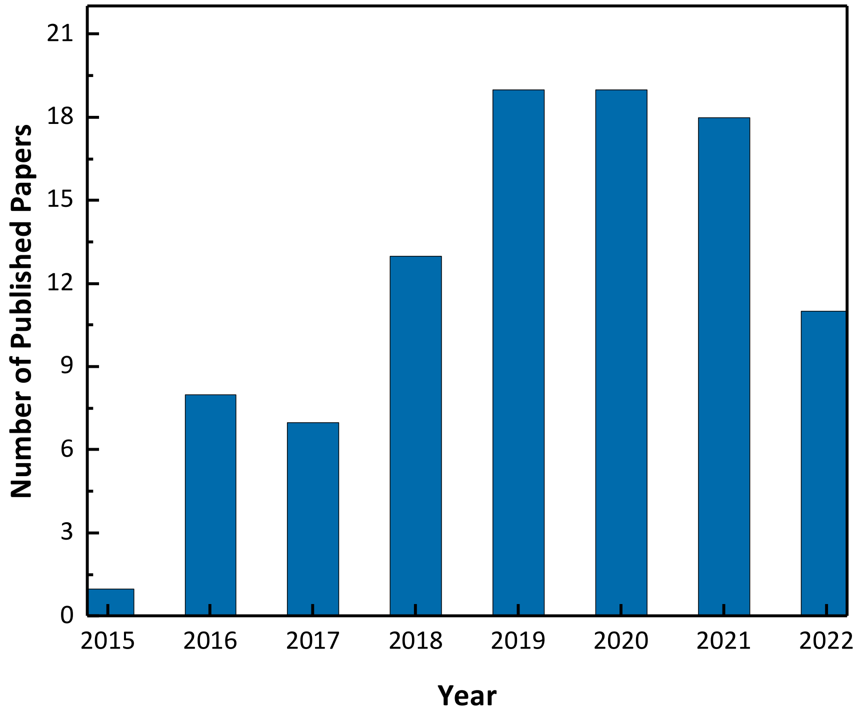

Figure 2.7: The total battery-less NFC sensor articles reported in the literature.

In recent years, various battery-less and battery-assisted wireless sensing solutions have been developed that use NFC and RFID technology in multiple application domains. These applications require the sensing of multiple disparate parameters that are discussed in Sub-section 2.3.1.

In order to develop a battery-less NFC sensor transponder for various IoT applications, the NFC transceiver based on ISO/IEC 14443 (i.e., NFC Type 2 and Type 4) and ISO/IEC 15693 (i.e., NFC type 5) has been widely used in literature.

2.3.2.1 NFC sensor transponder based on ISO/IEC 14443 standard

This sub-section briefly describes the battery-less NFC sensor transponders that are based on ISO/IEC14443 i.e., NFC Type 2 and Type 4. In [26], an NFC sensor transponder was reported that could sense real-time determination of Carbon dioxide (CO_2) inside an FFP2 (FFP stands for filtering face piece). A circuit diagram of the reported NFC CO_2 sensor transponder along with interconnection is shown in Figure 2.8 (a).

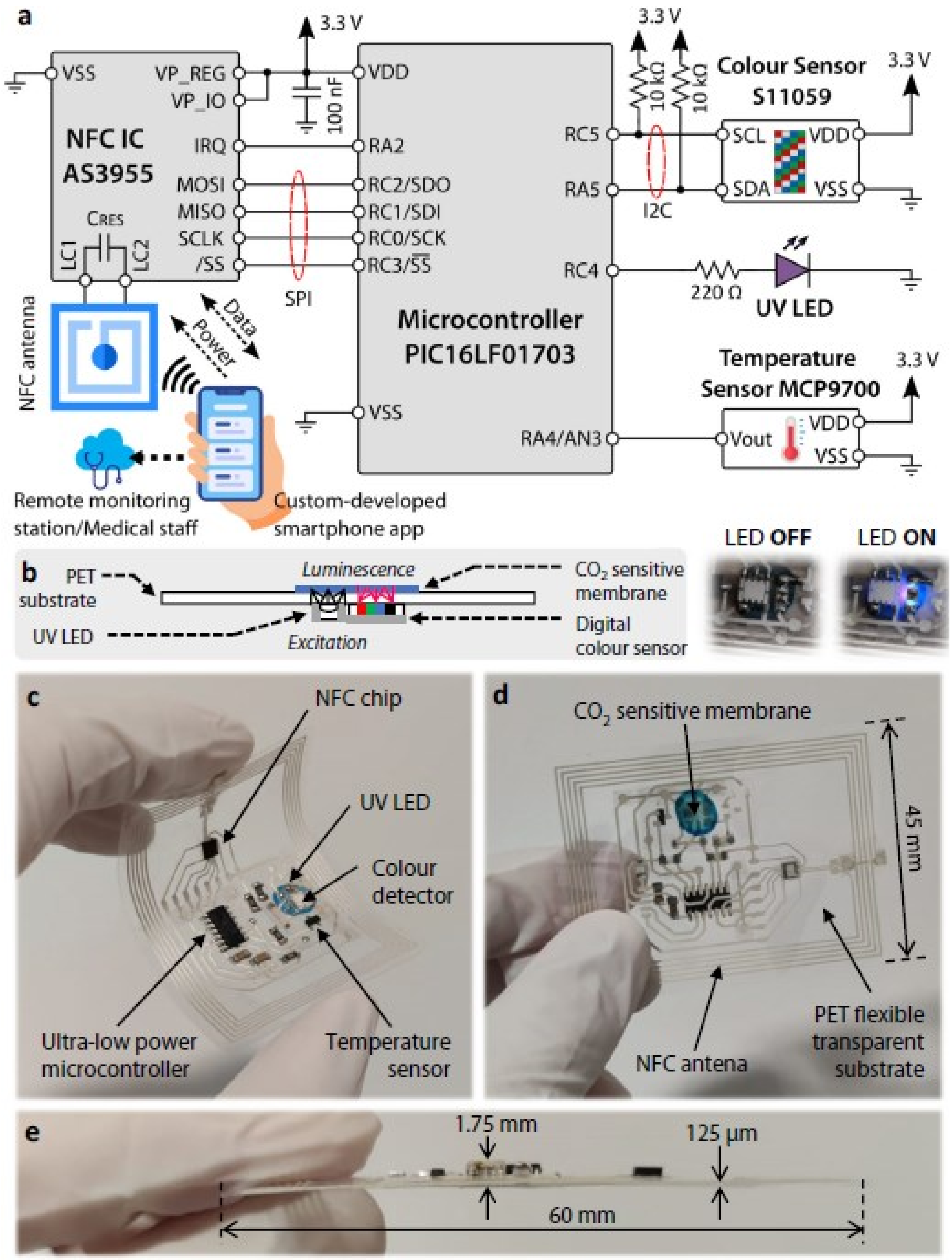

Figure 2.8: NFC sensor (a) schematic (b) CO_2 sensor (c)-(e) prototype (Fig.3 of [26]).

As shown in Figure 2.8 (a) the circuit diagram comprises of a microcontroller (Part Number: PIC16LF10703) and NFC transceiver (Part Number: AS3955) [26]. In addition, the circuit diagram also consists of the sensing elements, including ultraviolet light emitting diode (UV LED), digital colour sensor (Part Number: S11059) and temperature sensor (Part Number: MCP9700). As shown in Figure 2.8 (b) to sense CO_2, the sensing module is aligned with a carbon dioxide-sensitive membrane. The luminescent response of the UV LED after the exciting CO_2 membrane was detected by the colour sensor. In addition, to correct the temperature dependency of the chemical sensor, a temperature sensor was also included in the transponder design. The NFC CO_2 sensor transponder was fabricated on a 125 μm thick PET flexible substrate as shown in Figure 2.8 (c) to (e). The reported transponder consumes 4.45 mW DC power to perform sensing operations while yielding a maximum wireless communication range of 1.9 cm with an NFC-enabled smartphone as a reader.

Furthermore, in [22] a battery-less NFC-enabled tire pressure monitoring system (TPMS) for bicycles has been reported. Figure 2.9 shows the top and bottom view of the NFC sensor transponder that incorporates a pressure sensor to sense tire pressure. The TPMS is fully wirelessly powered by a magnetic field induced by the reader, i.e., NFC enabled smartphone. The pressure-sensing element is a force-sensing resistor (FSR) and is interfaced with a timer-based oscillator integrated circuit, i.e., IC 555. The oscillator frequency is then read and computed by the MCU. As shown in Figure 2.9 hardware prototype was fabricated on an FR4 substrate and includes a microcontroller (MCU) and NFC transceiver (Part Number: NT3H2111) [22]. A maximum wireless communication range of 0.8 cm was reported after integration within the bicycle tire. In addition, pressure sensor accuracy of 0.1 bar has been reported over a pressure range from 0.5 to 2.2 bar.

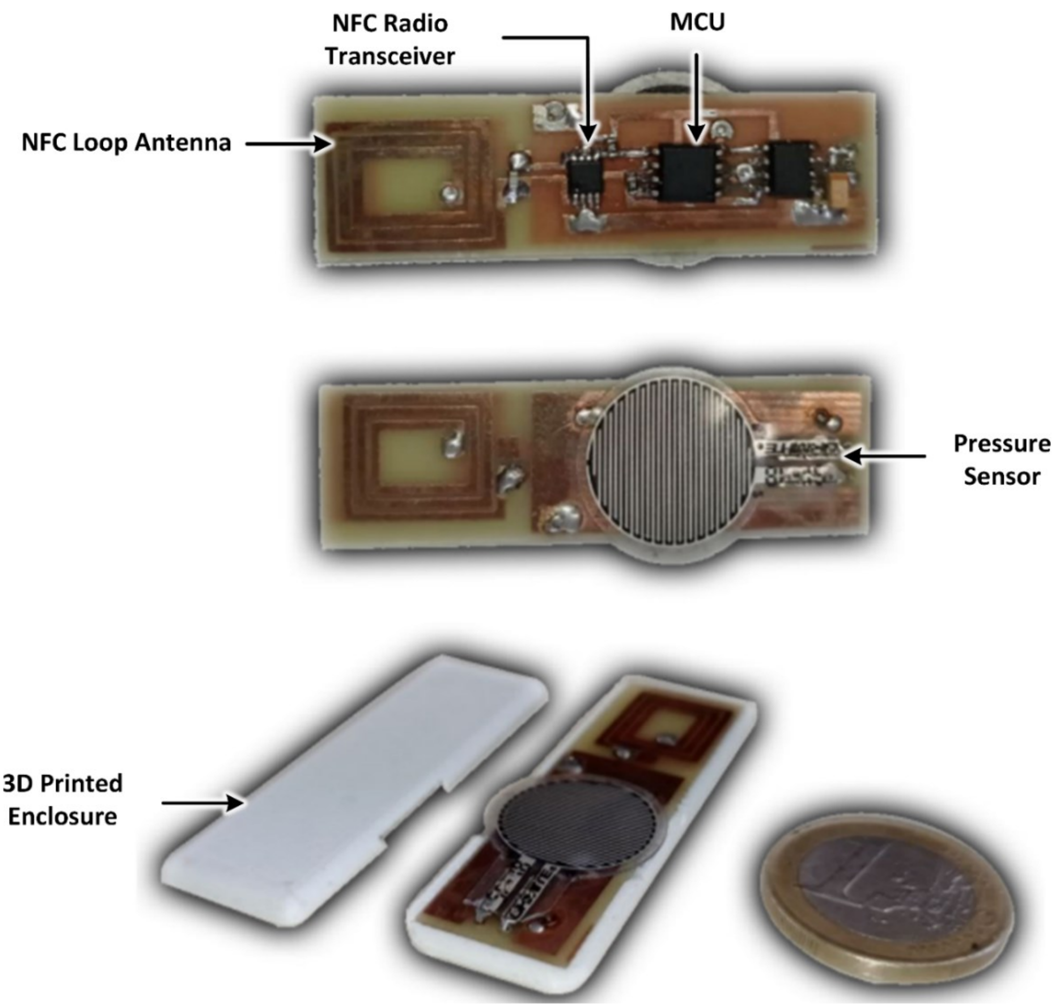

Figure 2.9: Top and bottom view of NFC sensor prototype (Fig. 7 of [22]).

Likewise, in [77], battery-less NFC sensor transponder was reported for monitoring transepidermal water Loss (TEWL) and skin wittedness factor (SWF) monitoring. Figure 2.10 shows the system architecture and prototype of the reported transponder. This transponder is based on a commercial NFC transceiver (Part Number: RF430CL330H). The transponder design comprises a compact antenna size with diameter of 2.6 cm and provided a wireless communication range of approximately 1 cm when an NFC-enabled smartphone was used as a reader.

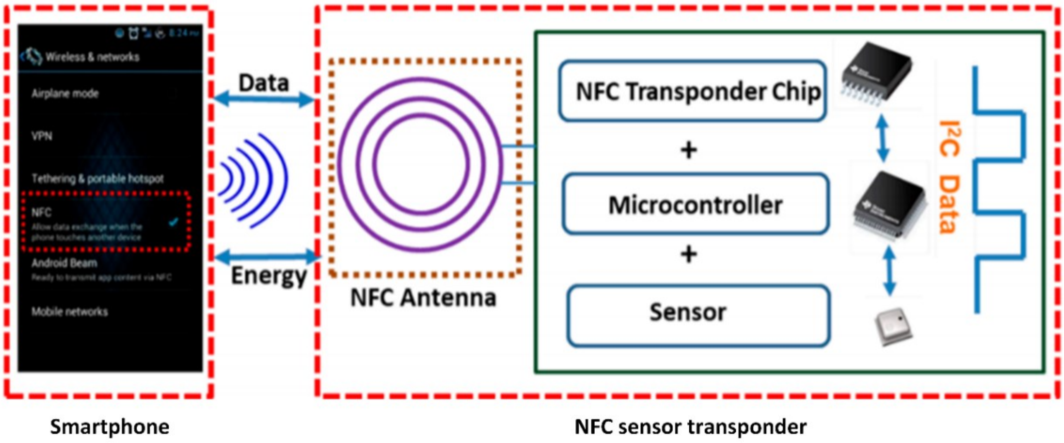

(a)

(b)

Figure 2.10: NFC skincare sensor (a) architecture (b) prototype (Fig. 2 & 3 of [77]).

The reviewed NFC sensor transponders that are based on ISO/IEC 14443 air interface and NFC type - 2 or type - 4 reported a shorter wireless communication range of less than 2 cm [22, 24, 26, 28, 30, 77-80].

2.3.2.2 NFC sensor transponder based on ISO/IEC 15693 standard

As discussed in 2.2.3, an NFC radio transceiver based on the ISO/IEC 15693 air interface standard can provide enhanced wireless communication range compared with an ISO/IEC 14443 based transceiver [1, 2, 81]. For example, in [82] a battery-less NFC enabled smart bandage has been reported and consists of a strain and temperature sensor. The block diagram and the hardware prototype of the smart bandage are shown in Figure 2.11.

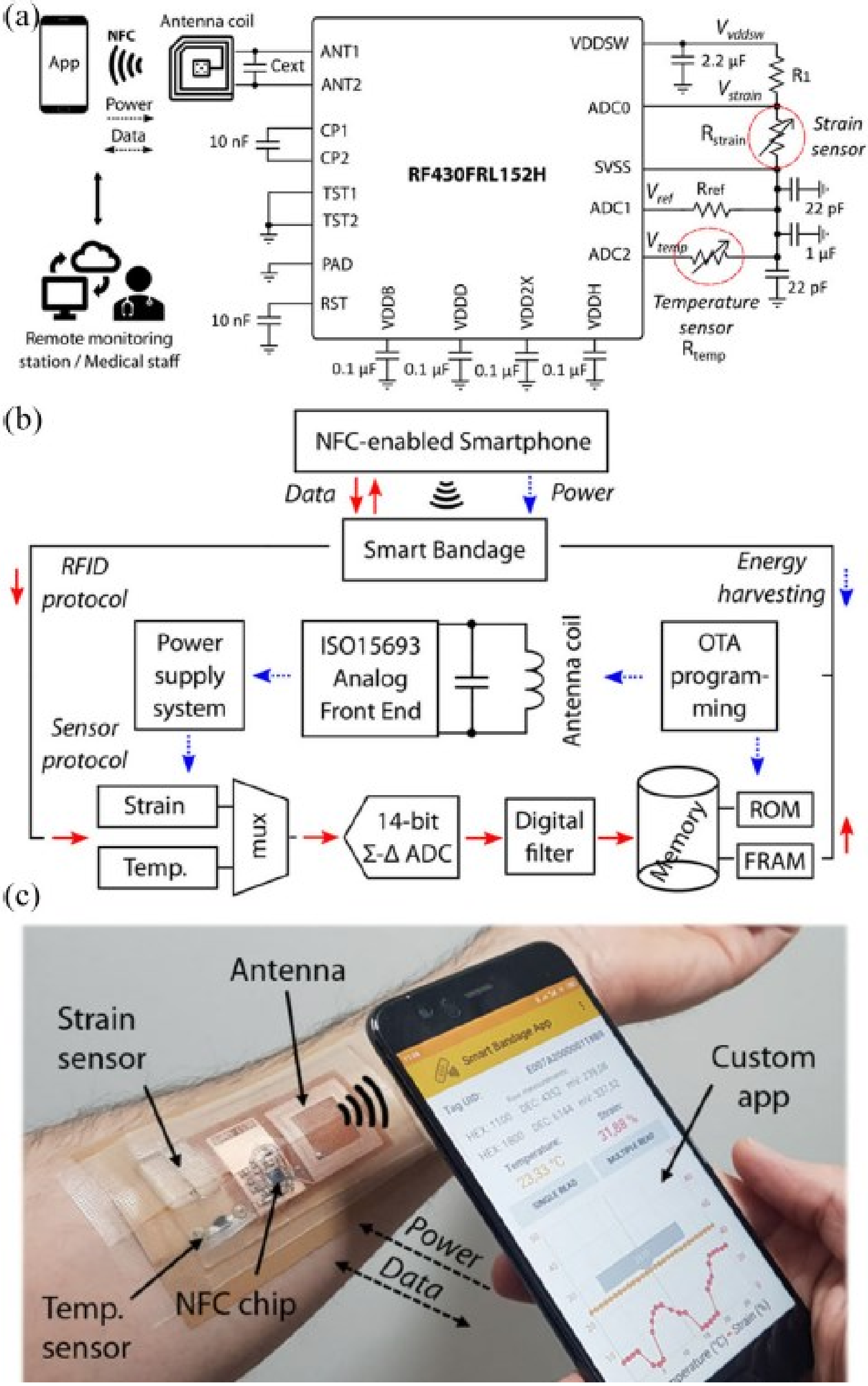

Figure 2.11: NFC bandage (a) schematics (b) diagram (c) prototype (Fig. 5 of [82]).

The smart bandage comprises of an NFC transceiver (Part Number: RF430FRL152H) and an analogue resistive type temperature and strain sensor. The RF430FRL152H is a programmable NFC radio transceiver with an integrated data processing unit. The transponder is wirelessly powered using an NFC-enabled smartphone and provided a wireless communication range of 4.3 cm. Similarly, the wireless communication range of NFC sensor transponders reported in [83] and [84] were 4 and 3 cm, respectively. Both NFC sensor transponders were based on an identical NFC radio transceiver (SL13A) has an integrated data processing core.

In order to process sensor data, the RF430FRL152H and SL13A do not require an additional microcontroller (MCU). This significantly reduces the overall DC power consumption of the transponder and leads to improved wireless communication range (described in Chapter 3). However, SL13A and its substitute NFC radio transceiver AS38513 were discontinued by the manufacturer (AMS AG, Austria) in 2015 and 2021, and both transceivers are now obsolete and not available on the market [85, 86]. On the other hand, the NFC radio transceiver RF430FRL152H is available in the market but can only deliver approximately 675 μW of DC power to external electronics such as sensors [82]. This limited wireless power harvesting capability restricts the use of RF430FRL152H in applications where more harvested power is required. Consequently, the NFC radio transceivers that interface with an external microcontroller as a processing unit are employed for most of the NFC sensor transponder designs reported in the literature, i.e., in [7, 9, 27, 29, 87].

For example in [25] a battery-less NFC sensor transponder for pH monitoring has been reported. The hardware prototype for a battery-less pH sensor transponder is shown in Figure 2.12. The transponder comprises of an Atmel Tiny85 microcontroller and NFC radio transceiver (Part Number: M24LR04E). In addition, the transponder also consists of a LED and light-to digital converter (Part Number: CS3472) as the sensing element. In order to sense pH, the transponder consumes 2.9 mW of DC power while yielding a maximum wireless communication range of 1.8 cm. In addition, the microcontroller clock frequency was set to 1 MHz to minimize DC power consumption.

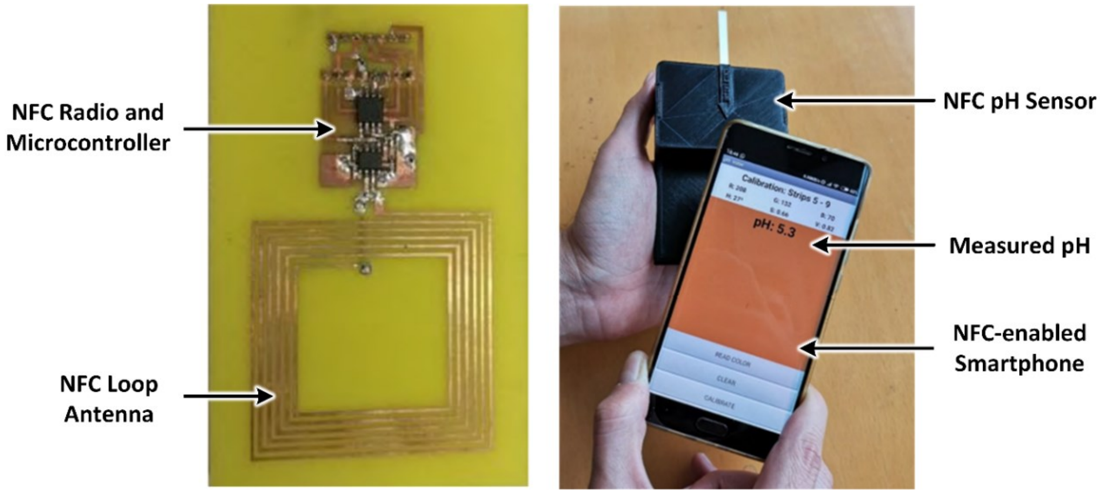

Figure 2.12: Hardware prototype of battery-Less NFC pH sensor (Fig. 21 of [25]).

Likewise, a battery-less flexible NFC sensor transponder for sensing the total mineral content of drinking water has been reported in [27]. Figure 2.13 shows a hardware prototype and measurement of the NFC sensor that uses a smartphone. The transponder comprises an external microcontroller (Part Number: MSP430FR2433) and an NFC transceiver (Part Number: M24LR16E). The transponder also implements a planar interdigitated capacitive sensing element that interfaces to the MCU using a capacitive to digital converter (Part Number: PCAP02). The NFC sensor transponder has a DC power consumption of 2.1 mW and provides a maximum wireless communication range of 3 cm with a smartphone as a reader. The clock frequency of the microcontroller was specified at 1 MHz to reduce the DC power consumption.

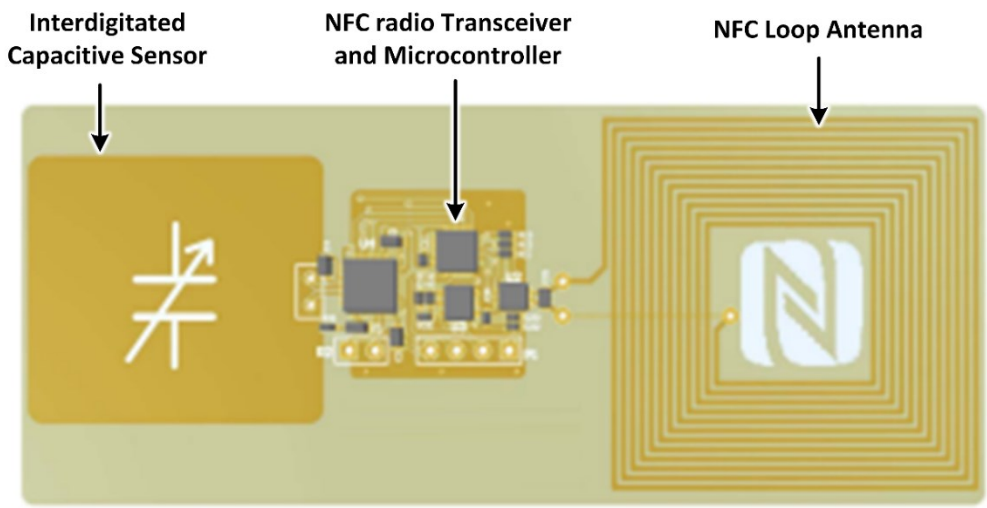

(a)

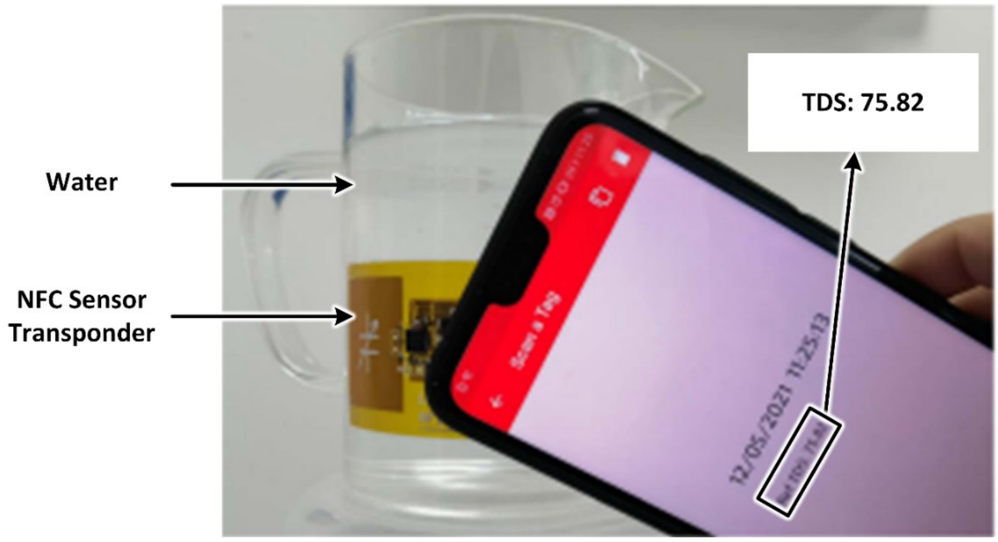

(b)

Figure 2.13: NFC minerals sensor (a) prototype (b) measurement (Fig. 6 & 8 of [27]).

2.4 RFID and NFC Sensor Transponder for Artefact Monitoring

This sub-section briefly describes the state-of-the-art in RFID and NFC transponders for museum artefact monitoring applications. In order to prevent the degradation of museum artefacts, battery-assisted or battery-powered NFC or RFID sensor transponders have been reported in the literature. For example, in [88], the long-term preventive care of fine art objects is reported. A battery-assisted NFC sensor transponder is described and that can monitor temperature and humidity. The sensor was deployed for a duration of six months to monitor the microclimatic conditions within a dedicated enclosure that was used to house a late 16th century panel painting as in Figure 2.14. The transponder is based on the ISO/IEC 15693 standard and compliant with NFC type 5. This study explicitly detailed the critical role of object-specific sensor transponders used for long-term preventive care of fine art objects.

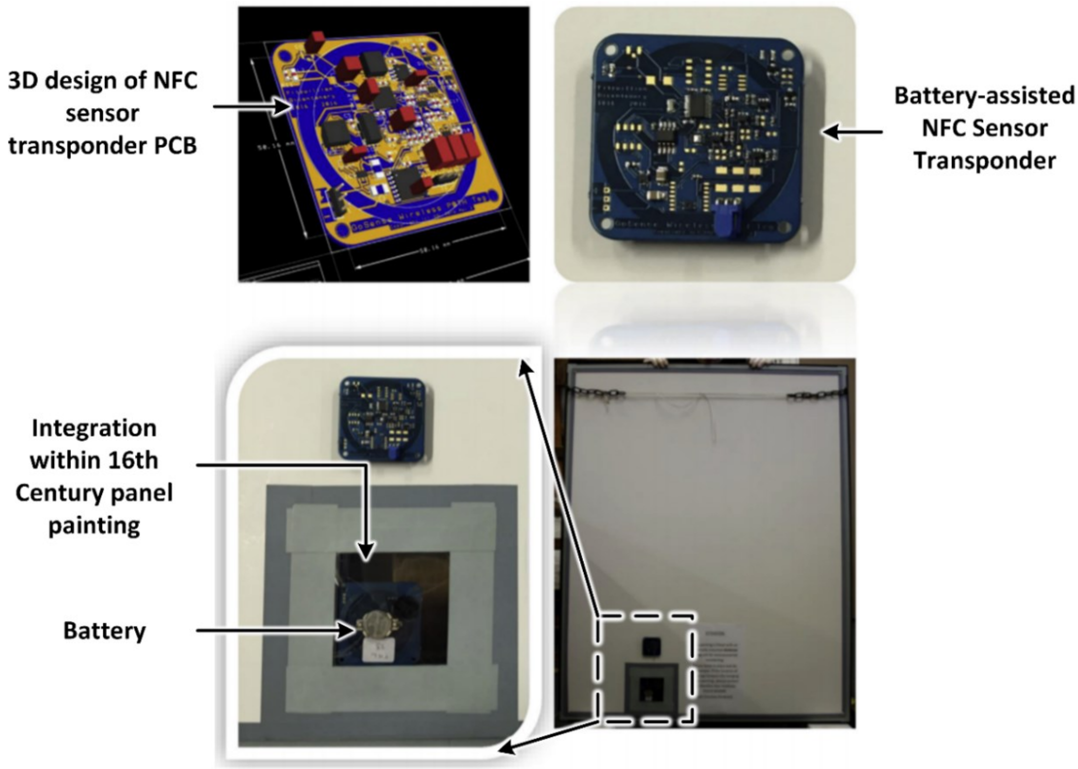

Figure 2.14: Battery-assisted NFC sensor for monitoring of painting (Fig.2 of [88]).

Similarly, the identification of cultural relics in museums, as well as the capability for environmental monitoring using RFID technology has been reported in [89, 90]. However, these reported artefact-monitoring solutions [88-90] require a battery as a power source.

2.5 Performance Comparison of State-of-the-Art NFC sensors

Table 2.4 summarizes the key performance characteristics of 17 state-of-the-art battery-less NFC sensor transponders from the literature. For ease of reading, each column in Table 2.4 is labelled A to H. Each entry lists the references number of each research article, the RFID air interface standard employed, the integrated processing unit, MCU clock frequency clock frequency (f_{CLK}), dimension of the NFC loop antenna in mm (*L*= length, *W*=width, or ∅ = diameter), DC power consumption of the NFC sensor transponder in mW, maximum wireless communication range in cm with NFC enabled smartphone, and parameters sensed using the reported transponder, respectively.

2.5.1 NFC sensor performance comparison

As summarized in column B of Table 2.4, two types of RFID air interfaces are used for these applications, i.e., ISO/IEC 14443 and ISO/IEC 15693. It is also evident from Table 2.4 that approximately 60 % of these NFC sensor transponders use the ISO/IEC 15693 standard.

Table 2.4: Performance comparison summary for state-of-the-art NFC sensor.

A	B	C	D	E	F	G	H
Ref	**RFID air Interface**	**Integrated processing unit**	**MCU clock (MHz)**	**Tag Coil Size (mm)**	**DC Power consumption (mW)**	**Range (cm)**	**Sensing parameters**
[22]	ISO14443	No	1	12 × 16	1.74	0.8	Pressure
[23]	ISO14443	No	1	⌀ 26	1.72	1	Skin moisture & Ultraviolet light
[77]	ISO14443	No	1	⌀ 26	NA[3]	1	Skin moisture
[24]	ISO14443	No	NA	35 x 25	1.8	1	ECG & sweat pH
[28]	ISO14443	No	NA	10 × 5	0.9	1	Arterial SPO_2 & Temperature
[29]	ISO15693	No	1	25 x 25	NA	1.4	Moisture
[25]	ISO15693	No	1	50 x 50	5.29	1.8	pH
[26]	ISO14443	No	NA	43 × 58	4.45	1.9	Carbon dioxide
[7]	ISO15693	No	1	50 x 50	3	2	Soil moisture, RH Temperature &
[9]	ISO15693	No	1	50 x 50	5.29	2	Color
[30]	ISO14443	Yes	NA	45 × 30	NA	2	Ascorbic acid
[10]	ISO15693	No	1	50 x 50	8	1.9	Color
[31]	ISO15693	Yes	NA	70 x 70	NA	3	pH
[84]	ISO15693	Yes	NA	34 × 46	1.3	3	Blood flow
[27]	ISO15693	No	1	35 × 35	2.1	3	Water minerals
[83]	ISO15693	Yes	NA	25 x 35	NA	4	pH
[82]	ISO15693	Yes	NA	26 × 26	NA	4.3	Strain & Temperature

Note: This table is sorted in the increasing order of wireless communication range in column G.

[3] NA = Information not reported in literature

2.5.2 DC power consumption and wireless communication range

Table 2.4 column F shows the overall DC power consumption of battery-less NFC sensor transponders that included a microcontroller as a processing unit exceeds a value of 0.9 mW. In addition, it is evident from Table 2.4 (column G) that a wireless communication range of the NFC sensor transponder that included a microcontroller is reported less than 3 cm. It is known [91-93] that magnetic field strength decays proportionally to the cube of the distance between two mutually-coupled coils [1]. In other words, there is a limit to the available harvested RF power for the NFC sensor for a given distance from the Smartphone. Therefore, in order to reduce overall DC power consumption and increase the communication range, the MCU clock frequency (f_{CLK}) of over half of the NFC sensor transponders reported in Table 2.4 was decreased and set to 1 MHz (also referred to as the frequency scaling technique). The overall power consumption also can be reduced by decreasing the CPU core voltage (V_{CORE}) of the MCU (also referred to as a voltage scaling technique) [1]. However, to the best of the author's knowledge, the voltage scaling technique to reduce the overall DC power consumption of NFC sensor transponder was not investigated in literature.

2.6 Gaps in the State-of-Art and Research Hypothesis

From the literature review discussed in Section 2.5, several technology limitations or gaps are evident from the state-of-the-art NFC sensor transponders reported in the literature. Some specific limitations are also evident, particularly for museum artefacts monitoring applications.

- The harvested DC power consumption of battery-less NFC sensor transponders that includes a microcontroller as a processing unit is mostly higher than 1.5 mW. In [28], DC power consumption of 0.9 mW has been reported. Higher DC power consumption is one of the key factors that limits the wireless communication range [1].
- The maximum wireless communication range of NFC sensor transponders that included a microcontroller as a processing unit has been reported to be less than 3 cm with an NFC-enabled smartphone as a reader.

- Several challenges with commercial solutions are identified, including a limited operational life of 3 years maximum [32], a limited number of the solutions support battery-less operation [33, 34] and are not optimised for low-cost applications i.e., unit-costs of approximately €23 [33].
- Commercially available hygrometers or data loggers and other environmental monitoring are not suitable for integration into a large number of storage enclosures [21].
- The storage box often needs to be physically opened to enable the reading of sensor data and this, in itself, may cause artefact degradation by introducing contaminants when opening the box.
- To the best of the author's knowledge, a museum archive box that features a fully integrated wireless powered temperature and humidity sensor has *not* been reported in the literature.

In museum artefact monitoring, cost, wireless communications range and operational life of NFC sensor transponder are important requirements [1]. In addition, NFC sensor integration in the box or packaging material without using adhesive is also a vital requirement [1]. To the best of the author's knowledge, there are no convenient cost-effective batteries-less wireless solutions available to solve the above problem in this application domain at the present time. Therefore, the work presented in this thesis aims at addressing the above challenges identified in the literature by designing a new, performance improved NFC sensor transponder that is optimized for museum artefact monitoring applications.

The research hypothesis for this work focuses on optimizing the overall harvested DC power consumption of the NFC sensor to enhance wireless communication range when compared to the state-of-the-art NFC sensor transponder. In addition, research also focuses on integrating NFC sensor transponders within the artefact storage enclosure without using adhesive by developing a collapsible archive box in collaboration with the project partner, i.e., ZFB Germany[4].

[4] Website: https://zfb.com/

With this interdisciplinary approach, the proposed wirelessly powered museum archive box with an integrated NFC sensor transponder enables a low-cost, long term and intelligent solution for artefact storage and monitoring.

2.7 Conclusions

This chapter has presented the background of RFID and NFC transponders. In addition, this chapter also presented a comprehensive review of battery-less NFC sensor transponders that are reported in the literature. Firstly, an overview of state-of-the-art battery-less RFID and NFC transponders was been discussed. Furthermore, a detailed review of the battery-less NFC sensor transponder was conducted, and the associated challenges were outlined. In the literature, two types of RFID air interfaces, i.e., ISO/IEC 14443 and ISO/IEC 15693 standards were shown to be used for battery-less NFC sensor transponders.

A performance comparison of battery-less NFC sensor transponders reported in the literature was performed to highlight the main characteristics and limitations of this technology. In particular, gaps in the state-of-the-art relating to the limitation on DC power consumption, wireless communication range, operational life, and cost of the NFC sensor transponder for museum artefact monitoring application were identified and the need for a new NFC sensor design, in particular for museum artefact monitoring applications, was identified.

This thesis aims to develop novel wireless sensor transponder to address the above gaps identified in the state-of-the-art NFC sensor transponders.

Chapter 3: Battery-less NFC Sensor: Hardware and Software Development

3.1 Background

As discussed in the literature review in Chapter 2, the emergence of NFC enabled battery-less sensing devices with multiple sensing parameters, including temperature, humidity, pressure CO_2 and pH is part of a growing wireless sensing application [31, 77, 81, 83, 94-108]. Such battery-less devices with enhanced wireless communication range can play a significant role in wireless sensing applications, for example, museum artefact monitoring. This chapter describes the embedded hardware and software development of a battery-less NFC sensor transponder and its integration within a museum artefact storage box (also referred to as an archive box). This chapter also explains the rationale for the consideration of the embedded hardware and software design based on the literature review and user requirements defined by the stakeholders including museum conservation scientists and the artefact storage box manufacturer. It was concluded in the literature review (see Chapter 2) that commercial NFC sensors have a limited operational life of approximately 3 years [32]. In addition, only a limited number of the reported solutions support battery-less operation [33, 34] and are not optimized for low-cost applications [32-36]. Furthermore, the harvested DC power consumption of battery-less NFC sensors reported in the literature is generally greater than 1.5 mW [32-36], which is one of the factors that limits wireless communication range. In addition, to the best of this author's knowledge, a smart museum archive box that features a fully integrated wireless powered temperature and humidity sensing has *not* been reported in the literature.

As described in [1, 40], museum artefact monitoring requires low-cost NFC sensor transponder with wireless communications range of less than 4 cm and long operational life as essential parameters.

In addition, NFC sensor integration on the inner wall of an archive box *without* using adhesive is also required to avoid contamination of the atmosphere inside the box from the gluing process and materials. As discussed in Chapter 2, currently, there is no commercial solution available, which can meet all the above-mentioned requirements for monitoring the museum artefacts. Therefore, there is a need for the development of a novel solution to address the challenges outlined above and this is the focus of this research.

With the aim to increase the wireless communication range, this chapter presents the design of a battery-less NFC sensor by optimizing harvested DC power consumption and integrating a multi-modal energy harvester. In addition, this chapter also presents the integration of a custom, relative humidity, sensor with the developed NFC sensor transponder. Finally, a fully integrated artefact storage box, manufactured without the use of any adhesive and featuring wireless powered temperature and humidity sensing capabilities is presented. The NFC sensor designs presented in this chapter have been reported in [1-3].

3.2 Prototype Development of Battery-less NFC Sensor

This section summarizes the architecture of the proposed NFC sensor transponder (also referred to as NFC sensor), driven by the user requirements from several stakeholders. The system design was tailored for a low-cost implementation using commercial-off-the-shelf (COTS) components. The proposed NFC sensor hardware prototype comprises the following COTS components: An NFC radio transceiver (ST25DV16K-JFR6D3) [109], microcontroller (STM32L031K6U6) [110], voltage regulator (STLQ015M18R) [111], and temperature and humidity sensor (SHTC3) [112]. The development of the proposed battery-less NFC sensor involves the following key design steps: defining the user requirement, design of hardware prototype, development of firmware, and integration of laser-induced graphene (LIG) based humidity sensor, multi-modal energy harvester and NFC sensor within a cardboard archive box.

3.2.1 User requirements

The user requirements as defined by the museum conservators and the artefact storage box manufacturer for the proposed NFC sensor are summarized in Table 3.1. The NFC sensor is required to cost less than €5 per unit for quantities of greater than 10,000 and have an operational life of greater than 5 years. An integrated memory (EEPROM) is essential to temporarily store measured temperature, humidity and metadata (such as archive box identification ID, artefact type, and location).

Table 3.1: NFC sensor technical and user requirements (Table 1 of [1]).

Requirement	**Specification**
Power Source	Wireless power transfer
Harvested DC Power	> 1 mW
NFC sensor cost	< €5 in 10k quantities
NFC sensor operational Life	> 5 years
Wireless communication Range	< 4 cm (With NFC enabled smartphone)
User memory (EEPROM)	< 20 kbits RF and I2C dual interface access
Wireless communication data rate	25 kbps
Communication standard	ISO/IEC 15693 and NFC Type - 5
NFC sensor form factor	85.60 mm × 53.90 mm × 2 mm
NFC sensor packaging	Integration in cardboard box packaging material without adhesive
Sensed environmental parameters	Temperature and Humidity
Temperature accuracy	< ± 0.5 °C
Relative humidity accuracy	< ± 1 %
Operational temperature range	–40 to +125 °C [112]
Operational humidity range	0 to 100 % [112]
Response time at τ (63 %)	8 s for relative humidity, 5 to 30 s for temperature [112]
Sensor parameter reading	Wireless using Smartphone

The NFC sensor is required to transmit measured data at a minimum data rate of 25 kbps. The presented design does not necessitate a battery and is wirelessly powered by an NFC enabled smartphone and is required to provide a harvested DC power of greater than 1 mW [40]. This enables the smartphone to monitor the internal environment of the archive box by placing the smartphone close to the outside surface of the box. Furthermore, in most small and medium-size museum archive boxes, the available real estate is limited. Hence, a low profile 'credit-card' implementation with dimensions of 85.60 mm × 53.90 mm × 2 mm is required.

3.2.2 Block diagram of the proposed NFC sensor

Figure 3.1 shows a block diagram of the proposed NFC sensor with an NFC enabled smartphone used to wirelessly power the sensor. In operation, with NFC enabled, the smartphone provides wireless power to the NFC loop antenna via inductive coupling. The antenna then provides RF power to the NFC radio (see Chapter 2, for further details). Energy harvesting circuitry within the NFC radio provides a harvested DC output that was then regulated using a low dropout voltage regulator (LDO) and which provides a 1.8 V DC output to power the microcontroller (MCU), temperature and humidity sensor (also referred to as sensor), and all the other circuitry. Digital communication between the NFC radio transceiver, MCU and sensor were implemented using the inter-integrated circuit protocol (I2C) [109].

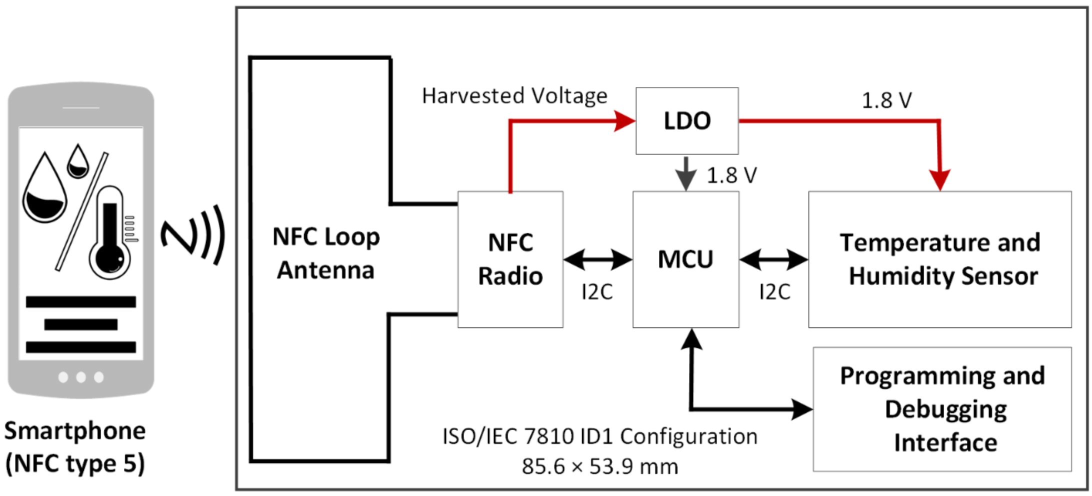

Figure 3.1: Block diagram of NFC sensor, powered using a smartphone (Fig. 2 of [1]).

In order to upload firmware for the NFC sensor transponder, a programming and debugging interface was also provided (see section 3.2.3.3 for further details). Upon power-up, temperature and humidity parameters were measured and metadata were read by the MCU and written to the NFC radio's integrated non-volatile memory (EEPROM). The measured sensor data can then be read upon command from the smartphone for later transfer, display and analysis on the smartphone.

3.2.3 Circuit design

This section describes the circuit design methodology of the proposed battery-less NFC sensor, as described in detail below.

3.2.3.1 Component selection

To meet the requirements defined in Table 3.1, the selection of appropriate COTS electronic components was critical. The key electronic components include a temperature and humidity sensor, MCU, NFC radio transceiver and LDO, whose electrical characteristics were taken from the relevant datasheet and are summarized in Table 3.2. In order to identify a suitable temperature and humidity sensor, the technical specifications of several temperature and humidity sensors were studied and matched against the user requirements.

Based on the sensors comparison, a Sensirion SHTC3 temperature and humidity sensor [112] was chosen because of its low DC supply voltage (1.8 V) requirement, low DC current consumption (270 μA) and high temperature and relative humidity accuracy of 0.2°C and 2 %, respectively. An added advantage of SHTC3 sensor is its small form factor (2 mm × 2 mm × 0.75 mm).

Similarly, a STMicroelectronics STM32L03 series MCU was chosen because of its ultra-low power consumption. The STM32L031K6U6 MCU has the capability to operate down to 49 μA/MHz using an external DC/DC converter and 76 μA/MHz using low drop voltage regulators in dynamic run mode [110]. An added benefit of the STM32L03 series MCU is that it supports dynamic supply voltage and clock frequency scaling [113], low DC supply voltage (1.8 V) requirement and is compact in size (4 mm × 4 mm × 0.55 mm).

Table 3.2: Electrical specifications of chosen components.

Component and part number	Minimum V_{DD} (V)	Maximum V_{DD} (V)	Maximum I_{SLEEP} (μA)	Maximum I_{ACTIVE} (mA)	Size (mm)	Ref
MCU (STM32L031K)	1.65	3.6	55	2.7	4 × 4 × 0.55	[110]
NFC radio (ST25DV16K)	1.8	5.5	2	0.33	2 × 3 × 0.55	[109]
Sensor (SHTC3)	1.62	3.6	0.6	0.57	2 × 2 × 0.75	[112]
LDO (STLQ015M18R)	1.5	5.5	Not Applicable	Not Applicable	1.6 × 2.9 × 0.9	[111]

Furthermore, in order to select a suitable NFC radio transceiver (also referred to as NFC radio) for the intended application, the technical specifications of various NFC radio transceivers were first evaluated against the user requirements.

In addition, wireless communication range tests were conducted with potential NFC radio transceiver's evaluation boards, including STEVAL SMARTAG1 (NFC radio: ST25DV64K) from STMicroelectronics [114], RF430FRL152HEVM (RF430FRL152H) from Texas Instruments [115] and NHS3152TEMOADK (NHS3152) from NXP [116]. This analysis showed that the STMicroelectronics’s ST25DV16K NFC radio transceiver best met the user requirements. An added benefit of ST25DV16K NFC radio transceiver is that the radio can harvest 12.59 mW of DC power at 5.5 A/m magnetic field when amplitude modulation (AM) = 10 % is considered [68, 117].

This level of wireless power transfer is sufficient to power the microcontroller as well as the temperature and humidity sensor (see user requirement Table 3.1). Similarly, this NFC radio transceiver is also compliant with NFC type 5 specifications, and ISO/IEC15693 air interface [109].

The selected NFC radio transceiver also supports low DC supply voltage of 1.8 V, consumes DC current of 330 μA and it requires a maximum size of 2 mm × 3 mm × 0.55 mm.

Finally, the linear low dropout voltage regulator (LDO) from STMicroelectronics (STLQ015M18R) was selected because this LDO was capable of providing a regulated DC output voltage of 1.8 V. In addition, this LDO has a wide input DC voltage range of 1.5 V to 5.5 V (as harvested DC voltage varies with distance), a low dropout voltage of less than 50 mV and a low quiescent current of approximately 1.2 μA at 1 mA output current.

The viability of the proposed architecture for the NFC sensor was verified by developing an evaluation kit based prototype including the X-NUCLEO-NFC04A1 (NFC radio transceiver) [118], NUCLEO-L031K6 (microcontroller) [119] and MIKROE-3331 Temp-Hum 9 click (temperature and humidity sensor) [120]. As a proof of concept, the early stage results for the proposed NFC sensor architecture is published in [40].

3.2.3.2 Wireless Power Transfer, Communication and Power Management

The schematic of the proposed NFC sensor was designed using a schematic entry tool, Mentor Graphics PADS Logic version 9.2. As discussed previously in section 3.2.3.1, the STMicroelectronics NFC radio transceiver (ST25DV16K) was chosen for wireless communication and wireless power transfer (WPT). In order to enable WPT and wireless communication between the reader (in this case, NFC enabled smartphone) and the NFC sensor, an NFC loop antenna is connected to the AC0 and AC1 pins of the NFC radio as shown in Figure 3.2 (a) and (b) on the next page. The NFC radio has an internal typical capacitance (C_{IC}) of 28.5 pF at a 13.56 MHz [109]. The integrated capacitor (C_{IC}) connects in shunt with the loop antenna, which forms a parallel LC circuit with a specified resonant frequency of 13.56 MHz.

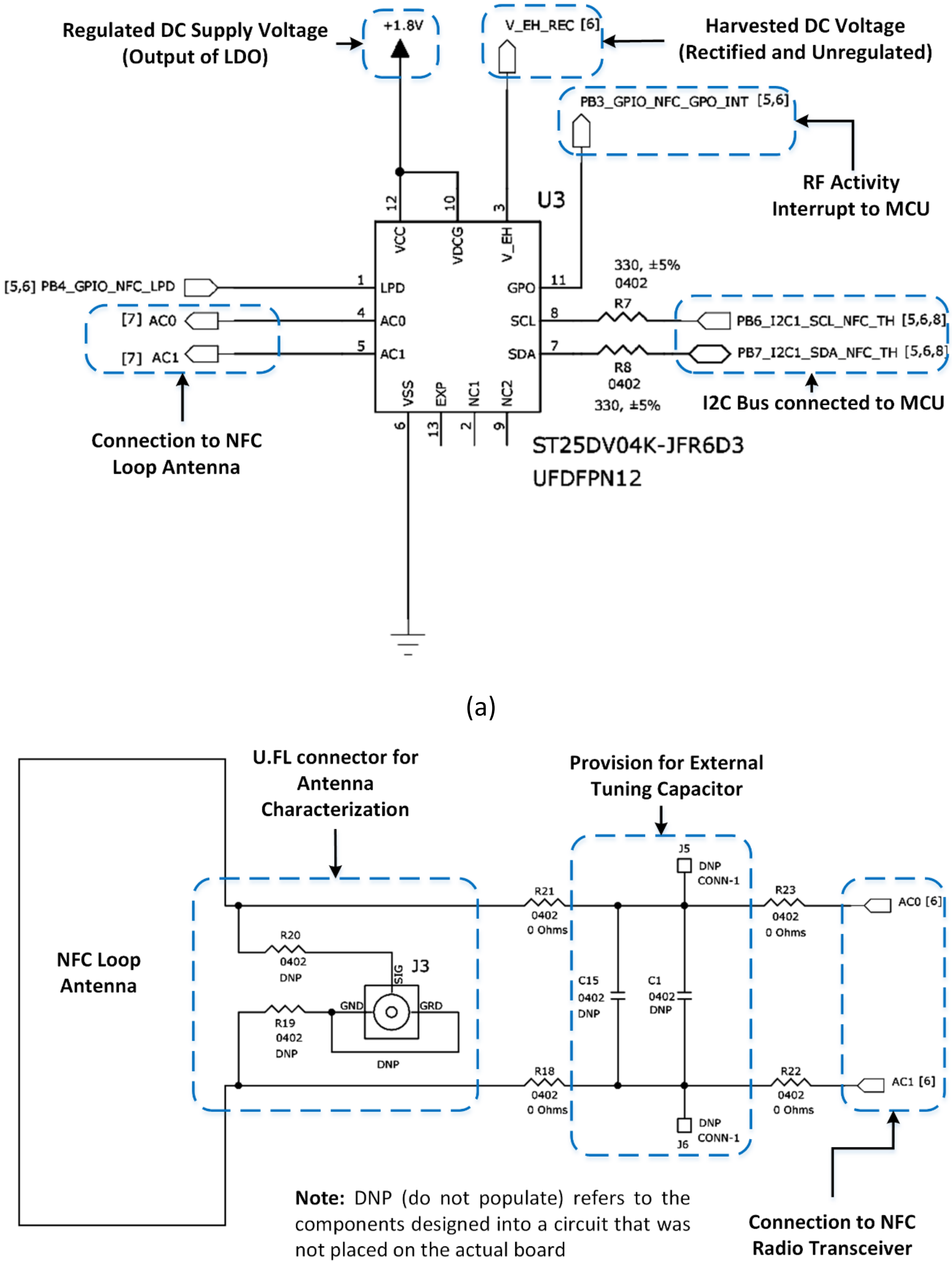

(a)

(b)[5]

Figure 3.2: Schematic of (a) NFC radio transceiver (b) NFC loop antenna.

[5] DNP (do not populate) and 0 ohm components were used to enable RF impedance characterization of the antenna.

The NFC radio incorporates a dedicated energy harvesting analogue output pin, V_EH. The internal static register (EH_CTRL_Dyn register[6]) of the NFC radio was used to define the default status of the V_EH pin after boot. The EH_EN and EH_MODE bit of the EH_CTRL_Dyn register is set to 1 to activate energy harvesting. The output voltage on the V_EH pin is generated by RF signal rectification which is limited to less than 5.5 V by the RF input clamping circuit [117]. In order to limit power supply noise (ripples), the output on V_EH pin was filtered using a capacitor C2 of 4.7 μF, 10 V, X5R as shown in Figure 3.3. The rectified and filtered DC voltage was further regulated to a constant 1.8 V DC using LDO (STLQ015M18R) as shown in Figure 3.4. Then the regulated voltage (also referred as DC supply voltage or V_{DD}) is used to power up the electronics, including MCU and sensor. The V_{DD} was also used to power some driving blocks of the NFC radio, such as the electrically erasable programmable read-only memory (EEPROM) during I2C access via the V_{CC} pin (described shortly in this section), and a general purpose output driver block driven via the "driver supply voltage (V_{DCG}) pin" (see Figure 3.2, a).

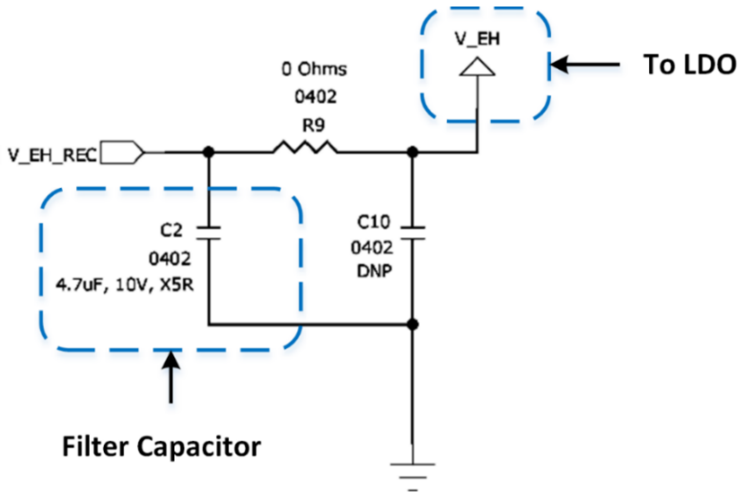

Figure 3.3: Schematic of the filter circuit to filter ripple from harvested DC voltage.

[6] EH_CTRL_Dyn is a static register but has a dynamic image with the static value of a register.

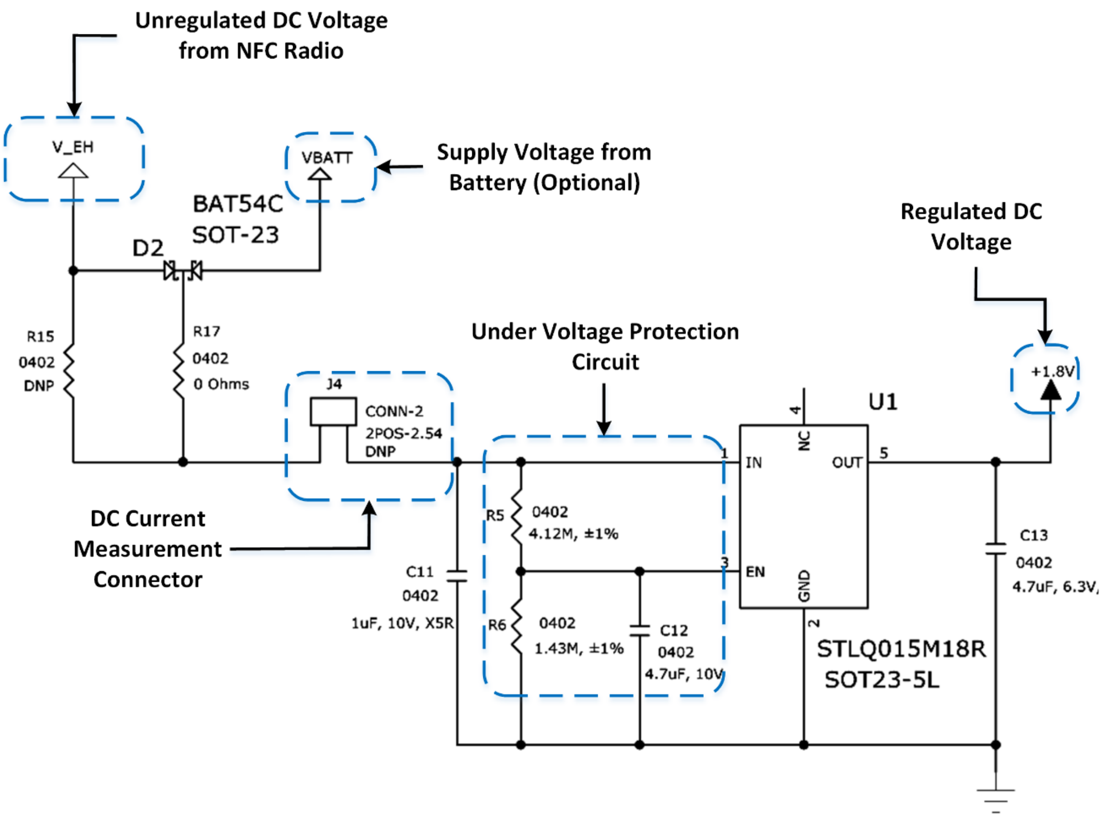

Figure 3.4: Schematic of the power supply block of NFC radio.

In addition, the EN pin of LDO was configured to turn ON the regulated DC power supply using a voltage divider network (R5 and R6) when the rectified DC voltage exceeds 2.6 V as shown in Figure 3.4. This voltage divider network on the EN pin acts as an under voltage protection circuit to prevent the NFC sensor operating from low supply voltage conditions. It has also been experimentally shown in [117] that the harvested DC voltage of greater than 2.6 V is required to operates NFC radio in energy harvesting and wireless communication domain.

The NFC radio also consists of I2C (wired) and RF (contactless) dual interface electrically erasable programmable read-only memory (EEPROM). The *I2C interface* of the EEPROM was powered from a regulated DC supply voltage (see Figure 3.2) and contains up to 16 kbit of user-accessible memory or user area memory.

In order to facilitate sensor data acquisition the serial clock and data bus (SDA and SCL) of the NFC radio are connected with the I2C port of the MCU (PB6 and PB7 pin) with the help of pull-up resistors R1 and R2 (see Figure 3.2 (a), Figure 3.5, Figure 3.7). The pull-up register is used to pull the I2C bus high when it is not driven low by the open-drain interface.

The *RF interface* of the EEPROM is powered by the received carrier signal and was activated when the NFC radio acts as a contactless memory (i.e., during wireless communication). In RF interface mode, the user memory of the NFC radio contains up to 512 blocks of 4 bytes following the ISO/IEC 15693 and NFC forum type 5 recommendations [109]. The NFC radio (ST25DV16K) also offers a fast data transfer mode between the radio and reader using a half-duplex 256 bytes volatile buffer (called Mailbox) with a data rate of 53 kbit/s. However, the mailbox functionality has not been used in the developed design.

As shown in Figure 3.2, the general-purpose output (GPO) pin of the NFC radio was used to provide RF activity information to the MCU, such as RF field detection and EEPROM write operation completion.

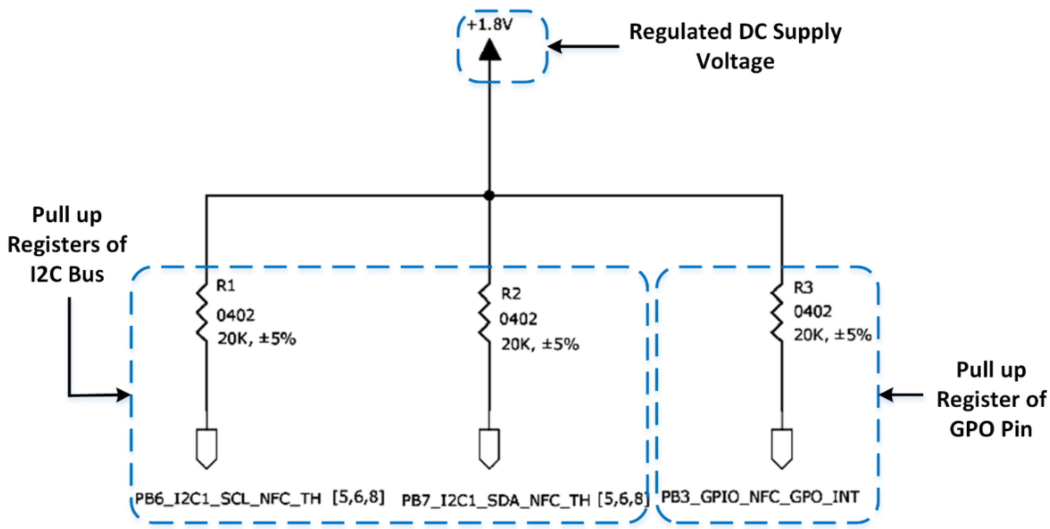

Figure 3.5: Pull up registers network.

The GPO pin was connected to the MCU (PB5 pin) as shown in Figure 3.7. The NFC radio used in this work provides GPO complementary metal-oxide-semiconductor (CMOS) output, which requires connecting the GPO pin to V_{DD} using a pull-up resistor R3 as shown Figure 3.5. As per the ST25DV design recommendation, the driver supply voltage (V_{DCG}) pin has also been connected to V_{DD} that supplies power to the GPO driver and also pulls the GPO pin logically high [109] (see Figure 3.2).

The NFC radio also supports a low power down (LPD) operation. The LPD is an input signal to the NFC radio, which was used to control the internal voltage regulator that delivers power to the internal blocks. When the LPD pin is set high, the internal regulator turns off and NFC radio goes into sleep mode. The LPD functionality has not been used in this design and the LPD pin was connected to the ground using a resistor R24 = 1 kΩ.

3.2.3.3 Temperature and humidity data acquisition

The SHTC3 used in this design is a digital temperature and humidity sensor and covers a relative humidity range from 0 to 100 % with a typical accuracy of ±2 %.

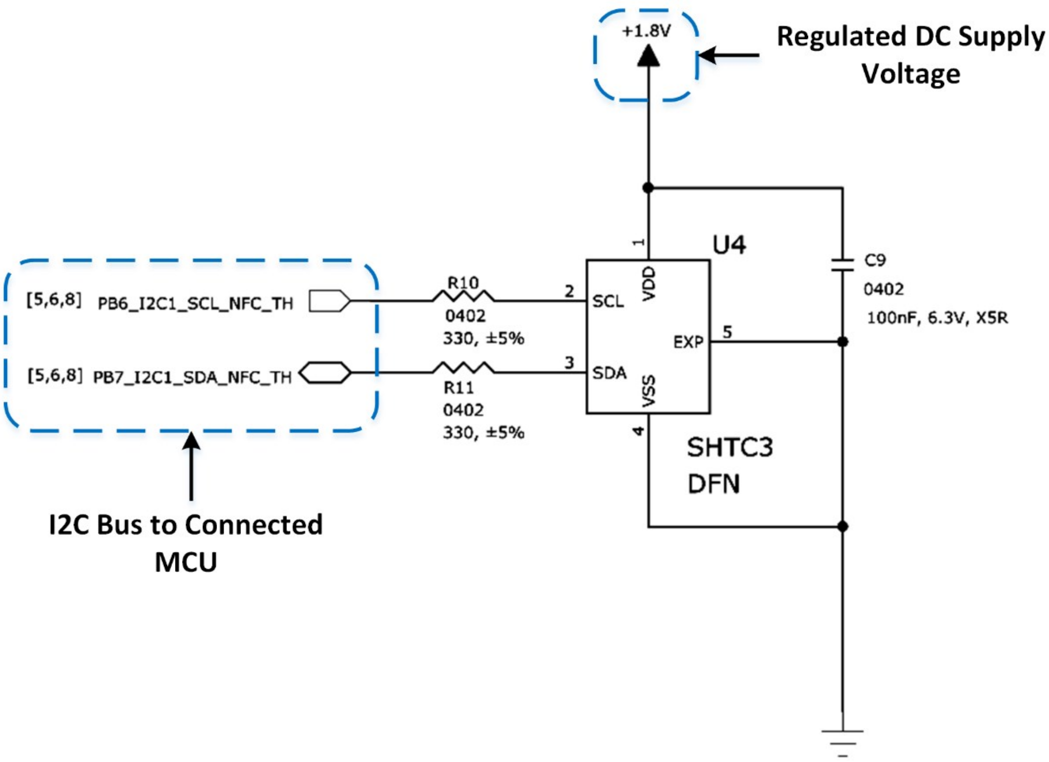

Figure 3.6: Schematic of the temperature and humidity sensor interfacing.

Similarly, with a typical accuracy of ± 0.2 °C, this sensor also covers a temperature measurement range of - 40 °C to +125 °C. The I2C bus (SCL and SDA) of SHTC3 sensor was connected to MCU I2C port PB6 and PB7 pin with the help of pull-up resistors R1 and R2 as shown in Figure 3.5 to Figure 3.7.

To reduce the power consumption during inter-circuit communication; the *standard-mode* of I2C commination was used. The standard mode operates at 100 kHz frequency and provides a data rate of 100 kbit/s that is sufficient for this application. The standard mode operation has a maximum rise time (t_R) of 1000 ns which is high in comparison to the fast mode (300 ns) and fast-mode plus (120 ns) operations [121].

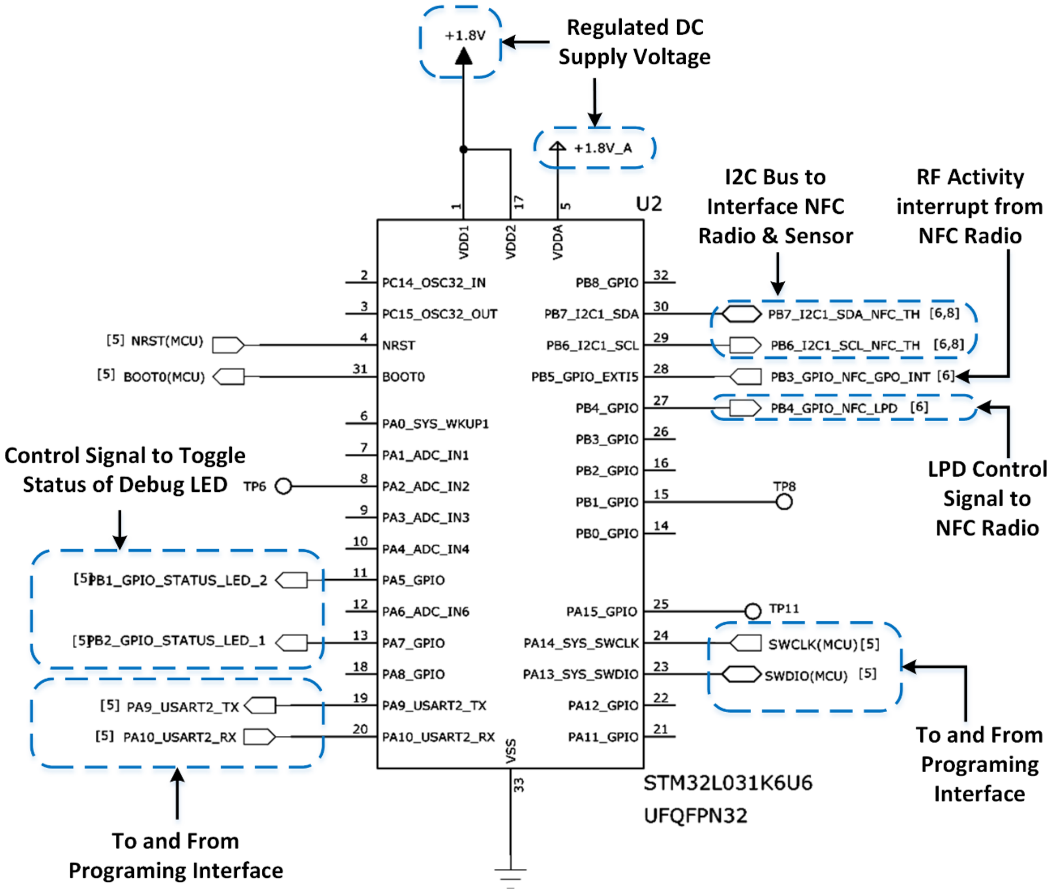

Figure 3.7: Schematic of the microcontroller unit (MCU).

This high-rise time (t_R) of 1000 ns allows the use of larger values of pull-up resistors, and the calculated value for this application is 20 kΩ. Note that, both SHTC3 and ST25DV16K were sharing the same I2C bus to connect to MCU as shown in Figure 3.7. Two series registers (R10, R11 for SHTC3 and R7, R8 for ST25DV16K) of value 300 Ω have also been used to protect the I2C port from a high voltage spike [see Figure 3.2 (a) and Figure 3.6].

In order to manage the operation of the proposed battery-less NFC sensor, an ultra-low-power MCU (STM32L031K6U6) from STMicroelectronics was chosen. The MCU performs serval tasks, such as process temperature and humidity sensor data, copying metadata from EEPROM location 0xA4 (written by smartphone using RF access) and creating NFC data exchange format (NDEF) text record (discussed in next section, section 3.2.4).

The MCU supports four different oscillator clock sources namely, a high-speed internal (HSI) clock, a high-speed external (HSE) clock, a phase locked loop (PLL) clock and a multi-speed internal (MSI) clock. In the proposed NFC sensor design, the MSI clock source was used to drive the CPU clock (HCLK and FCLK) and the peripheral clock of the MCU. An added benefit of the MSI clock is that it is low power and low-cost (no external components). The frequency range of the MSI clock was adjusted by modifying the MSIRANGE bit in the internal clock sources calibration register (RCC_ICSCR). The desired output clock frequency of the MSI clock source was ensured by factory calibration with 1 % accuracy. The MCU clock tree is discussed in section 3.2.4.1.

The MCU programming and debug interface is shown in Figure 3.8 (a) and (b) and includes a 12 position flexible flat cable (FFC) connector from Molex, USA (part number: 5034801200) that connects with an external programming board from STMicroelectronics (part number: ST-LINK/V2). In order to load firmware in the flash program memory of the MCU, the BOOT0 pin is connected to logic 0, i.e., ground, as shown in Figure 3.8 (a). After reset, the boot mode configuration is latched on the fourth rising edge of the system clock (SYSCLK). The software serial wire debug signals (SWCLK and SWDIO) were used to upload firmware and enable software debug.

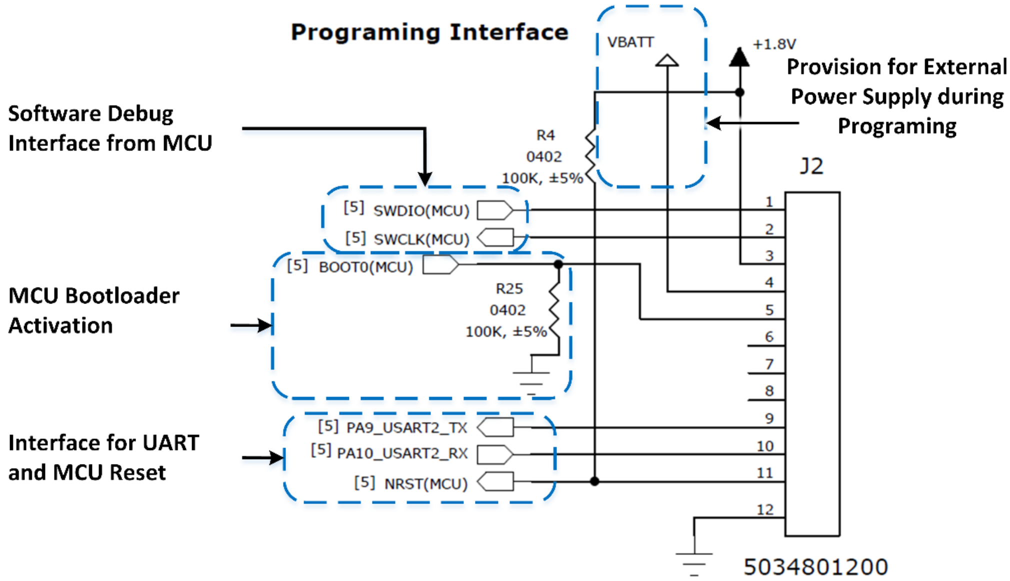

(a)

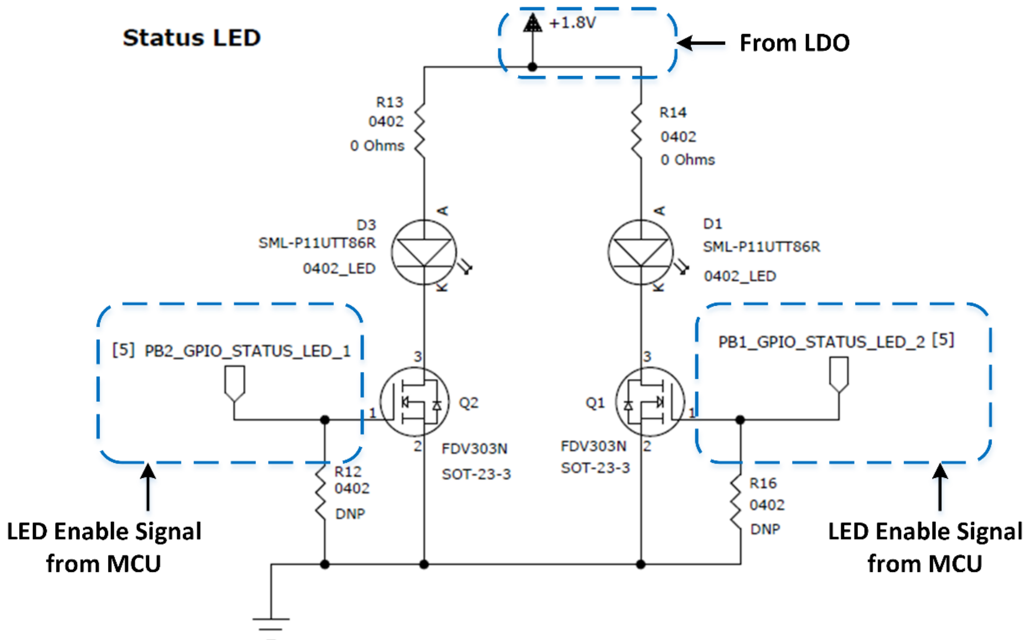

(b)

Figure 3.8: Programmer hardware configuration (a) interface (b) status indicators.

In addition, a connection for an external power source was also provided to power up the MCU during the firmware updates. Low power light emitting diodes (LEDs) were used to indicate debug status.

3.2.4 Firmware development

As discussed in section 3.2.1, continuous data logging is not required for this work. Therefore, the proposed battery-less NFC sensor has two modes of operation namely, active and shutdown mode.

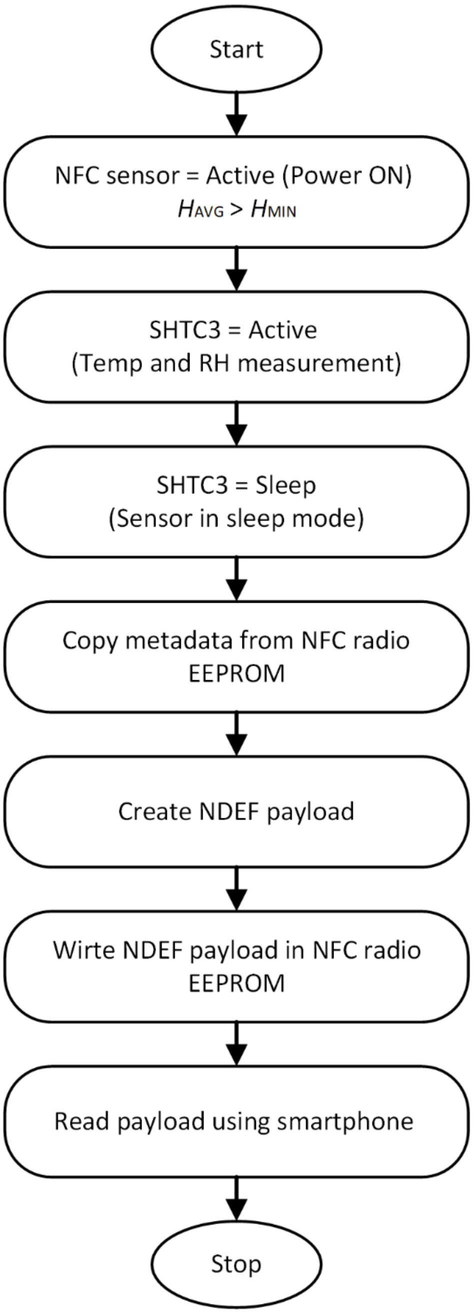

Figure 3.9: NFC sensor transponder workflow diagram.

The NFC sensor firmware was developed with the help of a workflow diagram as shown in Figure 3.9. Initially, the smartphone provides wireless power to the NFC sensor. Upon power-up, RF activity information including field detection was sent to MCU using the GPO pin of the NFC radio.

Then MCU and other electronics initiate the measurement process (active mode) when the average magnetic field strength (H_{AVG}) exceeds the threshold magnetic field (H_{TH}) of 150 mA/m [122].

Following that, the temperature (Temp) and relative humidity (RH) parameters were measured and read by the MCU. After measurement, the sleep mode of the SHTC3 sensor was activated to minimize the peak power consumption. In addition, metadata[7] was also read from EEPROM using I2C access and NDEF record was created by the MCU and written to the NFC radio's EEPROM user area 1 (see Figure 3.10 on next page). The type name format (TNF) "well-known" with text (T) record type was used to create an NDEF record (see Section 2.2.5 for further details).

The memory organization of NFC sensor is shown in Figure 3.10. A capability container (CC) file manages the information related to the NFC Type-5 specification and enables RF access of the NFC sensor to any NFC Type-5 enabled smartphone [123]. For the NFC sensor design, a 4-byte CC file is used with a 1-byte address mode (Magic number bit = E1 in the CC file), which makes the NFC sensor compatible with a smartphone running on Android version 8 or lower. The memory organization also includes static registers located in system configuration area of EEPROM. The static registers are set during device configuration including the GPO function and energy harvesting default strategy. The content of the static registers is read during boot-up. However, the dynamic registers, which used dynamic configuration of the EEPROM, are volatile and thus do not restore their content after booting. Finally, the measured sensor data and metadata were read upon receiving a command from the smartphone and data is displayed on the smartphone screen.

---

[7] Metadata of 44 bytes can be directly written in EEPROM from 0xA0 to 0xD0 location using RF (contactless) access.

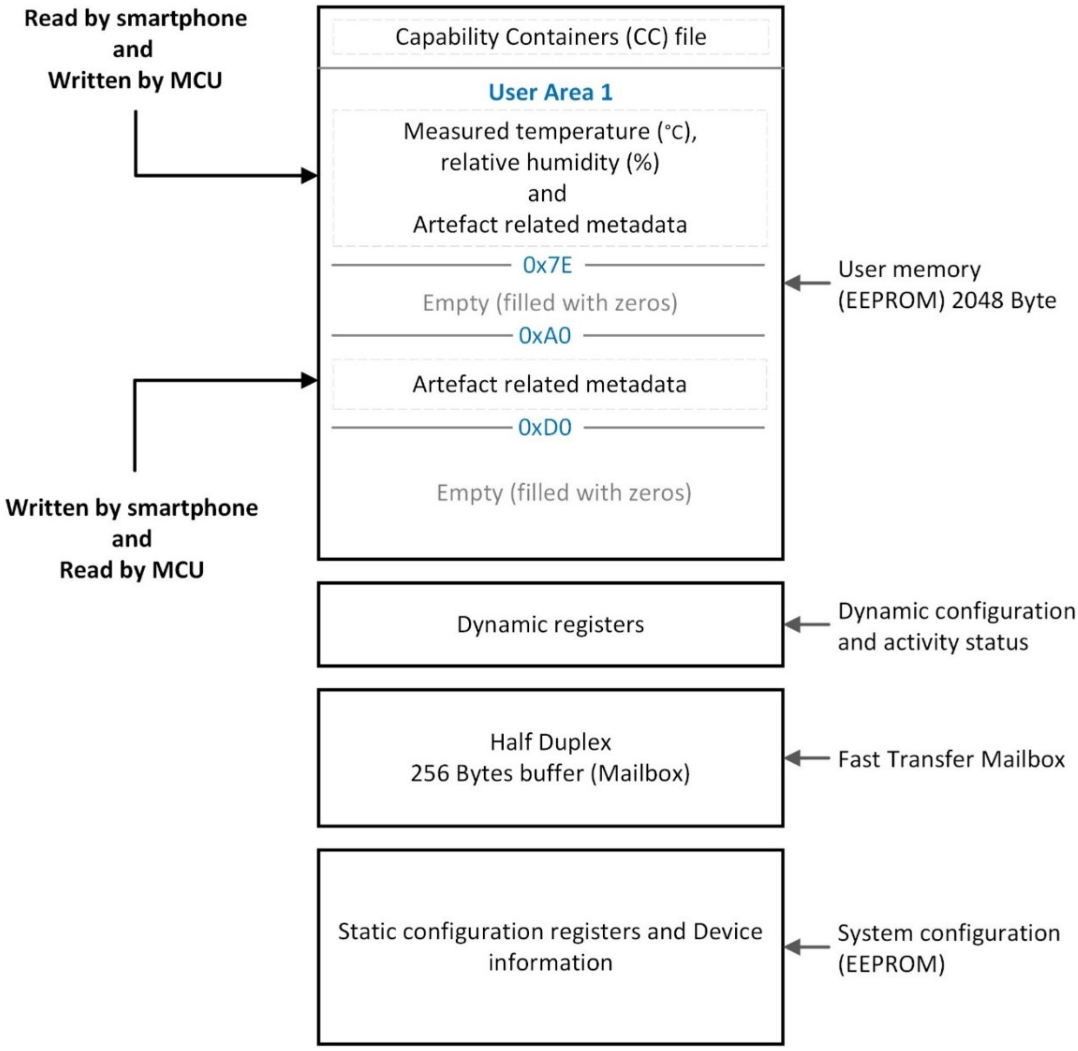

Figure 3.10: NFC sensor memory (EEPROM) organization.

3.2.4.1 Optimization of MCU power consumption

This subsection describes the methods used to minimize the harvested DC power consumption of the proposed NFC sensor. It is known [91-93, 124] that the magnetic field strength decays proportionally to the cube of the distance between two mutually coupled coils (Smartphone Coil and NFC sensor coil).

In other words, there is a limit to the available harvested RF power for the NFC sensor for a given distance from the smartphone. The harvested DC power consumption of the NFC sensor is therefore of key interest and NFC sensor was optimized for low power operation as described below. The electrical characteristics of the MCU, NFC radio transceiver, temperature, and humidity sensor reported in the datasheet are summarized in Table 3.3. From Table 3.3 it can be observed that the overall DC power consumption for the main components is 11.07 mW using datasheet specified values [109, 110, 112]. In this case, the microcontroller has an estimated DC power consumption of 8.10 mW, which is *73.17 %* of the overall DC power consumption for the NFC sensor and therefore needs to be optimized.

Table 3.3: Electrical specifications for IC components (Table 2 of [1]).

Component and part number	**Maximum Power consumption (mW)**	**Operating condition**	**Supply voltage range (V)**	**Ref**
MCU (STM32L031K6U6)	8.10	$V_{DD} = 3.0$, $V_{CORE} = 1.8$, $f_{CLK} = 16$ MHz	1.65 – 3.6	[110]
NFC radio (ST25DV16K-JFR6D3)	1.09	$V_{DD} = 3.3$, f_C (I2C) = 1 MHz (< 50 ns), Write operation	1.8 – 5.5	[109]
Sensor (SHTC3)	1.88	Low power mode, $V_{DD} = 3.3$	1.62 – 3.6	[112]
Total estimated DC power consumption = 11.07 mW				

The DC power consumption of digital CMOS integrated circuits, such as MCUs, varies with the square of the supply voltage [125, 126]. In addition, the DC power consumption varies in direct proportion with the MCU clock frequency. For this NFC sensor design, both voltage and frequency scaling techniques have been used to minimize DC power consumption with detailed measurement information described in Chapter 4.

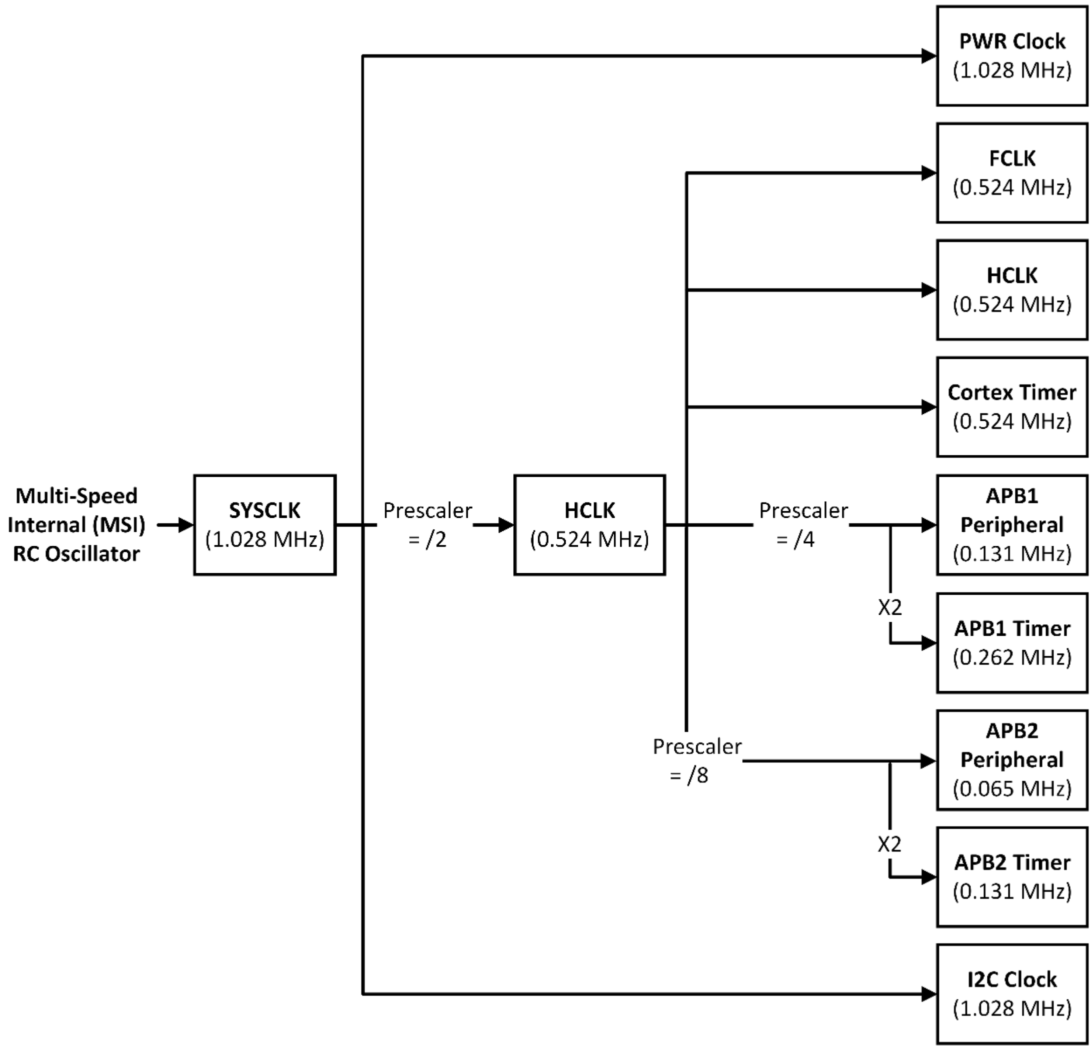

Figure 3.11: Summary of microcontroller clock tree.

In addition to a supply voltage *(V_{DD}) of 1.8 V DC*, an internal voltage regulator (V_{CORE}) was configured to provide a lowest possible supply voltage of 1.2 V DC to the MCU core (voltage scaling). As shown in Figure 3.11, a *low power* multispeed internal (MSI) RC oscillator clock with a frequency of 1.028 MHz is used as a system clock and clock source for the I2C core. Furthermore, to match trade-off between computational speed and power consumption, the clock frequency to the CPU and peripherals was adjusted using an internal prescaler, which was used to reduce the clock frequency. As a result, the MSI RC oscillator frequency of 1.028 MHz was optimized to the lowest possible value of 0.524 MHz, and used as a clock source for the CPU (HCLK and FCLK). Other peripheral clocks, such as the advanced peripheral bus (APB) clock, were also optimized to the lowest possible value of 0.131 MHz and 0.065 MHz for APB1 and APB2, respectively. The lowest harvested DC power consumption was achieved with the MCU clock scheme shown in Figure 3.11, where CPU Clock *(f_{CLK})* = 0.524 MHz, I2C core input clock *(f_{I2C_IN})* = 1.028 MHz, V_{CORE} = 1.2 V, and V_{DD} = 1.8 V.

3.2.5 Hardware prototype of NFC temperature and humidity sensor

The printed circuit board (PCB) of the proposed NFC sensor was designed using a Mentor Graphics PADS version 9.2. Figure 3.12 show the fabricated hardware prototype of the developed solution, implemented in a PCB size of 85.6 mm × 53.9 mm. The NFC loop antenna is shown on the left of Figure 3.12 (a). The inductive loop antenna was designed using an eDesignSuite tool from STMicroelectronics [127]. The designed NFC loop antenna has 7 turns, a trace width T_W = 0.6 mm, turns spacing T_S = 0.75 mm and a copper thickness of 35 μm that yields a measured inductance of 6.5 μH at 13.56 MHz. An integrated capacitance within the NFC radio transceiver connects in shunt with the loop antenna to form a parallel LC circuit with a nominal resonant frequency of 13.56 MHz. The MCU, Temperature (Temp) and relative humidity (RH) and LDO are also shown as well as the programming interface in Figure 3.12.

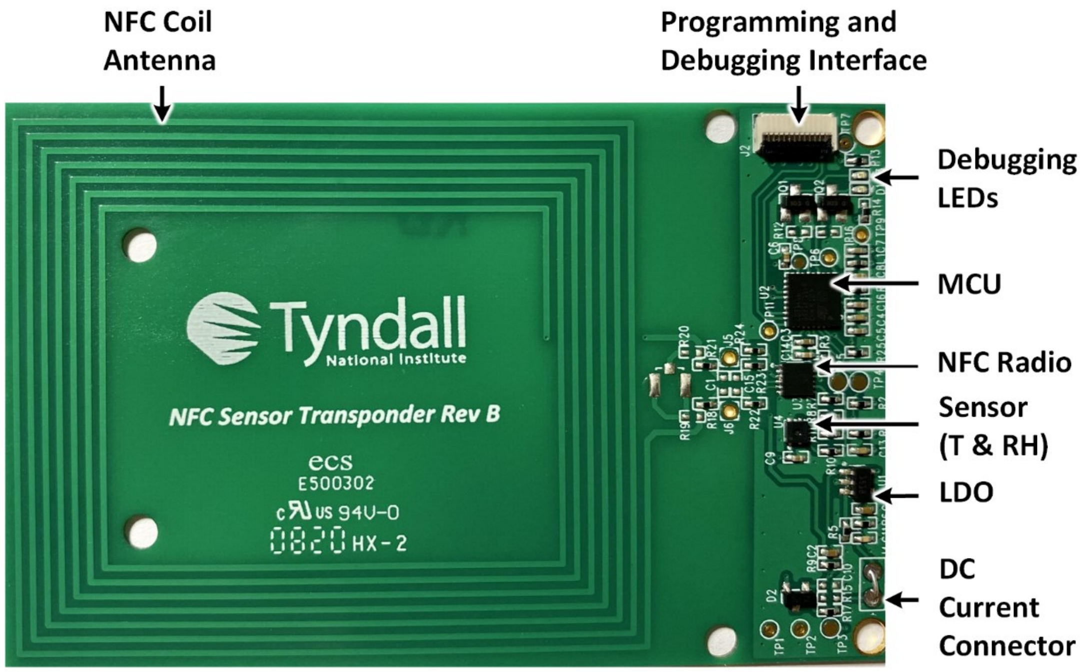

(a)

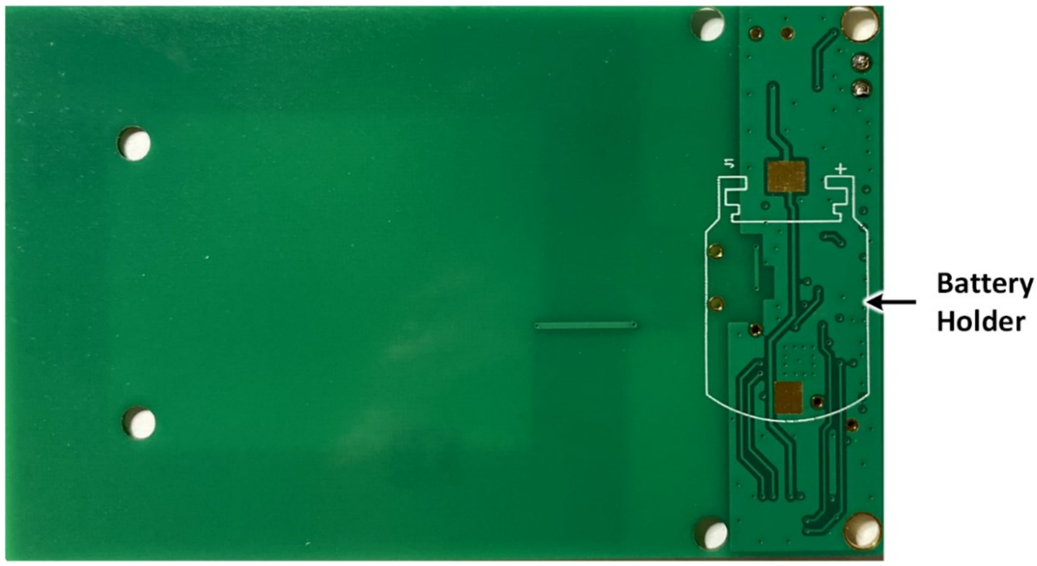

(b)

Figure 3.12: NFC sensor hardware prototype (a) top, (b) bottom side (Fig.3 of [1]).

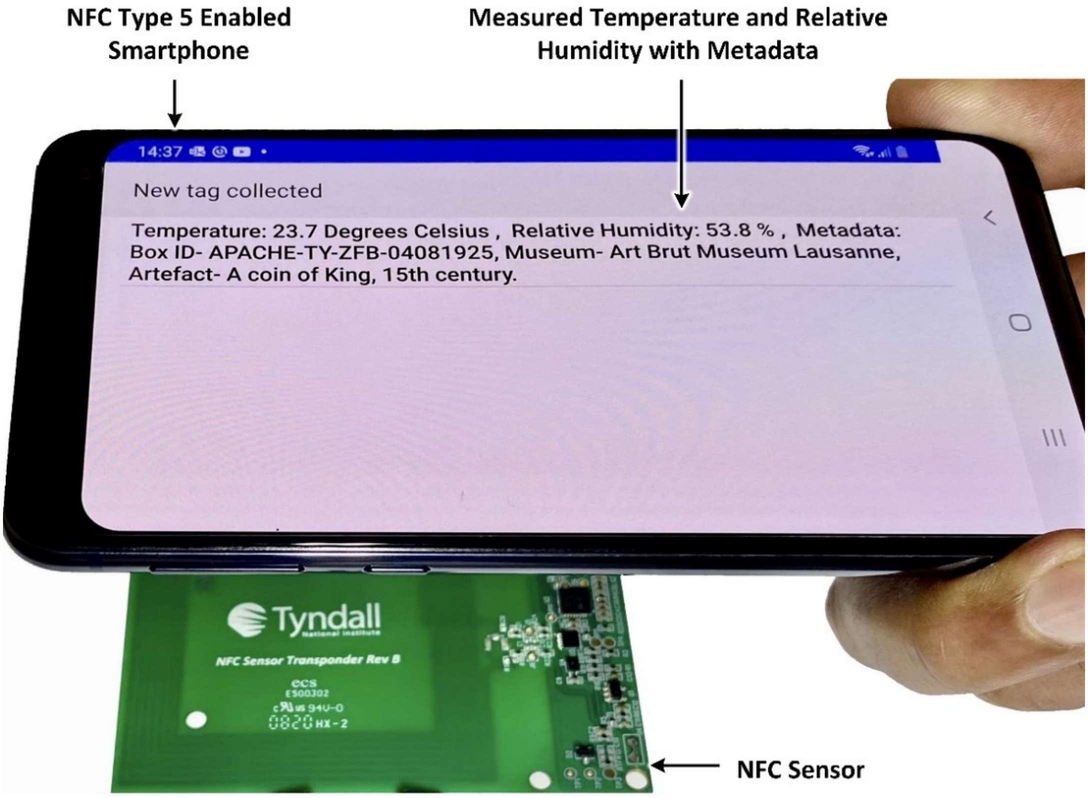

Figure 3.13*:* Demonstration of wirelessly powered NFC sensor (Fig.4 of [1]).

A 4-layer, 0.8 mm thick PCB stack-up was employed for this design with all components placed on the top layer to yield a planar structure for ease of later integration within the cardboard archive box. The developed NFC sensor also has the capability for continuous monitoring and data logging of temperature and relative humidity data when an optional coin-cell battery was included as shown in Figure 3.12 (b). However, the coin-cell battery was not inserted and the inclusion of the data-logging functionality would be a valuable addition for future work through the addition of some additional Flash memory.

Figure 3.13 demonstrates wireless power transfer and communication between the NFC sensor and smartphone. As shown in Figure 3.13, when the smartphone is placed within a distance of < 5 cm to the sensor, it enables the NFC sensor and temperature and relative humidity values with additional metadata was measured wirelessly, with no requirement for battery power on the sensor. Any smartphone with NFC type 5 capability can operate the sensor as shown. The final optimized NFC sensor has a measured harvested DC power consumption of approximately 597 μW.

In order to measure the range of the wireless communication, a Samsung Galaxy S20 smartphone was used. The maximum wireless communication range obtained for the NFC sensor was measured at approximately 5 cm in free-space (see Chapter 4 for further details).

3.2.6 NFC sensor cost estimation

The cost estimation includes all the necessary components that were used to develop the NFC sensor and summarized in Table 3.4. This cost estimate shows that the NFC sensor can be manufactured for approximately €4.91 per device in 10k quantities, as shown in Table 3.4. The cost estimate was based on quotations from an electronics components supplier, Digi-Key and a PCB manufacturer, PCBWay [128].

Table 3.4: NFC sensor cost estimation at 10k quantities (Table S1 of [1]).

Components Name	Component Description / Part Number	Cost per Sensor (€)
Microcontroller	STM32L031K6U6	1.16
PCB	PCB manufacturing and component assembly	1.03
Temperature and Humidity Sensor	SHTC3	0.99
NFC radio transceiver	ST25DV16K-JFR6D3	0.54
Programming Connector	FFC FPC 12 POS connector	0.40
Capacitors	X5R, 0402 package capacitors	0.19
Connector	Conn header 2 POS 2.54 mm	0.14
Voltage regulator	STLQ015M18R	0.13
Debug LED	Indication LED V_F = 1.8 V, I_F = 1 mA	0.13
MOSFET	N channel MOSFET 25V	0.08
Resistor	1/16W 0402, package resistor	0.06
OR’ing Diode	Schottky diode array	0.04
Ferrite bead	Ferrite bead 600 Ohm	0.02
Total per unit cost of sensor at 10 thousand quantity (€)		**4.91**

3.3 Battery-less NFC Humidity Sensor Transponder

After the development of the battery-less NFC sensor using commercial-off-the-shelf temperature and humidity sensors, the NFC sensor design was tailored to integrate a custom highly-sensitive humidity sensor. Figure 3.14 shows a block diagram of the battery-less NFC-enabled LIG/GO humidity sensor, in which the newly added or modified blocks for this design are highlighted in blue, and functionalities are described in this section.

The humidity sensor was developed using Laser induced graphene (LIG) electrodes and fabricated by direct laser writing of polyimide films as reported in [129]. Polyimide films were "written" with a KKmoon compact automatic desktop laser-engraving machine equipped with a laser with 3 W power and illumination wavelength of 450 nm. A glass slide was used as a rigid substrate to support the polyimide tape, which was irradiated at 30% laser power to obtain the designed spiral electrode structures by laser raster scanning. Obtained structures were washed with acetone, followed by isopropanol (IPA) and deionized (DIW) water to remove any residues from the laser engraving process.

Spiral-like structures were used as interdigitated electrodes as shown in Figure 3.15. The overall pattern had a dimension of 150 mm^2. Copper wires and Ag paints were used to connect the sensors to signal conditioning circuit. The humidity sensing layers were created by the drop casting of 150 μl graphene oxide (GO) on the LIG electrodes. The humidity sensor displayed a wide operating range (0 – 97% RH) and short response/recovery times. The optimized sensor consists of a 0.33 mg/mL GO drop-deposited on spiral LIG electrodes that exhibited high sensitivity up to 1800 pF/% RH at 22 $^{\circ}$C, which is higher than previously reported LIG/GO sensors [3]. This development of a battery-less NFC enabled LIG/GO humidity sensor was carried out in close collaboration with the Nanotechnology group within Tyndall National Institute, Cork, Ireland responsible for the LIG deposition activity. The Nanotechnology group carried out the LIG/GO humidity fabrication. Additional information available regarding the process steps has been reported in [3].

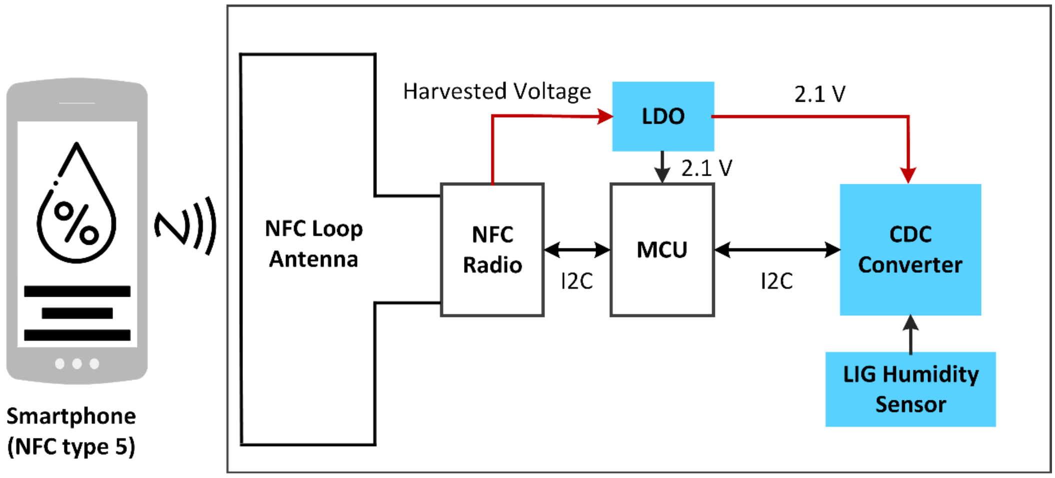

Figure 3.14: Block diagram of battery-less NFC-enabled LIG/GO humidity sensor.

Figure 3.14 shows a block diagram of the battery-less NFC-enabled LIG/GO humidity sensor with an NFC-enabled smartphone to power the relative humidity sensor wirelessly. The developed sensor was connected to a capacitance-to-digital converter (CDC) which was further interfaced with a microcontroller unit (MCU) using the inter-integrated circuit (I2C) protocol, as shown in Figure 3.14. The NFC sensor system comprised an NFC loop antenna, with the smartphone providing wireless power to the sensor via inductive coupling. The CDC requires a minimum of 2.1 V DC voltage. Therefore, in this design the low drop voltage regulator (LDO) was changed (STLQ015M21R) to obtain a regulated voltage of 2.1 V DC.

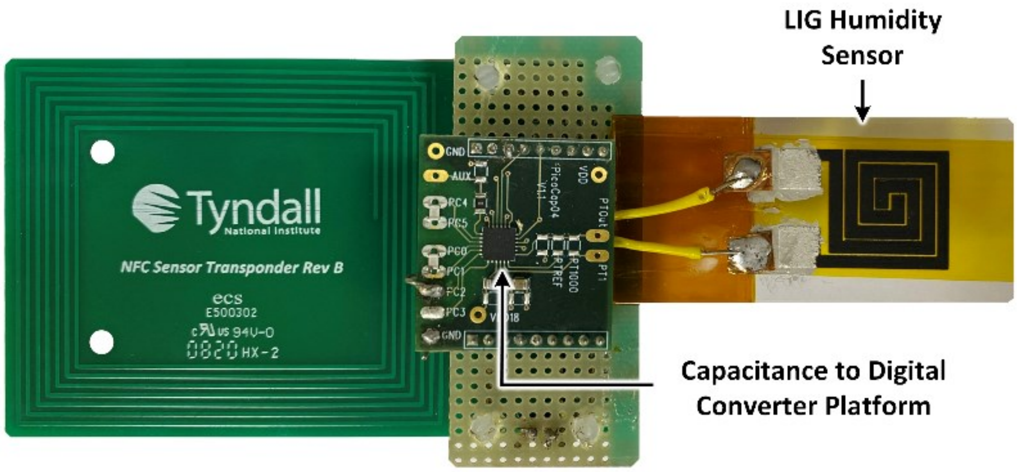

Figure 3.15: Battery-less LIG/GO humidity sensor using NFC (Fig.7 of [3]).

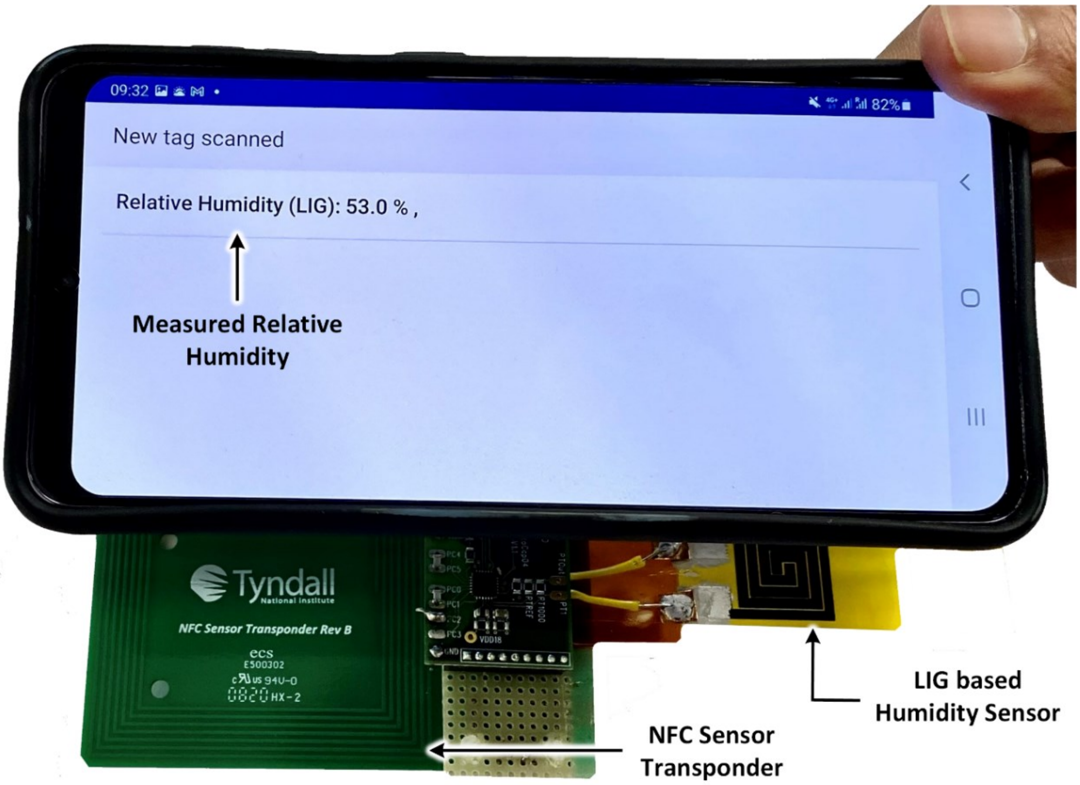

Figure 3.16: Demonstration of battery-less LIG/GO humidity sensor (Fig.7 of [3]).

The regulated voltage was used to power the CDC, MCU and NFC radio. On power-up, the ambient relative humidity was sensed using the developed LIG electrode based humidity sensor. The humidity sensor's change of capacitance was digitized using the CDC. In addition, the MCU first reads the digital values from the CDC then calculates the relative humidity. The measured relative humidity data was read using an NFC-enabled smartphone with the help of a read command, as illustrated in Figure 3.16.

In the NFC-enabled LIG/GO humidity sensor design, both voltage and frequency scaling techniques were used to minimize the harvested DC power consumption of the developed NFC sensor with the aim to maximize wireless communication range (see section 3.2.4.1). To achieve sub-mW DC power consumption, the NFC-enabled humidity sensor was designed with optimal settings, namely CPU clock (f_{CLK}) = 0.524 MHz, I2C core input clock (f_{I2C_IN}) = 1.028 MHz, MCU core voltage (V_{CORE}) = 1.2 V with a supply voltage (V_{DD}) of 2.1 V.

As a result, the NFC-enabled LIG/GO humidity sensor required a peak DC power of 900 μW. Furthermore, a Samsung Galaxy S21 smartphone was used to measure the wireless communication range, and a maximum range of 4.5 cm in free space was achieved.

3.4 NFC Sensor with Improved Wireless Communication Range

The wireless communication range of the battery-less NFC sensor depends on several factors, such as power transmitted by the reader, antenna size, coupling between the NFC reader and transponder antenna, air interface standard and power consumption of the NFC sensor. As discussed earlier in section 3.2.5, with a NFC type 5-enabled smartphone as a reader, a maximum wireless communication range of approximately 5 cm can be achieved. As the battery powers the NFC electronics associated with the NFC sensor, the power harvested through the NFC aids in communicating the data-modulated signal. However, the degradation of the battery life owing to thermal/mechanical stress as well as chemical reactions pose a great challenge in the usage of batteries for NFC sensor nodes. Hence, assisting the NFC sensor with an energy harvester to power the electronics (instead of a battery) and to enhance the range of communication appears to be a viable approach that would open wider fields of wireless sensing application. In this NFC sensor design, the mechanical energy harvesting capability of the vibration energy harvester (VEH) is used to assist in powering the NFC sensor.

The resonant FR4 based concertina shaped VEH was developed to power the NFC sensor [2]. The developed VEH comprises interleaved springs that were connected in series, building a concertina shape that exhibits a large amplitude of displacement (2.5 mm) within a small footprint of 9 cm^3 when subjected to external excitation. Owing to this enhanced out-of-plane (vertical) compliance, the VEH offers a power density of 455.6 $\mu W/cm^3 g^2$ when operating at resonance (75 Hz). This makes the concertina shape VEH a potential candidate for assisting the developed low power NFC sensor node.

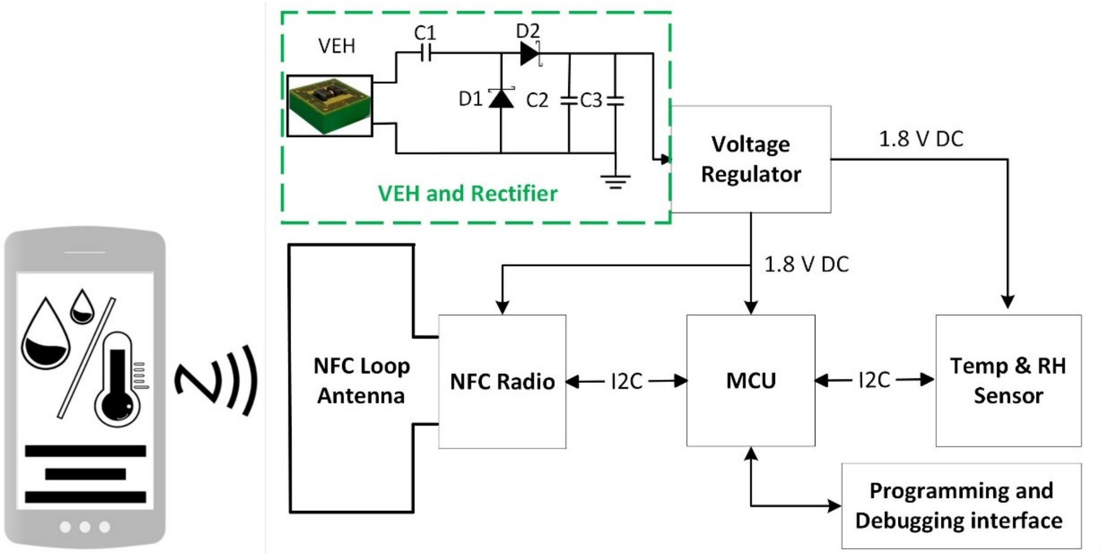

Figure 3.17: Block diagram of the NFC sensor assisted with the VEH (Fig. 8 of [2]).

The development of the VEH assisted NFC sensor was completed in close collaboration with the Micropower-Nanomagnetics group within Tyndall National Institute, Cork, Ireland and the Micropower-Nanomagnetics group carried out the development of the VEH. Additional information available regarding the VEH design and development steps has been reported in [2]. The functional block diagram of the VEH assisted NFC sensor is shown in Figure 3.17 and Figure 3.18 shows NFC sensor along with the AC-DC rectification unit.

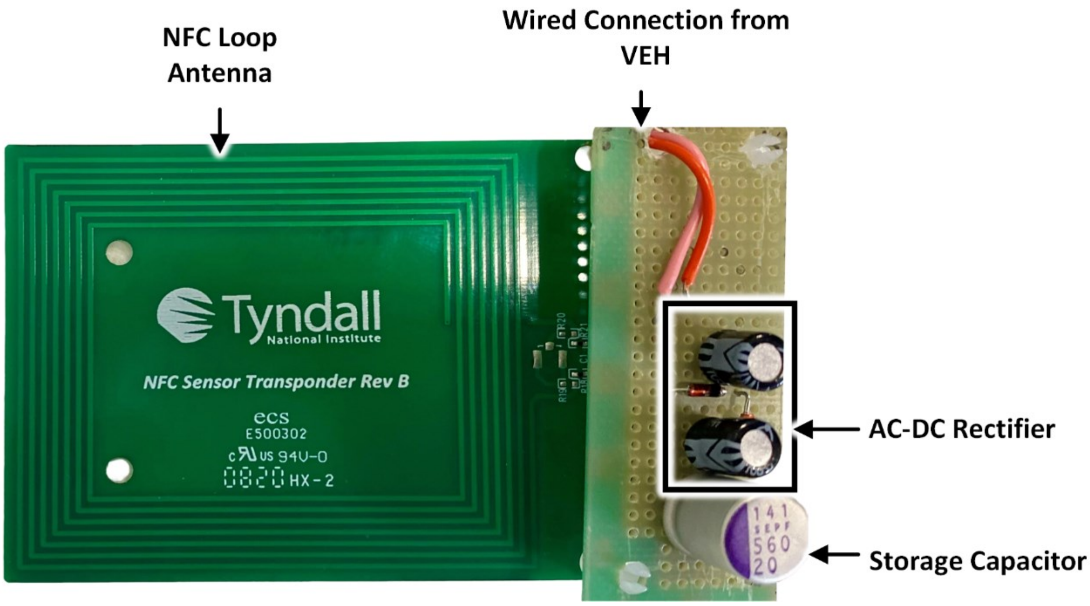

Figure 3.18: NFC sensor with the AC-DC rectification stage (Fig. 8 of [2]).

By connecting the VEH energy harvester, the RF energy harvested from the smartphone can be focused to facilitate the wireless communication of the data acquired by the NFC sensor back to the smartphone. The VEH would act as a sustainable power source that offers the capability of continuously providing power to the electronics interface to support the NFC sensor hardware, as a replacement of batteries that only offer limited lifetime. To allow for an extraction of sufficient electrical energy, even from a low amplitude vibration, a double-stage voltage multiplier circuit comprising of two capacitors (10 μF each) and two diodes (Small-signal Schottky Diode, part number BAT85-T/R) was employed for the rectification of the incoming AC signal from the VEH. Following the rectification stage, a 560 μF, 20V conductive polymer aluminium solid capacitor (SEPF series) was added to store the energy and to supply it to the NFC sensor hardware circuitry when required.

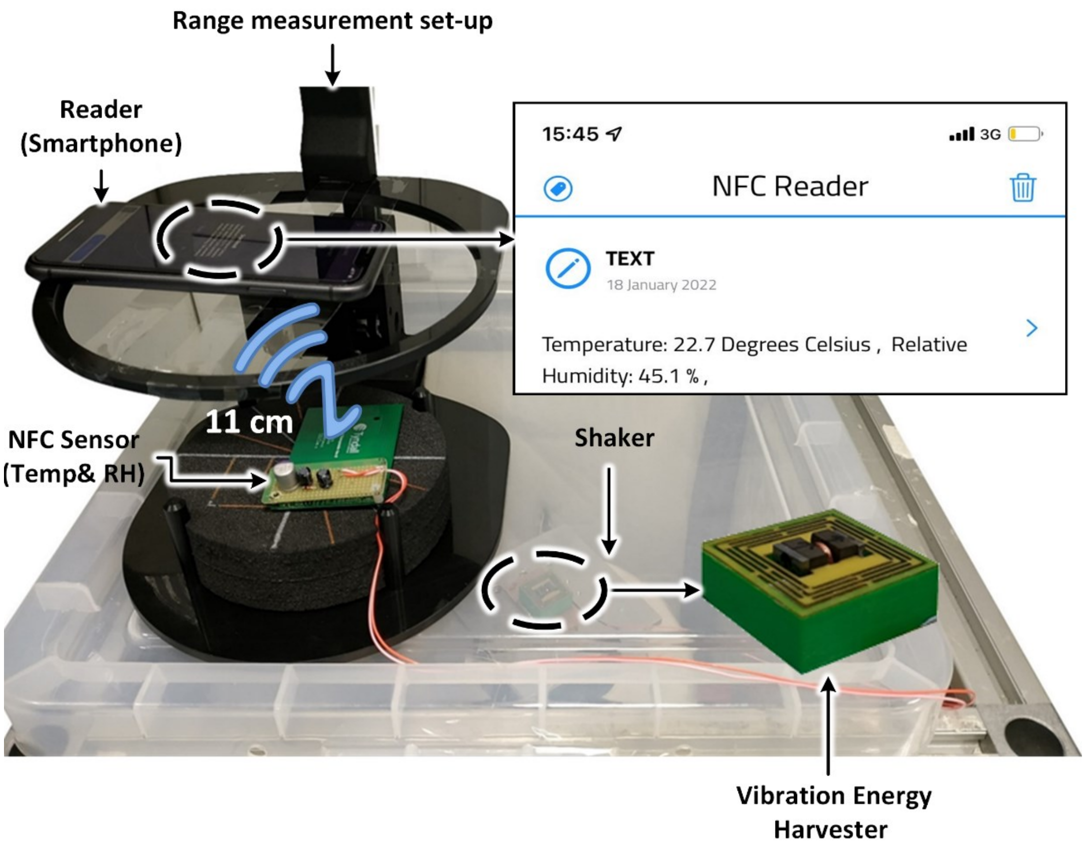

Figure 3.19: Demonstration of VEH assisted NFC sensor (Fig. 9 of [2]).

For lower (0.2 g) amplitudes of mechanical excitation, the VEH generates 164 μW of DC power and the storage capacitor provides a steady DC supply to the NFC sensor. However, for moderate acceleration levels (0.6 g), the concertina shaped VEH generates considerably large power (1.2 mW) that making the capacitor redundant for steadily powering the sensor electronics due to harvested DC power from VEH is greater than required DC power. The voltage regulator was activated upon receiving a minimum voltage of 2.6 V from the VEH. This regulator then provides a steady 1.8 V DC supply to the rest of the associated sensor electronics (see section 3.2.3.2). To maintain the overall footprint of the system small, the voltage multiplier circuit along with the storage capacitor was implemented on a PCB board mounted on top of the remaining electronics of the NFC sensor node with a vertical spacer. For the VEH assisted NFC sensor design, a voltage and frequency scaling method was used, which is discussed in 3.2.4.1. In this experimental setup, an NFC-enabled smartphone was used to measure the wireless communication range, and a maximum range of 11 cm in free space was achieved as shown in Figure 3.19 (described in Chapter 4).

3.5 Integration of the NFC Sensor within an Industry Standard Archive Box

The primary motivation for integrating the NFC sensor (discussed in section 3.2 and shown in Figure 3.12) within a museum archive enclosures is to quantify and measure the temperature and relative humidity conditions inside the archive box itself, without having to open the box and disturb the environment. For the successful integration of NFC sensors into archive boxes, the following requirements need to be fulfilled:

1. The NFC sensor needs to be directly exposed to the “packed air” in contact with the stored museum artefact within the box.
2. The measurement of temperature and relative humidity needs to take place at a position that ensures the most representative environmental data within the box.
3. The NFC sensor is required to be readily accessible for wireless reading using the smartphone, even when the boxes are stacked upon each other or lined up together.

4. The NFC sensor is required to be wirelessly connectable even through multiple layers of cardboard box material.
5. The NFC sensor needs to be protected from direct contact with the packed goods within the box to prolong its useful life.
6. The NFC sensor needs to be integrated without the use of adhesives to avoid contamination of the atmosphere inside the box.

The NFC sensor system described in this work focuses on a commonly used standard "telescope box[8]" [130] with an interior size of 10.5 x 25.4 x 33.7 cm^3 and the following descriptions illustrate the methodology to meet the NFC sensor integration requirements as is shown in Figure 3.21.

Although the storage of objects within archive boxes usually aims to maximize the utilization of the available space, this often leaves little residual volume of atmosphere around the artefact due to the use of standard sized boxes that are manufactured in large quantities. It is therefore advantageous to expose the sensor to a residual or "dead" space environment that is directly interacting with the stored artefact.

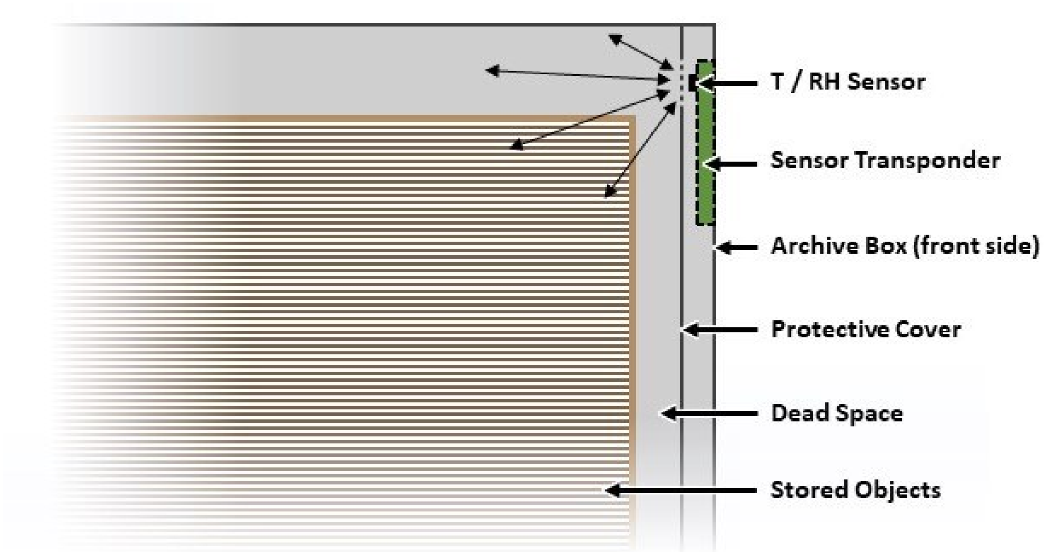

Figure 3.20: Packed archive box with integrated NFC sensor (Fig. 5 of [1]).

[8] The telescope box is the cardboard box with a two-piece box in which the sides of one part fit over those of the other.

In addition, the positioning of an NFC sensor on the interior of the box needs to provide a convenient means for an operator to read the sensor using a smartphone, without having to move the boxes when they are laid horizontally on the top of the other or stored vertically alongside each other. The boxes' front side, which directly faces the operator, was therefore chosen for the installation of the NFC sensor, since it provides a convenient means to read the NFC sensor by simply placing the smartphone close to the surface of the archive box.

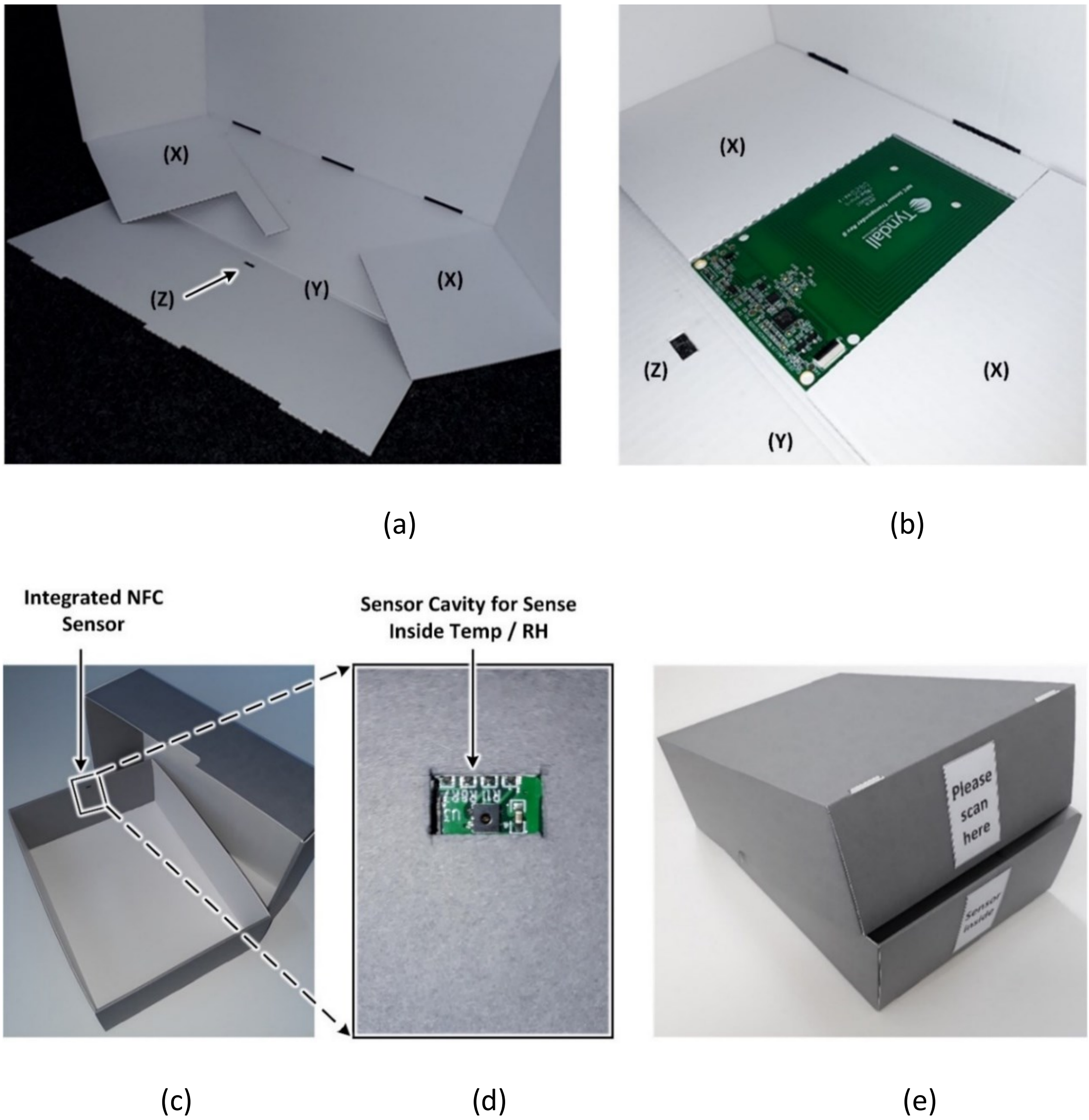

Figure 3.21: Integration (a)-(c) integrated view (d) cavity (e) label (Fig. 6 of [1]).

Protection of the sensor from direct contact with the packed object (and vice-versa) can be provided by incorporating an additional cover layer of material, as illustrated in Figure 3.20. The NFC sensor was placed in a shape-specific recess in one of the fastening flaps "(*X*)", as shown in Figure 3.21 (a) and (b), which were folded inside to be covered by the front flap "(*Y*)".

This location represents the operator-facing front side of the box and the sensor faces towards the interior space to sample the environmental conditions within the box. An aperture on flap "(*Z*)" is indicated by the arrow in Figure 3.21 (a) is used to position the temperature and humidity sensor in air contact within the box. For any particular NFC sensor size and sensor location, the recess in flap "(*X*)" and the position of cavity "(*Z*)" can be customized. The integration of the upright NFC sensor shown best fulfils the requirement number 2 but is, however, limited to telescope boxes having a height of 9 cm and flap boxes having a width of 5 cm minimum, according to the NFC sensor size. A label indicating the location of the NFC sensor is used to guide the operator to position the smartphone during a NFC sensor read operation.

The sensor integration described allows for a reliable detection of microclimates within the archive box to which the artefact is exposed. While its unhindered exposure to the enclosed atmosphere was ensured, the direct physical contact between the sensor and the stored object is avoided. This not only protects the artefact from the electronics, but also protects sensitive electronic components and circuits. A straightforward and simple construction of the collapsible enclosure is presented, comparable to conventional archive boxes, which are well known to conservators. It does not require any additional components or adhesives and can be offered as a low cost uncomplicated modular system of 'box + sensor'. With this interdisciplinary approach, the proposed battery-less archive box with integrated NFC sensor enables a low-cost, long term and intelligent solution for artefact storage and monitoring.

3.6 Conclusions

This chapter presents, for the *first time*, a novel smart archive box for microclimate monitoring in museum artefact storage applications. The developed NFC sensor does not require a battery and is wirelessly powered using a standard smartphone. A low-cost prototype of the battery-less NFC sensor was successfully developed and demonstrated. The developed NFC sensor is uniquely integrated (without using adhesive) in a low-cost cardboard archive box for real-world deployments.

The developed NFC sensor has also been optimized for low power operation using voltage and frequency-scaling techniques, leading to a peak harvested DC power consumption of 597 μW. Wireless communications performance tests on the prototype sensor show a maximum range of 5 cm, using a Samsung Galaxy S21 smartphone.

The developed battery-less sensing solutions are especially beneficial for small and middle-size museums with critical or inappropriate storage climates and budget constraints that preclude the use of expensive air conditioning systems. The developed smart archive box in this chapter, for the first time, enables accurate microclimate environmental monitoring without the need for movement or opening of the archive box with no battery replacements being required. This feature is especially advantageous for museum conservators to readily monitor and reduce the risk of degradation of valuable Cultural Heritage artefacts in storage.

In addition, highly sensitive and ultra-responsive humidity sensors based on graphene oxide (GO) active layers and LIG electrodes was integrated with an NFC sensor transponder to function as a wireless, battery-less humidity sensor platform for museum artefact monitoring. The NFC humidity sensor design has also been optimized for low power operation with a measured peak harvested DC power consumption of 900 μW while yielding a 4.5 cm wireless communication range.

Finally, a battery-less vibration energy harvester (VEH) assisted NFC sensor transponder was developed and demonstrated. A wireless communication range of the battery-less VEH assisted NFC sensor transponder was measured with NFC-enabled smartphone and maximum wireless communication range of *11 cm* in free space was achieved.

Chapter 4: Battery-less NFC Sensor Characterisation and Deployment

4.1 Background

In Chapter 3, the development of three types of battery-less NFC sensor transponder prototypes were presented:

1. NFC temperature and humidity sensor
2. NFC-enabled LIG/GO humidity sensor
3. Vibration energy harvester (VEH) assisted NFC sensor transponder

In addition, Chapter 3 also presented a fully integrated smart artefact storage box and featuring wirelessly powered temperature and humidity sensing for museum artefact monitoring.

This chapter presents the performance measurement and characterization of the three battery-less NFC sensors transponders. The key measurement parameters include RF receiver sensitivity (i.e., the RF power level required for the NFC sensor to be able to respond to the command from the reader), DC power consumption, wireless communication range, and temperature and humidity sensing accuracy.

In addition, the NFC temperature and humidity sensor was successfully demonstrated to the project stakeholders during three APACHE project public training events, which were held in Paris (France), Turin (Italy) and Budapest (Hungary). Finally, the NFC temperature and humidity sensor (also referred to as NFC sensor) is currently deployed in Cork Public Museum, Cork, Ireland, in the Guggenheim museum, Venice, Italy and Fondazione Scienza e Tecnica (FST) in Florence, Italy with museum catalogue number 1588.

The NFC sensor performance parameters presented in this chapter have been reported in [1-3].

4.2 NFC Sensor Characterization

This section presents the performance measurement of the developed NFC sensor. The accuracy of temperature and relative humidity sensor measurements is compared against a calibrated standard. In addition, the result of various characterization and performance parameters for the NFC sensor transponder including, RF receiver sensitivity, resonant frequency (also referred as center frequency), DC power consumption and wireless communication range of the NFC sensor are also presented.

4.2.1 Measurement Setup

The RF performance of the developed NFC sensor was characterized using an industry standard Tagformance Pro measurement system from Voyantic Ltd, Finland [131]. Tagformance is a radio frequency identification (RFID) and NFC measurement system developed by Voyantic for evaluating the RF performance of the transponder [131]. Figure 4.1 shows block diagram of the NFC sensor characterization setup, which includes Tagformance Pro, NFC reader Antenna (Part Number: C145), distance control kit and laptop with software interface, i.e., Tagformance HF [131].

As discussed in Chapter 2, in a typical battery-less NFC sensor system, the RF carrier signal generated by the reader is used to power the NFC sensor transponder.

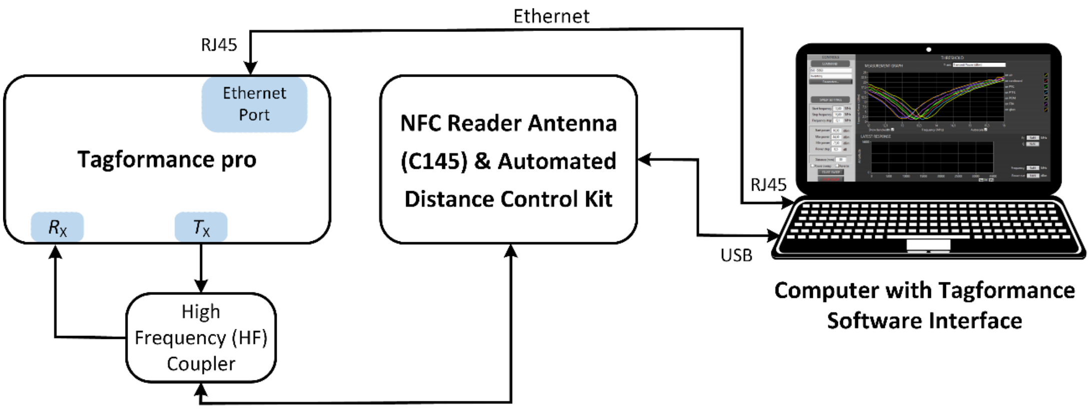

Figure 4.1: Block diagram of the NFC sensor characterization setup.

In order to send commands to the NFC sensor transponder, the reader modulates the carrier signal. Then, in turn, the NFC radio transceiver modulates the signal reflecting from it using load modulation. To evaluate the performance of the NFC sensor transponder, Tagformance uses dedicated commands that are defined by the ISO/IEC 14443 and ISO/IEC 15693 standards, i.e., *Inventory* and *Read Single Block*. After sending a command, the Tagformance acts as a time-domain network analyser that also provides a carrier signal for the transponder and records the backscattered response. To visualize the measured parameters, the measurement system uses a dedicated software interface running on a computer, as shown in Figure 4.1 [131].

Figure 4.2 shows the measurement setup for characterizing the key parameters, such as RF receiver sensitivity, load modulation and wireless communication range of the sensor in free space i.e., before integrating the sensor into an archive box.

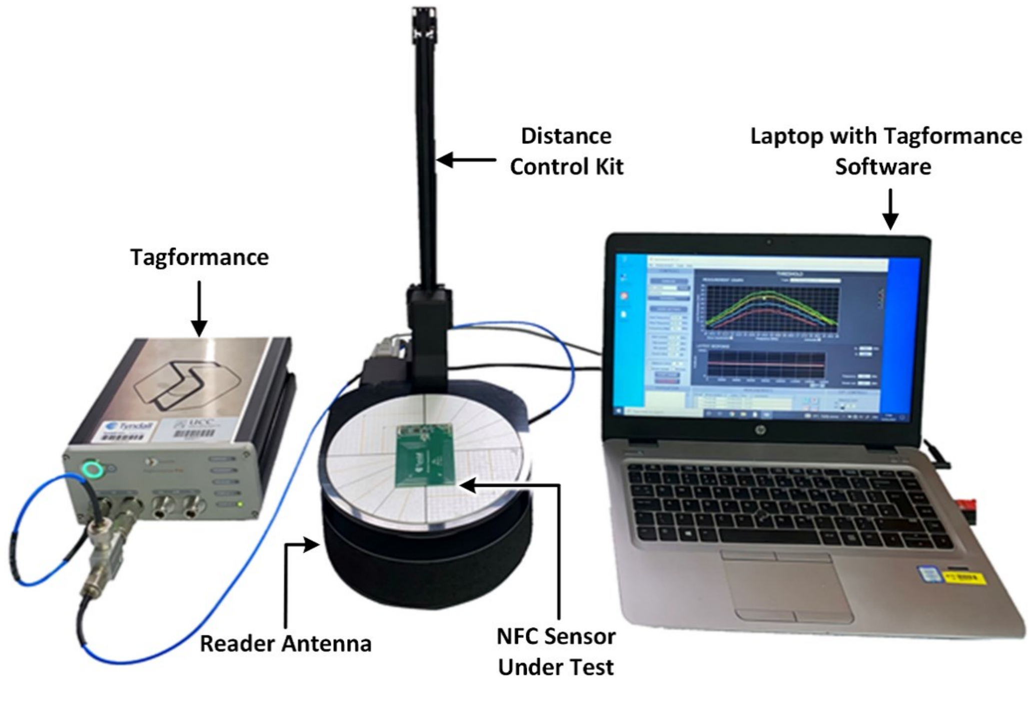

Figure 4.2: NFC sensor characterization in free space using Voyantic Tagformance.

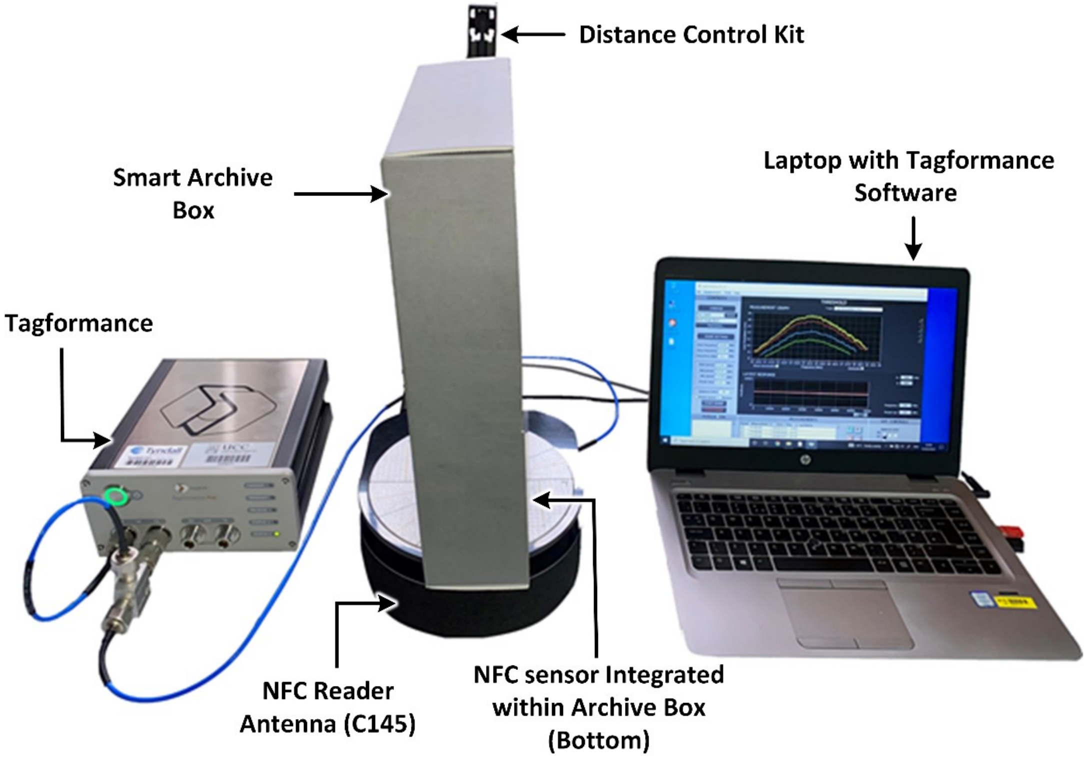

Figure 4.3: NFC sensor characterization after integration within archive box.

The measurement setup of the NFC sensor after integrating within an archive box is illustrated in Figure 4.3. For both cases, the measurement setup includes the Tagformance pro, distance control kit and laptop.

4.2.2 NFC sensor RF receiver sensitivity measurement

This sub-section describes the measured RF receiver sensitivity of developed NFC temperature and humidity sensor. The RF receiver sensitivity of NFC sensor determines the minimum RF power level that is required for the NFC sensor to respond to the command from the reader (in this case, *Read Single Block* command).

The RF receiver sensitivity of NFC sensor was measured by a performing transmit power sweep from -10 dBm to + 25 dBm in the frequency range of 10 MHz to 20 MHz. In order to measure the RF sensitivity, the wireless communication distance between the reader antenna (C145) and the NFC sensor was set to 3 cm in both cases i.e., NFC sensor in free space and after integration within the archive box.

Figure 4.4 shows the measured RF receiver sensitivity result. In free space, the NFC sensor requires a minimum magnetic field strength (H_{MIN}) of 67.8 mA/m at 13.74 MHz to be able to respond to the reader command from the reader and ensures the NFC sensor is readable by the reader. In addition, when the NFC sensor was integrated within the archive box, the NFC sensor requires a minimum magnetic field strength (H_{MIN}) of 87.6 mA/m at 13.59 MHz. The Tagformance software algorithm then calculates the centre frequency (f_C) and quality factor (Q) of the NFC sensor with the help of the measured H_{MIN}. As defined in the Tagformance technical manual [131], the threshold value of $\sqrt{2}\,H_{MIN}$ is used by the Tagformance software algorithm to calculate the minimum frequency (f_{MIN}) and maximum frequency (f_{MAX}). Then the centre frequency (f_C) is calculated for both cases using Equation 4.1.

$$f_C = \frac{f_{MIN} + f_{MAX}}{2} \tag{4.1}$$

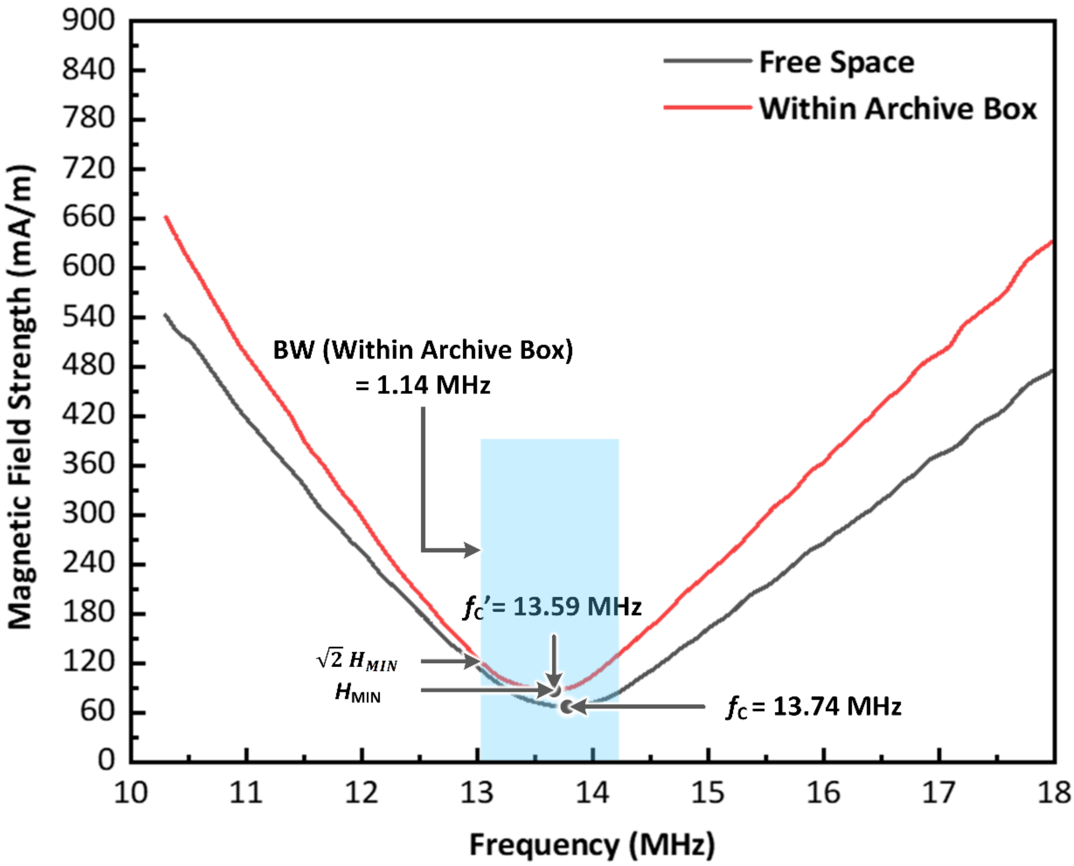

Figure 4.4: Measured RF receiver sensitivity, - 3dB bandwidth and f_C.

As evident from Figure 4.4, the calculated f_C in free space is 13.74 MHz. However, after integration within the archive box, the calculated centre frequency (f_C') is 13.59 MHz, which is close to the required centre frequency of 13.56 MHz with a difference of 30 kHz.

The centre frequency (also referred to as resonant frequency, f_R, in this case) of the NFC sensor was decreased by 0.15 MHz after integration within the archive box (f_C - f_C'). This reduction in the f_R can be described by the expression shown in Equation 4.2.

$$f_R = \frac{1}{2\pi\sqrt{L\,(C_{IC} + C_P + C_T)}} \tag{4.2}$$

Where L is the inductance of NFC loop antenna in Henrys and C_{IC} is the internal capacitance of NFC radio in Farads. Parameter C_P is the parasitic capacitance, which includes the parasitic capacitance of the loop, and C_T is the external capacitor that may required to adjust the f_R to the operation frequency. However, as shown in Figure 3.2(b) in Chapter 3, the external tuning capacitor C_T was not used in the NFC sensor design presented in this thesis.

The placement of the archive box close to the NFC sensor increases the inter-turn capacitance (C_P) of the NFC loop antenna [132]. This leads to reduction in the resonant frequency as given by equation 4.2.

The tagformance software algorithm uses the expression shown in Equation 4.3 to calculate the quality factor (Q) and -3 dB bandwidth (BW) of the NFC sensor [131, 133].

$$Q = \frac{f_C}{BW} = \frac{f_C}{f_{MAX} - f_{MIN}} \tag{4.3}$$

The measured and calculated performance parameters of the NFC sensor are summarized in Table 4.1.

Table 4.1: Comparison of the NFC sensor performance parameter with ISO15693.

Parameter	Free space	Integrated within Archive box	Required value as per ISO/IEC 15693 air interface & initialization
Minimum magnetic field strength (mA/m)	67.8	87.6	150 [122]
Centre frequency, f_C (MHz)	13.74	13.59	13.56 [122]
Quality Factor at f_C	11.80	11.91	Not Specified
-3 dB bandwidth (MHz)	1.16	1.14	0.908[9] [122]

This comparison table shows that the performance of the developed NFC sensor is in agreement with the ISO/IEC 15693 air interface and initialization specification [122].

4.2.3 DC power consumption

In order to decrease the harvested DC power consumption of the developed NFC sensor, voltage and frequency scaling techniques have been employed as discussed in Chapter 3. Table 4.2 and Figure 4.5 summarize the measured DC power consumption as a function of microcontroller (MCU) voltage and clock frequency. As summarized in Table 4.2 and depicted in Figure 4.5, a measured DC power consumption of 12.01 mW was observed at the first design iteration with the following clock and voltage settings: Supply voltage (V_{DD}) = 3.3 V, MCU core voltage (V_{CORE}) = 1.8 V, MCU clock source = high speed internal (HSI) RC oscillator, CPU clock (f_{CLK}) = 16 MHz and I2C core input clock (f_{I2C_IN}) = 16 MHz. In the second iteration, V_{DD} was reduced to 1.8 V (with V_{CORE} = 1.8 V, MCU clock source = HSI, f_{CLK} = 16 MHz and f_{I2C_IN} = 16 MHz) reducing the DC power consumption to 6.18 mW.

[9] When two subcarriers are used where the first subcarrier frequency (f_{S1}) = f_C/32 = 423.75 kHz, and the second subcarrier frequency (f_{S2}) = f_C/28 = 484.28 kHz, this gives a resultant bandwidth of 0.908 MHz.

Table 4.2: DC power consumption with MCU voltage and frequency scaling.

Design Iteration	MCU Clock Source	f_{CLK} (MHz)	f_{I2C_IN} (MHz)	V_{DD} (V)	V_{CORE} (V)	Measured DC Power Consumption (mW)
1	HSI	16	16	3.3	1.8	12.01
2	HSI	16	16	1.8	1.8	6.18
3	HSI	8	8	1.8	1.5	3.47
4	MSI	4.192	4.192	1.8	1.5	1.79
5	MSI	2.096	2.096	1.8	1.2	1.03
6	**MSI**	**0.524**	**0.524**	**1.8**	**1.2**	**0.597**

Further, design iterations changed the clock source to use a low power multi-speed internal (MSI) RC oscillator, reducing the clock frequency and core voltage as shown in Figure 4.5. The lowest DC power consumption was achieved at f_{CLK} = 0.524 MHz, f_{I2C_IN} = 1.024 MHz, MCU clock source = MSI, V_{CORE} = 1.2 V, and V_{DD} = 1.8 V.

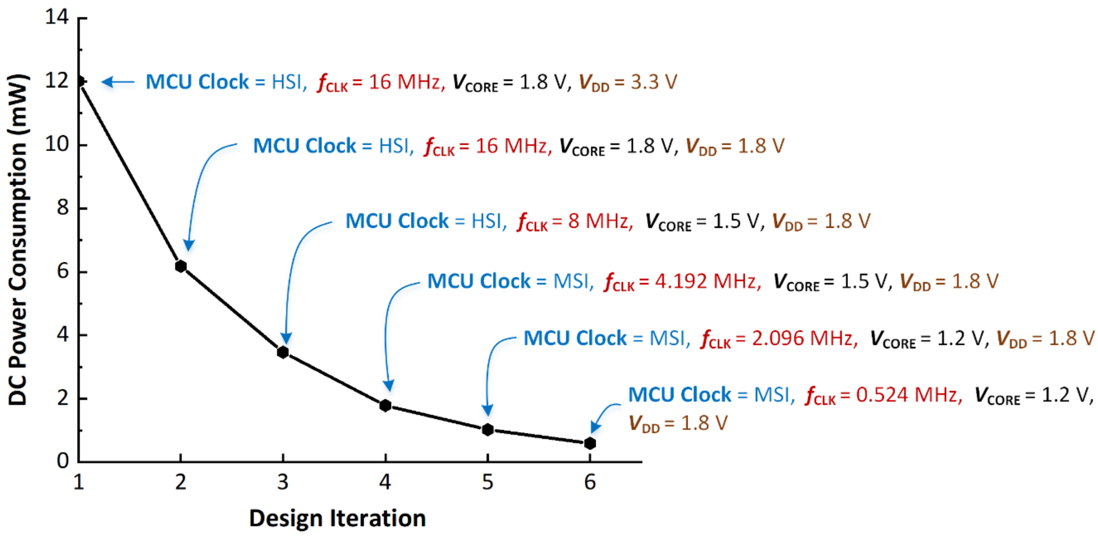

Figure 4.5: Measured DC power consumption with voltage and frequency scaling.

The final optimized NFC sensor has a measured DC power consumption of approximately 597 μW when the smartphone was placed at a distance of approximately 2 cm from the NFC sensor. As shown in Figure 4.5, the use of the described frequency and voltage scaling techniques enable a factor of greater than 20 reduction in DC power consumption for the NFC temperature and humidity sensor.

As discussed in Chapter 3, the vibration energy harvester (VEH) assisted NFC sensor also operates at optimal settings for low power, namely f_{CLK} = 0.524 MHz, f_{I2C_IN} = 1.024 MHz, V_{CORE} = 1.2 V, and V_{DD} of 1.8 V and consume DC power consumption of 597 μW.

Similarly, The NFC-enabled LIG/GO humidity sensor was also designed with optimal settings, namely f_{CLK} = 0.524 MHz, f_{I2C_IN} = 1.024 MHz, V_{CORE} = 1.2 V, and V_{DD} of 2.1 V. As a result, the NFC-enabled LIG/GO humidity sensor required a peak DC power of 900 μW.

4.2.4 Wireless communication range measurements

This section describes the wireless communication range of the developed battery-less NFC sensor, as described below.

4.2.4.1 Wireless communication range measurement using Tagformance

The wireless communication range of the NFC sensor in free space and after integration within the archive box was also measured using the measurement setup discussed in section 4.2.1. In order to automatically adjust the wireless communication range, a distance control kit within the Tagformance pro was used, as shown in Figure 4.2 and Figure 4.3. To measure the wireless communication range of the NFC sensor, the Tagformance was configured with the following parameters: (a) Wireless communication range sweep = 1 cm to 18 cm with a resolution of 0.1 cm, (b) Transmit power level = + 25 dBm, (c) Modulation Index = 100 %, (d) Command = Read single block, and (e) centre frequency (f_C) = 13.74 MHz for free space and 13.59 MHz for within archive box case.

For each wireless communication range distance settings i.e., 0.1 cm from 1 cm to 18 cm received signal strength (also referred to as load modulation or load modulated signal) of the NFC sensor was recorded. In this case, the load modulation is a modulated carrier signal that is reflected or returned from the NFC sensor in response to the “read single block” command. The measured wireless communication range of the NFC sensor as a function of received signal strength is shown in Figure 4.6. It is evident from Figure 4.6 that a wireless communication range of approximately 16.4 cm for the free space case and 14.9 cm for the archive box integration case was achieved. Note that the NFC sensor was integrated on the inner wall of the archive box which has a thickness of approximately 1.5 cm, as illustrated in Figure 3.21, in Chapter 3.

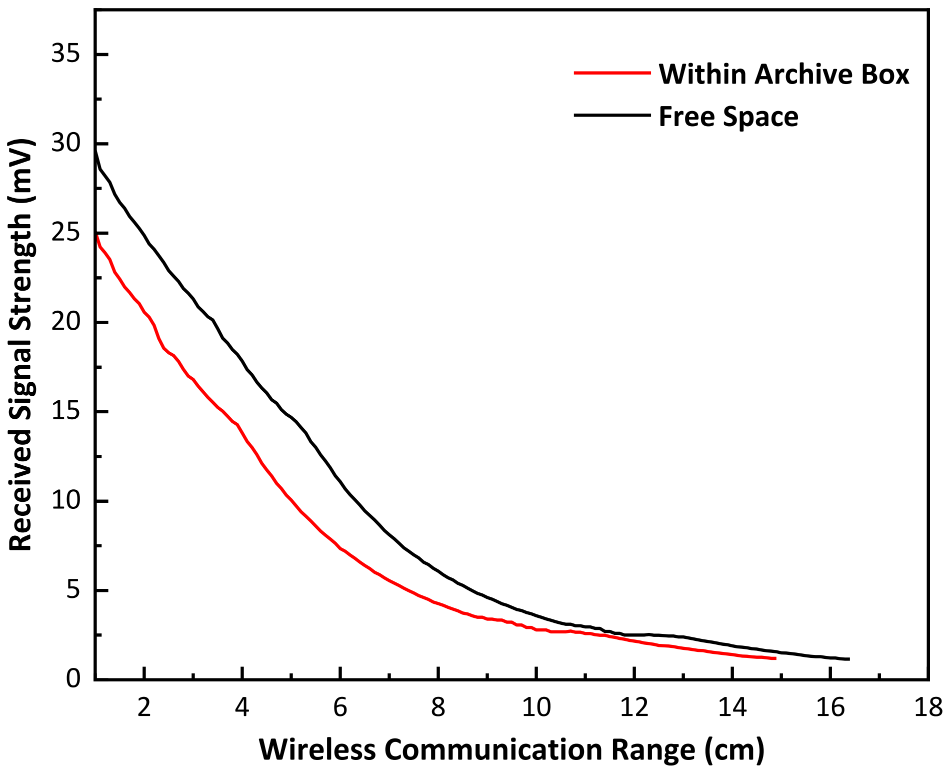

Figure 4.6: Wireless communication range measurement.

4.2.4.2 Wireless Communication Range Measurement using a smartphone

The wireless communication range of the NFC sensor was also measured using a Samsung Galaxy S20 smartphone. The low power consumption of the NFC sensor i.e., 597 μW yields a wireless communication range of approximately 5 cm in free space. Using the same smartphone, a wireless communication range of 3.5 cm was achieved when the NFC sensor was integrated within the archive box and the range was measured from the outside, as shown in Figure 4.7.

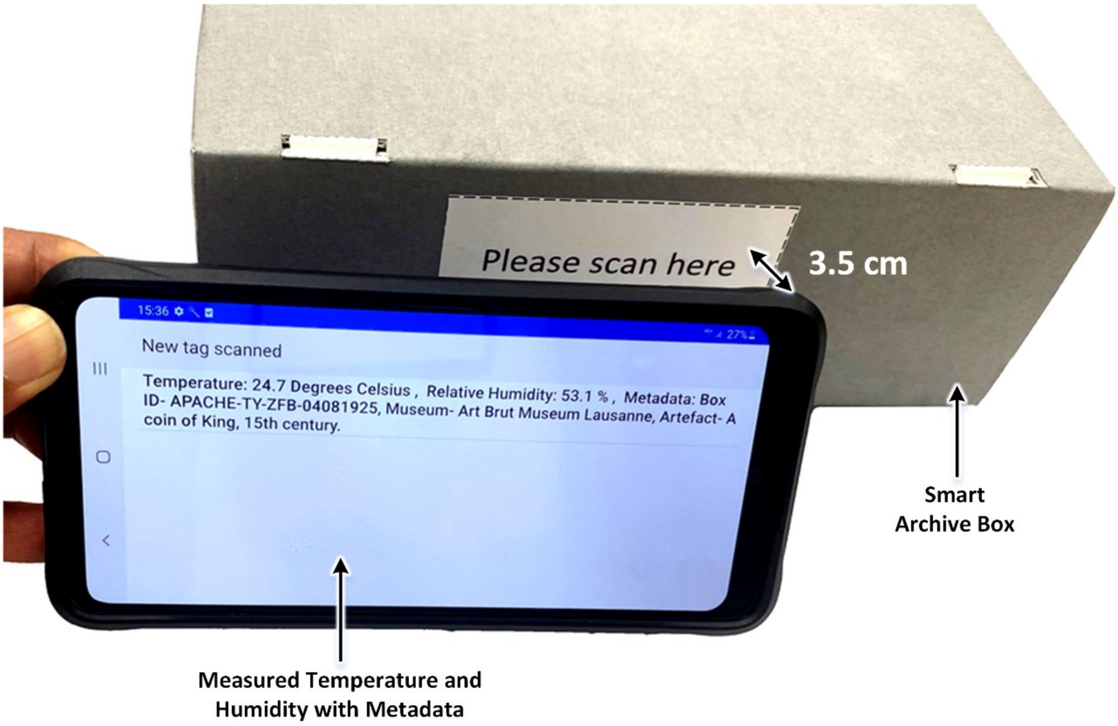

Figure 4.7: Measured wireless communication range using smartphone.

4.2.4.3 Wireless communication range of VEH assisted NFC sensor

As described in Chapter 3, in this work an NFC-enabled smartphone was mainly used to provide wireless power to the battery-less NFC temperature and humidity sensor. The power received from the smartphone is partly used to power the electronics in the NFC sensor. The RF signal strength left for the latter then determines the strength of the load modulated signal or equivalently, the communication range of the NFC sensor.

The battery-less NFC temperature and humidity sensor discussed in Chapter 3, Section 3.2 provides a wireless communication range of 5 cm using the smartphone as a reader when not connected to any additional energy source such as battery. In addition, as discussed in Chapter 3, Section 3.4, a vibration energy harvester (VEH) was used to power the NFC sensor and also to enhance the wireless communication range. Figure 4.8 shows the variation of the deliverable power of the VEH as a function of the amplitude of excitation. The DC power (P_{LOAD}) required by the NFC sensor hardware to be fully functional is measured to be 597 μW. It is noted that with a 0.2 g drive amplitude, DC power (P_{HAR}) of 164 μW was harvested. Such a low amplitude of excitation is investigated to be sufficient to power up the NFC sensor leading to an increased wireless communication range, though with a storage capacitor ($C_{STORAGE}$) of 560 μF [2]. It is interesting to note that by further increasing the amplitude of excitation to 0.6 g, the VEH provides substantial energy, which drives the NFC sensor autonomously. In this case, the storage capacitor at this stage would no longer be required to store and supply energy to the circuitry associated with the NFC sensor.

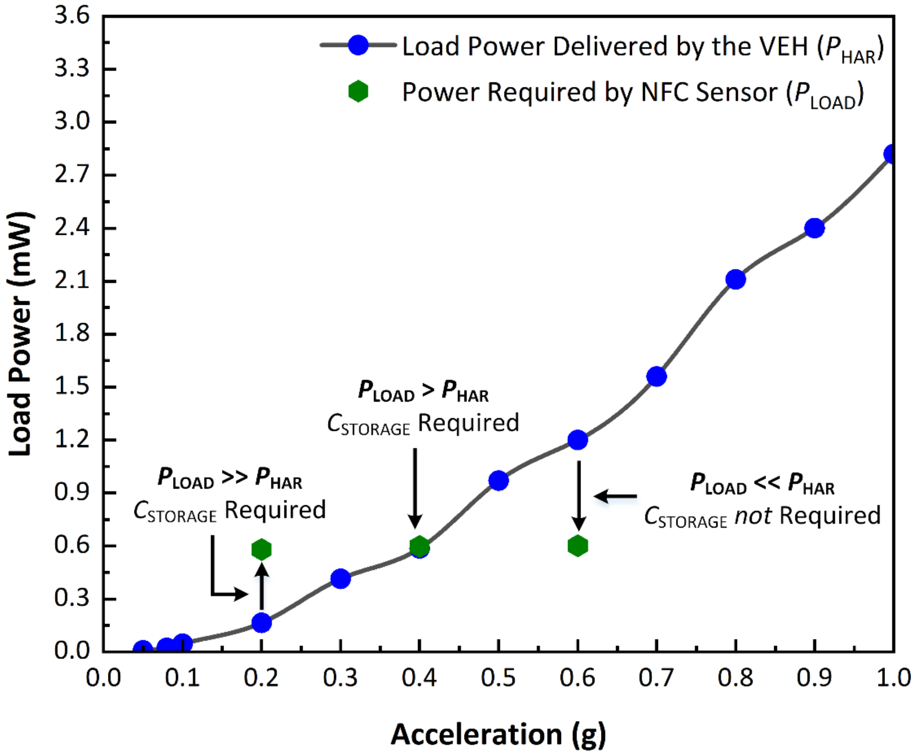

Figure 4.8: Measured DC power consumption when excitation varied (Fig. 8 of [2]).

Additional measurement-based information regarding the NFC sensor operation with various vibration levels, from 0.2 *g* to 0.6 *g*, has been reported in [2]. From Figure 4.8 it is evident that, the VEH is capable to provide required power to NFC sensor. Therefore, the NFC sensor can retain the RF signal strength from NFC reader only for wireless communication. As a result, the NFC sensor provides an improved wireless communication range, i.e., 11 cm, as shown in Figure 4.9.

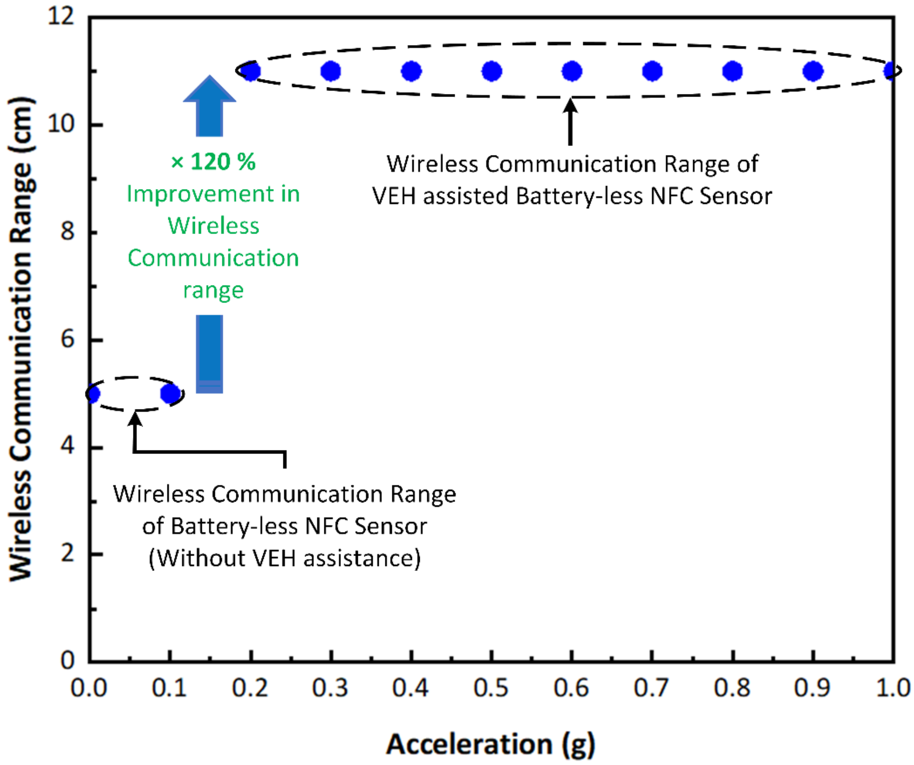

Figure 4.9: Measured wireless communication range (Fig. 10 of [2]).

4.2.5 Accuracy of temperature and relative humidity measurement

In order to determine the accuracy of the developed prototype sensor, the measured temperature and relative humidity values have been compared with a calibrated Fluke 971 temperature and humidity meter [134]. The testing was performed in the test setup shown in Figure 4.10 using an insulated pinewood enclosure [135, 136]. The NFC and Fluke 971-meter sensors were placed in close proximity within a distance of 2.5 cm. Initially, the NFC sensor, along with the smartphone and Fluke 971 meter was placed within the enclosure for a period of 60 minutes. During NFC sensor measurements, the transparent lid of the pinewood box was removed and the smartphone was placed over the NFC sensor to capture the measured temperature and relative humidity level within a period of less than one minute. The measured temperature and relative humidity level for the Fluke 971 meter were also recorded. Using this approach, 10 measurements for temperature and relative humidity were taken over a one-hour period.

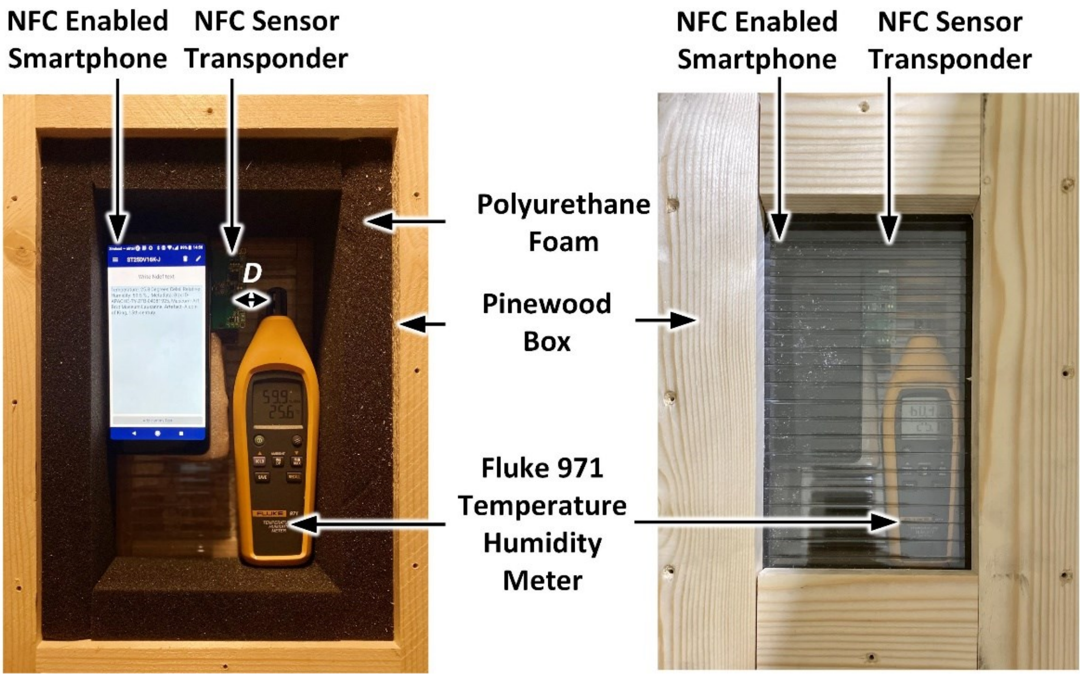

Figure 4.10: NFC sensor characterization setup (Fig. 7 of [1]).

During measurements, the ambient lab temperature and relative humidity varied from 24.6 °C to 26.5 °C and 59.9 % to 63.8 %, respectively. The measured temperature and relative humidity errors between the NFC and calibrated meter measurements are shown in Figure 4.11. Figure 4.11 (a) shows that a minimum error of 0.2 °C and a maximum error of 0.6 °C was recorded. Similarly, the measured relative humidity results are shown in Figure 4.11 (b) with a minimum error of 0 % and maximum error of 0.7 % being recorded. The measured results show that the NFC sensor exhibited a temperature and relative humidity mean error of ± 0.37 °C, ± 0.35 %, respectively. In Figure 4.11, the blue square symbols denote the mean error value. The mean error was calculated using the expression shown in Equation 4.4.

$$Mean\ error = \frac{\sum Measurment\ errors}{Total\ number\ of\ measurements} \tag{4.4}$$

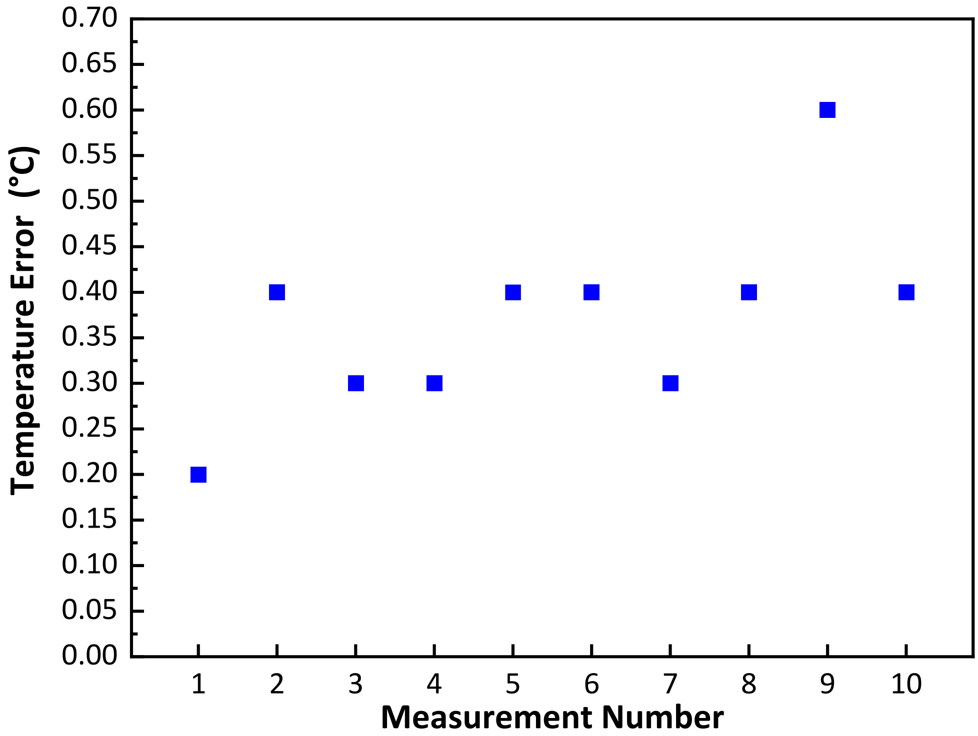

(a)

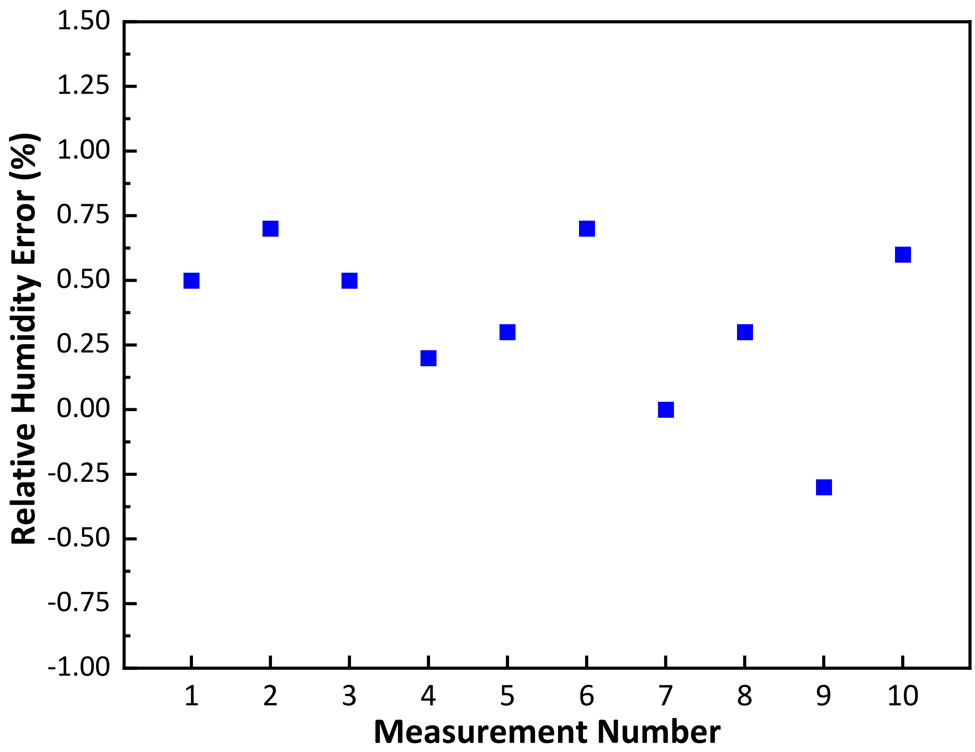

(b)

Figure 4.11: Accuracy testing (a) temperature (b) relative humidity (Fig. 8 of [1]).

The temperature accuracy of the developed NFC sensor was also characterized over a range of 6.8 to 50.6 °C. The testing was performed in the setup shown in Figure 4.12 using a cardboard box. As shown in Figure 4.12 (a) and (b), the sensing part of the Fluke 971 is inserted inside a cardboard box. In addition, the NFC sensor is integrated within the cardboard archive box, and a small aperture is created for temperature sensing, as depicted in Figure 4.12 (b). The Fluke 971-meter and NFC temperature sensors were placed in close proximity within a distance of 2.5 cm. During the measurements, the lid of the cardboard box was closed, and temperature was varied from 6.8 to 50.6 °C. The temperature of the NFC sensor was scanned from outside of the box, as shown in Figure 4.12 (a), simultaneously the Fluke 971-meter temperature measurement was recorded. Using this approach, 21 individual measurements were taken, and the temperature value of the NFC sensor was compared with the Fluke 971 meter recording. The measured temperature result is shown in Figure 4.13 with a minimum error of 0.2 °C and a maximum error of 0.6 °C being recorded. The above results show that the NFC sensor exhibited a mean error of ± 0.34 °C in temperature. As shown in Figure 4.13, the blue square symbols denote the mean error value.

As reported in [112], the temperature and humidity sensor (SHTC3) covers a temperature range from -40 °C to 125 °C (typical accuracy = ±0.2 °C for 0 °C to 60 °C).

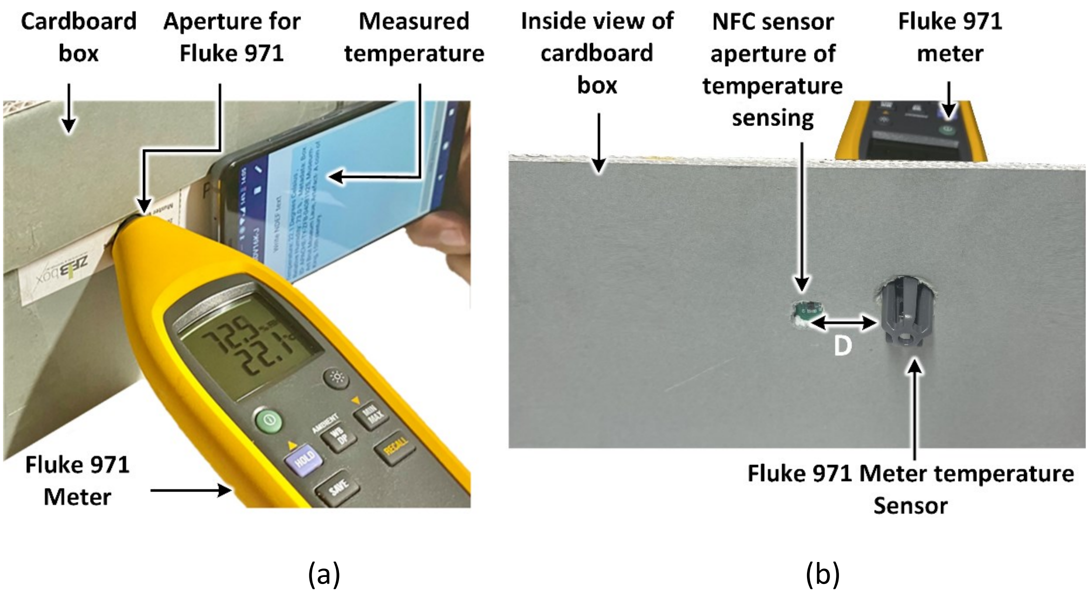

Figure 4.12: NFC sensor measurement setup (a) outside (b) inside view (Fig. S1 of [1]).

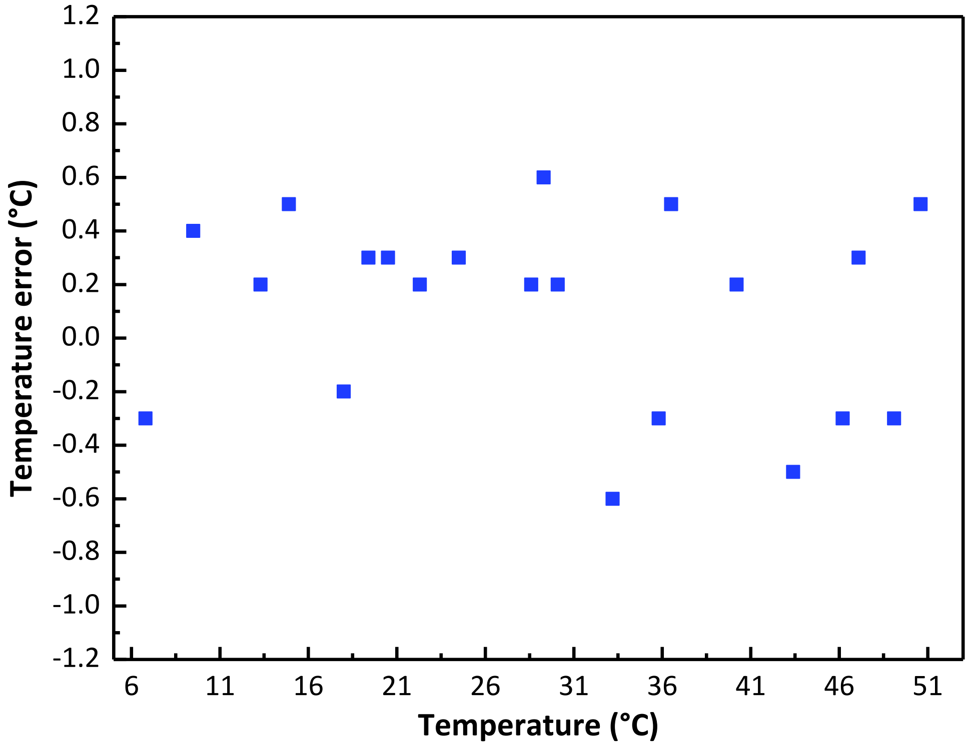

Figure 4.13: NFC sensor temperature comparison with a Fluke 971 (Fig. S2 of [1]).

Similarly, the humidity sensor covers a relative humidity range of 0 % to 100 % (typical accuracy = ±2 % for 20 % to 80 % at temperatures of 25 °C [112]).

4.3 Performance Evaluation of the NFC sensor

Table 4.3 shows a performance comparison of the developed the developed NFC sensor transponder with the state-of-the-art NFC sensor transponders to identify the performance improvements that the developed NFC sensor has enabled compared with other works in this research area. It is evident from Table 4.3 that the DC power consumption of the developed NFC sensor is the lowest in comparison with reported NFC sensor transponders in literature [28]. In addition, the wireless communication range of developed NFC sensor is the largest compared with the literature.

Note: Table 4.3 is sorted in increasing order of wireless communication range in column G.

Table 4.3: Comparing NFC sensor performance with the literature.

A	B	C	D	E	F	G	H
Ref	**RFID Air Interface**	**Integrated processing unit**	**MCU clock (MHz)**	**Tag Coil Size (mm)**	**DC Power consumption (mW)**	**Range (cm)**	**Sensing parameters**
[22]	ISO14443	No	1	12 × 16	1.74	0.8	Pressure
[23]	ISO14443	No	1	⌀ 26	1.72	1	Skin moisture & Ultraviolet light
[77]	ISO14443	No	1	⌀ 26	NA[10]	1	Skin moisture
[24]	ISO14443	No	NA	35 x 25	1.8	1	ECG & sweat
[28]	ISO14443	No	NA	10 × 5	0.9	1	Arterial SPO_2 & Temperature
[29]	ISO15693	No	1	25 x 25	NA	1.4	Moisture
[25]	ISO15693	No	1	50 x 50	5.29	1.8	pH
[26]	ISO14443	No	NA	43 × 58	4.45	1.9	Carbon dioxide
[7]	ISO15693	No	1	50 x 50	3	2	Soil moisture, RH Temperature
[9]	ISO15693	No	1	50 x 50	5.29	2	Color
[30]	ISO14443	Yes	NA	45 × 30	NA	2	Ascorbic acid
[10]	ISO15693	No	1	50 x 50	8	1.9	Color
[31]	ISO15693	Yes	NA	70 x 70	NA	3	pH
[84]	ISO15693	Yes	NA	34 × 46	1.3	3	Blood flow
[27]	ISO15693	No	1	35 × 35	2.1	3	Water minerals
[83]	ISO15693	Yes	NA	25 x 35	NA	4	pH
[82]	ISO15693	Yes	NA	26 × 26	NA	4.3	Strain & Temperature
This Work[11]	**ISO15693**	**No**	**0.524**	**49 × 59**	**0.597**	**11**	**Temperature, Humidity**

[10] NA = Information not reported in literature

[11] Vibration energy harvester (VEH) assisted battery-less NFC sensor

4.4 Demonstration and Deployment

This section describes the demonstration and deployment of the developed battery-less NFC sensor.

4.4.1 Demonstration of battery-less NFC sensor to stakeholders

The developed battery-less NFC sensor was practically demonstrated to stakeholders in three public training events organized by the APACHE project and host European museums.

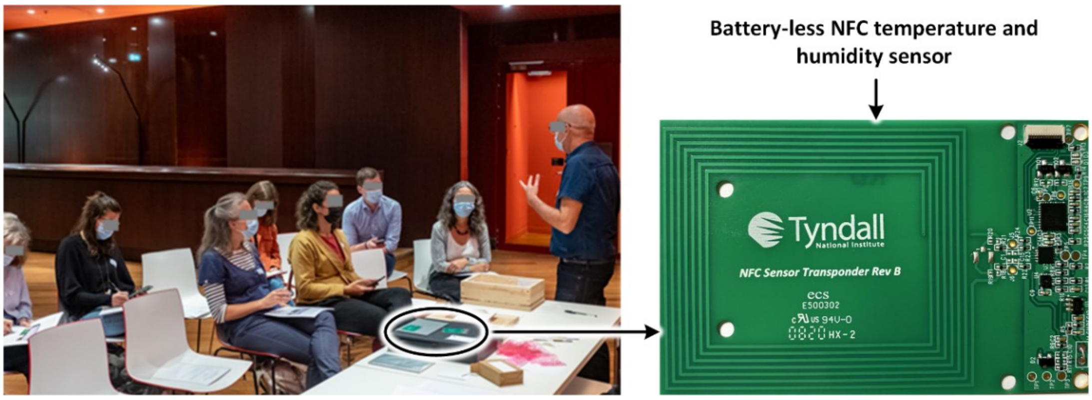

(a)

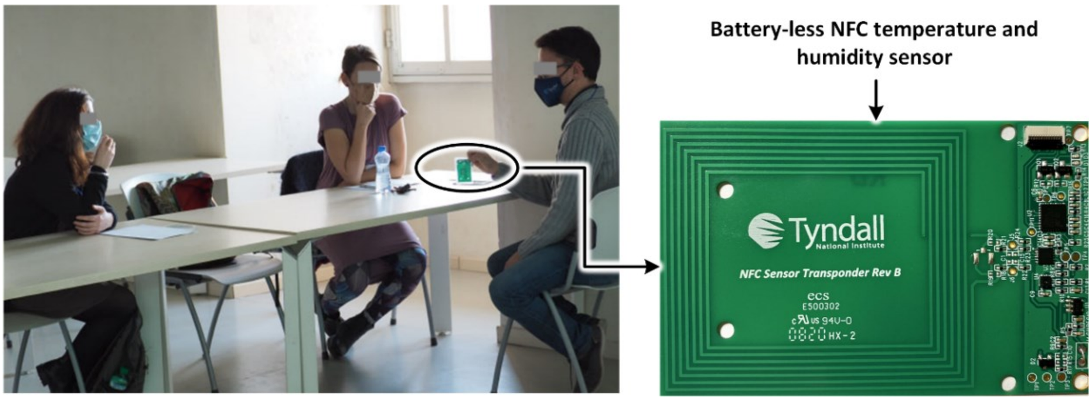

(b)

Figure 4.14: Demonstration in (a) Paris, France, (b) Turin, Italy.

The first public training was held at Musée du quai Branly – Jacques Chirac, Paris, France on 2nd and 3rd September 2021 and was organized by the APACHE project and Musée du quai Branly–Jacques Chirac, Paris. A photograph of the practical demonstration of the NFC sensor to museum conservators and conservation scientists during the first public training is depicted in Figure 4.14 (a). Additional information regarding the training has been reported in [137]. Similarly, the NFC sensor demonstrated in the second public training, which was held in Centro Conservazione e Restauro "La Venaria Reale" Venaria Reale, Turin, Italy on 2nd and 3rd December 2021. The practical demonstration of the NFC sensor to stakeholders during this training is shown in Figure 4.14 (b), and further information has been reported in [138]. Lastly, on 29th June 2022, the NFC sensor was also demonstrated to stakeholders in the final public training, which was held in the Hungarian National Museum, Budapest, Hungary [139]. Table 4.4 summarizes the details of the NFC sensor demonstration events.

Table 4.4: Summary of NFC sensor demonstration events.

Event Name	**Organizers**	**Demonstration Method**	**Location**	**Ref**
First APACHE public training	APACHE project and Musée du quai Branly–Jacques Chirac, Paris	*Theoretical* presentation followed by *Practical* demonstration	Paris, France	[137]
Second APACHE public training	APACHE project and Centro Conservazione e Restauro "La Venaria Reale" Venaria Reale, Turin	*Theoretical* presentation followed by *Practical* demonstration	Turin, Italy	[138]
Final APACHE public training	APACHE project and Hungarian National Museum, Budapest	*Practical* demonstration	Budapest, Hungary	[139]

4.4.2 Practical deployment of battery-less NFC sensor in museum

This subsection describes the *deployment* of the developed smart archive box with integrated NFC sensor in the Public Museum in Cork (CPM), Ireland, that was established in 1910 and housed more than 40 thousand artefacts [140].

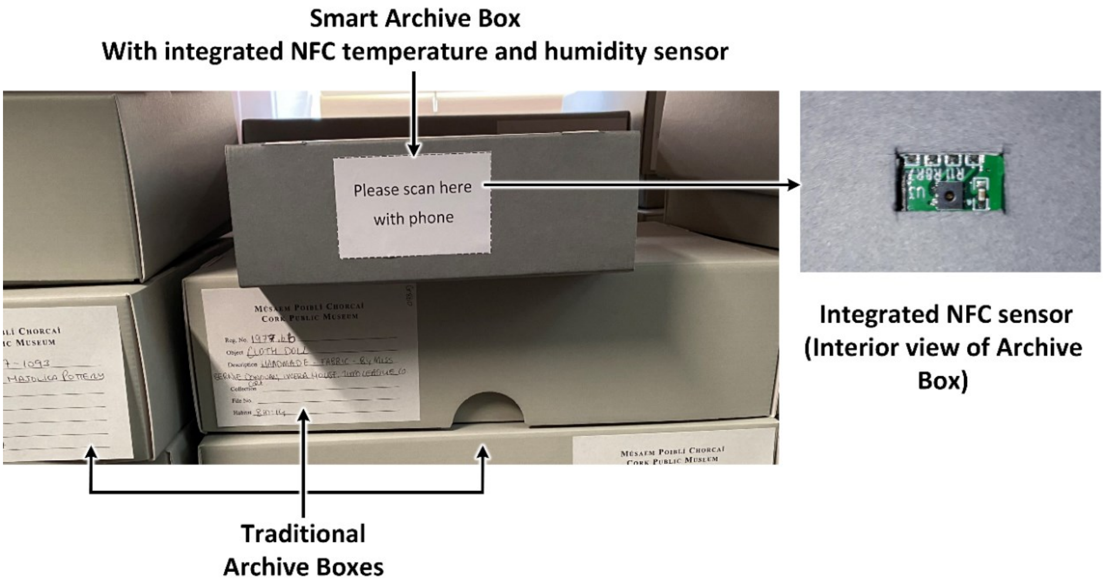

(a)

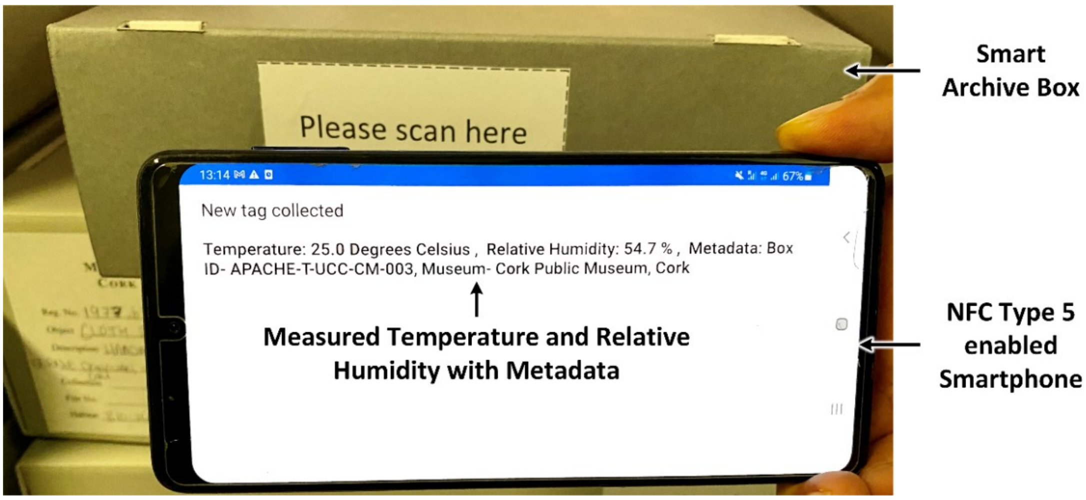

(b)

Figure 4.15: Deployment at CPM, Ireland (a) smart archive box, (b) measurement.

Figure 4.15 (a) shows the deployed smart archive box in the storage facility of the museum. Figure 4.15 (b) demonstrates the NFC sensor being wirelessly powered and read using a smartphone. The smartphone, when placed within a distance of < 5 cm of the sensor, enables the temperature and relative humidity values and additional metadata to be measured wirelessly, with no requirement for battery power for the sensor.

In addition, to monitor interior temperature and relative humidity of the historic *Andy Warhol's "Flowers"* which was painted in 1964, the NFC sensor was also *deployed* at the Guggenheim Museum, Venice, Italy. Figure 4.16 shows the NFC sensor integration within the painting frame. The deployed NFC sensor is working well as of 5th December 2022.

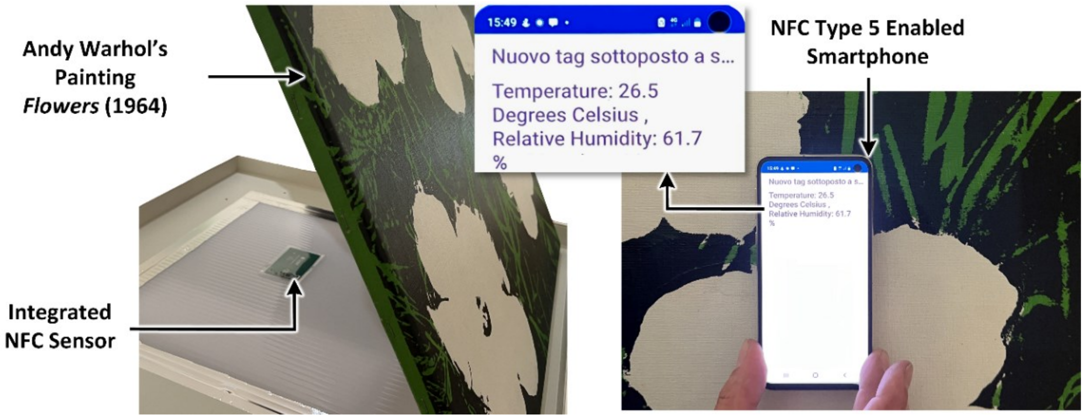

Figure 4.16: Deployment of NFC sensor at Guggenheim museum, Venice, Italy.

4.4.3 Summary of benefits and convenience of smart archive box to user

In terms of the developed NFC temperature and humidity sensor, it is also instructive to highlight the advantages of the smart archive box to the user and the convenience afforded as described in this subsection:

1. The developed temperature and humidity sensing solution is the **first reporting of a smart archive box** of its type in the literature for museum artefact monitoring.
2. The proposed method uses a battery-less NFC sensor that can be read conveniently with a standard NFC-enabled smartphone.
3. There is no requirement for a battery to power the sensor and the archive box does not need to be opened during the measurement so the internal environment is undisturbed.
4. Another convenient feature is that there is no requirement for maintenance of the NFC sensor such as battery replacement. This could be problematic in a situation where thousands of stored items exist in a large collection for example, requiring significant maintenance and personnel costs.
5. A low-cost sensor has been developed in this work with a cost of € 4.91 in volumes of 10,000 units making it economically viable for use in small to medium-sized museums.
6. The removal of the requirement for a battery means that there is a positive environmental impact with no need to dispose of depleted batteries.
7. The presented solution using passive wireless sensing is convenient for many small and medium sized institutions, making it possible to measure important artefact environmental data without large associated costs and effort being required.

4.5 Conclusions

The performance measurement and characterization results of the developed battery-less NFC sensor transponder prototype have been discussed in this chapter. The RF receiver sensitivity of the developed NFC sensor was measured using an industry-standard Tagformance Pro measurement system. The NFC sensor requires a minimum magnetic field strength (H_{MIN}) of 67.8 mA/m at 13.74 MHz and 87.6 mA/m at 13.59 to operate (i.e., respond to the read command) in the free space case and after NFC sensor integration within the archive box, respectively. In addition, the bandwidth (-3 dB) of the NFC loop antenna is calculated to be 1.16 MHz and 1.14 MHz for the case free-space and after integration within the archive box, respectively. Furthermore, the key performance parameters such as RF receiver sensitivity, centre frequency and bandwidth of the developed NFC sensor were compared with the ISO/IEC 15693 air interface specification and are in good agreement with it.

The developed NFC sensor has also been optimized for low power operation using voltage and frequency-scaling techniques for MCU, leading to a peak DC power consumption of 597 μW, which is the **lowest value found in the literature** [28]. Wireless communications performance tests on the prototype sensor in free space achieved a maximum range of 5 cm with a Samsung Galaxy S20 smartphone and 16.4 cm using the Tagformance pro measurement system. With a measured mean error of ± 0.34 °C in temperature from 6.8 °C to 50.6 °C, the developed NFC sensor qualifies for accurate temperature measurements for museum artefacts monitoring.

Finally, the wireless communication range of the battery-less vibration energy harvester-assisted NFC sensor transponder was measured with a NFC-enabled smartphone. A maximum wireless communication range of *11 cm* in free space was achieved. The wireless communication range of the developed battery-less NFC sensor is 120 % greater than similar devices described in the literature [26, 82].

Chapter 5: A Long-Range Wireless Communications Platform for Museum Artefact Monitoring

5.1 Background

In Chapter 3 and Chapter 4, the development, performance characterization, demonstration and deployment of the battery-less NFC sensor transponder prototypes for museum artefacts monitoring that are particularly conserved in museum archives facilities was been discussed. In museum settings, the vast majority of artefacts (up to 90 %) are deposited in dedicated storage areas of museum [141], representing large facilities with thousands of storage crates.

These storage crates are essential for the protection of museum artefacts from light, mechanical damage, volatile gases and dust in the prevention of deterioration of the housed objects. Depending on the variety of materials (such as paper-based, canvas or acrylics in paintings and modern art, metals, etc.), those objects often require specific temperature and relative humidity storage conditions, in which they can be best protected from material degradation [16]. At the same time, the material's varying moisture contents or emission of degradation products from the artefacts themselves can create an unfavourable microclimate in these closed containers, which can accelerate the natural ageing and damage to the artefacts. This ageing may be caused by temperature changes or adverse surrounding (indoor) climates, connected with the impermeable nature of the enclosures. Therefore, the preventive conservation of artefacts stored inside wooden storage crates in museum storage facilities requires continuous temperature and relative humidity monitoring within the crates themselves.

In addition, the wall thickness of a wooden storage crate's wall is several cm thick. This compares to only a few mm of wall thickness for cardboard-based archive boxes so making use of certain short-range wireless technologies such as NFC is appropriate.

As such, the employment of the battery-less NFC sensor solution discussed in Chapter 3 and 4 are challenging for this test case because of the short wireless communication range of less than 5 cm using NFC technology. Hence, development of long-range wireless communication platform is required.

In [142-144] museum artefact monitoring solutions are presented using various wireless sensing and Internet of Things (IoT) technologies. The selection of a suitable wireless technology for stored artefact monitoring is vital mainly because the museum storage areas are often located in protected buildings that may often feature stone wall construction. Building structures for historical buildings may include thick walls that attenuate more high-frequency radio signals (e.g., 2.45 GHz) compared to lower frequencies (sub-GHz), and this results in decrease in the wireless communication range and data throughput [145]. Similarly, artefacts owned by museums are generally stored in basement areas, and some museums are located in remote areas where the cellular network may be unavailable or have a poor cellular network connection [146]. Likewise, artefacts can be stored in large quantities that are housed in wooden crates and that are placed in dedicated storage areas. Wireless monitoring of the microclimate parameters of individual storage crates at regular intervals may create wireless signal congestion, which can decrease packet delivery ratio (PDR) [147].

This chapter aims to identify the optimum wireless technology for museum artefact monitoring of crate objects in museum storage facilities. Eight different wireless technologies are studied and compared. In addition, this chapter also discusses the development of a LoRaWAN testbed network using a commercial LoRaWAN gateway and an open-source hardware platform for sensor nodes for museum artefacts monitoring within a museum storage facility. Finally, a LoRaWAN testbed network was deployed in the Cork Public Museum, Cork, Ireland, as a proof of concept deployment in a relevant environment. The wireless technology selection methodology and validation LoRaWAN-based long-Range wireless communication platform is presented in this chapter and has also been reported in [4].

5.2 User Requirements

Table 5.1 summarizes the user requirements for monitoring of museum artefacts that are stored in museum storage facilities. These user requirements were defined by the stakeholders, including museum conservators and conservation scientists. The wireless sensor nodes need to cost less than €50 per unit in 10k quantities including the overhead cost of wireless communication network infrastructure and maintenance for an operational life of 10 years.

Table 5.1: Long-range sensor node user requirements.

Requirement	Specification
Electrical Power Source	Battery
Minimum operational Life	10 years
Maximum sensor node cost	< €50 in 10k quantities
Monthly or yearly subscription	No
Maximum wireless communication	< 100 m
Maximum museum storage area	40 m x 10 m x 5 m
Maximum required bitrate	250 bits/sec
Packet delivery ratio	> 0.995
Data transmission duration	1 packet per day
Maximum payload	10 bytes
Dependency on cellular coverage	No
Maximum airtime	< 1.5 Second
Sensed environmental parameters	Temperature and Humidity
Maximum temperature accuracy	< ± 0.5 °C
Maximum relative humidity	< ± 2 %
Operational temperature range	–40 to +120 °C [148]
Operational humidity range	0 to 100 % [148]
Maximum sensor response time at *t* (63 %)	8 seconds for relative humidity, 2 seconds for temperature [148]

The wireless sensor node is required to transmit 1 data packet per day at a minimum bitrate of 250 bits/sec with a wireless communication range of typically less than 100 meters. A low data rate, for example 100 bits/sec requires a couple of seconds of airtime to transmit a payload of 10 bytes. Because of the increasing number of sensor devices, this increased communication duration time may lead to an increased packet error rate [147] and, therefore, may not be feasible for this application. The desired wireless sensing solution is required to provide an operational lifetime minimum of 10 years without any maintenance, such as battery replacement. In addition, a network subscription and the dependency on cellular coverage are not desirable for this application [4, 146].

5.3 Choosing a Suitable Wireless Communication Technology

This section describes the selection methodology for the wireless communication technology envisaged for museum artefact monitoring, which is described in detail in the following sections. This chapter also describes the rationale for the consideration of the long-range wide area network (LoRaWAN) as a wireless communication technology for this application.

5.3.1 Comparison of wireless communication technologies

This subsection describes theoretical analysis and comparison of eight possible wireless communication technologies considered suitable for typical Internet of things (IoT) applications. In [149-151], comprehensive reviews of various wireless technologies have been reported. To select a suitable wireless technology for the museum artefact monitoring application, the analysis of several key wireless performance parameters is required. These parameters include power consumption during the different operational states including data transmission, data reception and during sleep mode (low power mode between operational cycles). The comparison should also include indoor wireless communication range as well as the data rate (baud rate) according to sensing modality requirements. Table 5.2 shows a comparison of the above technical parameters for the eight wireless technologies listed.

Table 5.2: Comparison of wireless technologies technical parameter (Table 1 of [4]).

Wireless Technology	Maximum Wireless Communication Range (m)	Maximum Data rate (kbps)	Maximum I_{SLEEP} (μA)	Maximum I_{TX} (mA)	Ref.
NB-IoT	10000	200	5	300	[150, 151]
SigFox	10000	0.1	0.7	22	[151, 152]
LoRaWAN	5000	50	1	32	[150, 151]
ZigBee	100	250	0.9	46	[151, 153]
WiFi	250	600k	4	229	[151, 154]
BLE	20	1000	0.97	6.40	[155, 156]
UHF RFID	15	640	0.7	0.350	[157, 158]
NFC	0.05	848	1.3	0.330	[1, 109]

Narrowband Internet of Things (NB-IoT) is a low power wide area network (LPWAN) technology with a wireless communication range of approximately 1 km typically with a data rate of 200 kbps [149]. However, an NB-IoT radio transceiver requires a peak DC current of approximately 300 mA during transmission and 5 μA current in sleep mode [159]. In addition, the network subscription cost (€0.02/MB) [160] is significant and the dependency of this type of communications system on cellular coverage makes NB-IoT difficult to be employed for this application.

SigFox is an another LPWAN technology developed for low-power and low bitrate applications, which requires a peak DC current of 22 mA during transmission and 0.7 μA in sleep mode [152]. However, because of a limited data rate of 0.1 kbps, SigFox requires a period of 2.08 seconds of airtime to transmit a payload of 12 bytes. When networks such as these need to be scaled up, the increasing number of wireless sensor devices, and the associated increase in transmission may lead to an increased packet error rate [147].

ZigBee and WiFi are short to medium-range wireless technologies with high data rates of 250 kbps and 600 Mbps, respectively [159].

As shown in Table 5.2, ZigBee and Wi-Fi technologies have limited wireless communication ranges, and in addition, both technologies consume more power during transmission when compared to other LPWAN technologies, such as LoRa (Long-Range). Therefore, ZigBee and Wi-Fi are not suitable for the intended application of cultural heritage monitoring with the identified application requirements (See Section 5.2).

In comparison, ultra-high frequency radio-frequency identification (UHF RFID) and near field communication (NFC) technologies can operate in both battery-less and battery-assisted power mode and consume a low DC current of respectively 350 μA [157] and 330 μA [109]. However, as shown in Table 5.2, the wireless communication range of both UHF RFID and NFC technologies is low and, therefore, additional infrastructure cost is required to enable autonomous sensor data collection.

LoRaWAN is another LPWAN radio technology that enables long-range wireless communications while consuming a DC current in the range of 32 mA [159]. LoRaWAN also has an acceptable data rate for this museum application. In addition, the user does not have to subscribe to third-party network providers like NB-IoT, and several years of battery lifetime can be achieved. Similarly, Bluetooth Low Energy (BLE) also meets data rate and power consumption requirements. However, the communication range of BLE is typically less than 20 m in an indoor environment [156], Thus, multiple relay nodes are generally required especially when the node deployment involves a wide coverage, or when the BLE gateway is located a large distance from the storage crates. Nevertheless, some performance test results for LoRaWAN and BLE technologies are performed and described in the next section.

5.3.2 Validation of LoRaWAN and BLE technologies

This subsection describes the experimental validation of two potential wireless communication technologies concerning LoRaWAN and BLE for this application. A LoRaWAN testbed network, BLE mesh server, and the client node were developed for the purpose of performance comparison as shown Figure 5.1. The implemented LoRaWAN testbed network comprises one LoRa sensor node and 4 gateways (TTN-GW868).

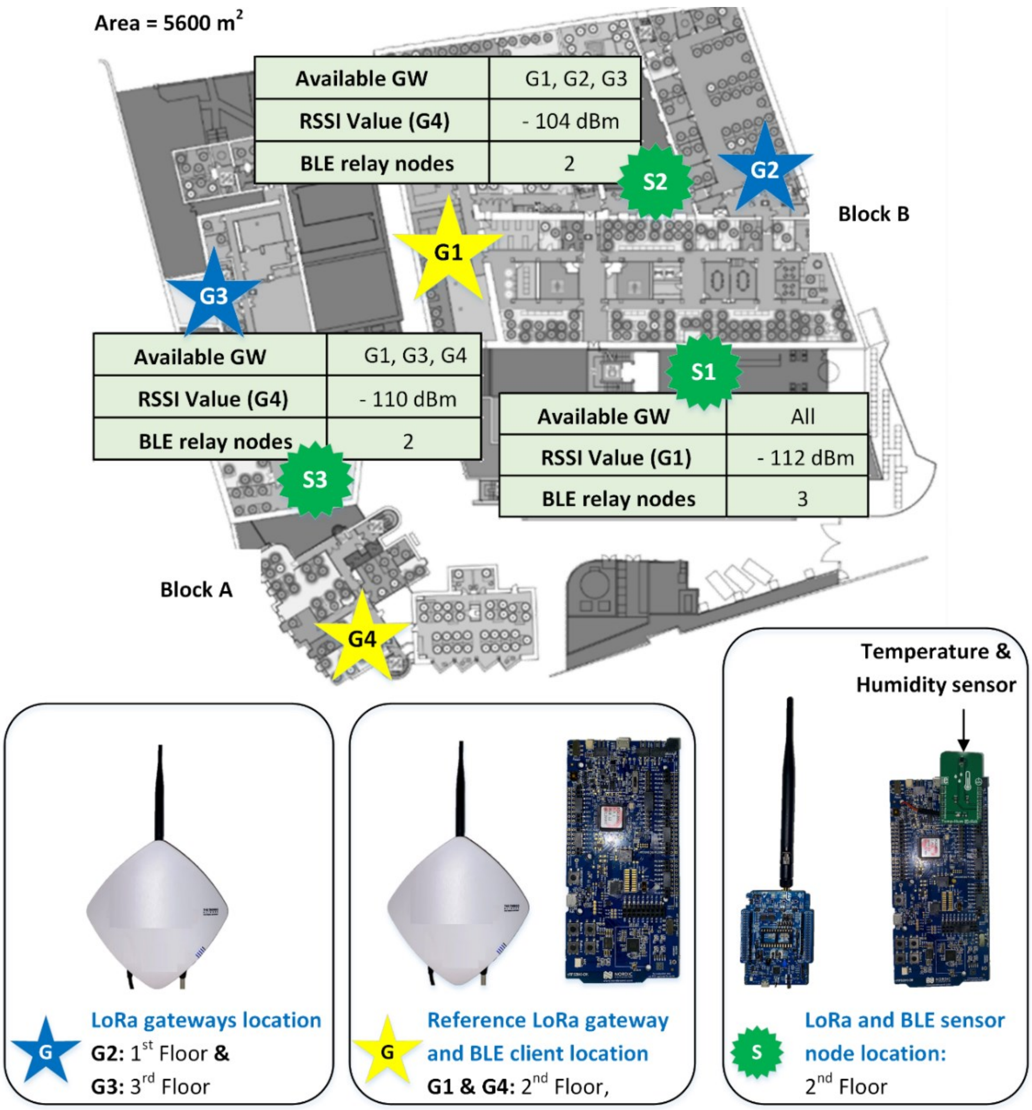

Figure 5.1: Indoor wireless communication test of LoRaWAN and BLE (Fig. 2 of [4]).

The LoRa sensor node was implemented using a commercial LoRaWAN evaluation kit (L072Z-LRWAN1) and sensor expansion board (X-NUCLEO-IKS01A2). Further, this LoRa sensor node was connected to a commercial 868 MHz whip antenna [161]. The LoRa sensor node is configured to transmit data with the adaptive data rate (ADR) feature enabled. ADR allows sensor nodes to operate with a high data rate (e.g. a spreading factor of SF7) when the node is close to the gateway [162]. Consequently, the sensor node spends less time on air and exploits the low link budget. ADR also allows data transfer with a lower data rate (e.g. SF12) for more distant nodes, and hence the wireless link budget is improved in this case. Similarly, a commercial evaluation kit of BLE (nRF52840-DK) was used to develop the BLE client and server node.

For the indoor wireless communication test, the LoRaWAN testbed network and the BLE nodes were deployed in one of the Tyndall National Institute's buildings as shown in Figure 5.1. This building is divided into two blocks: Block A (i.e., a protected building construction with thick walls that was constructed in 1812) and Block B is a modern style construction. As shown in Figure 5.1, the LoRa gateway and BLE client node were set up at location G1 in Block B, indicated by the yellow-coloured 5-star symbol. The LoRa sensor node was placed at locations S1 and S2 indicated by the green-coloured symbol. The LoRa Received Signal Strength Indicator (RSSI) metrics were then recorded at location G1 and were measured at -112 dBm and -104 dBm for location S1 and S2, respectively, showing the large RF attenuation levels associated with this environment. Similarly, to transmit data from S1 and S2 to G1, BLE required a total of 3 and 2 relay nodes, respectively. A similar performance test was conducted in Block A. The LoRa gateway and the BLE client node were set up at location G4. A LoRa RSSI value of -110 dBm was measured at the gateway location G4 from the sensor location S3. For BLE, 2 relay nodes were required to transmit data from S3 to G4.

Therefore, even though BLE presented a high PDR [163], it requires additional infrastructure, which increases the overall complexity and deployment cost. In this particular deployment, the increase in cost is about 200 % given that a BLE relay node (e.g., nRF52840-DK) unit costs approximately €41 [164]. Furthermore, if a large number of BLE end-devices are placed in the storage area, the additional battery replacement cost is significant, since the collected traffic must travel via the relay nodes, which must constantly be in active mode.

In order to evaluate the experimental configuration (i.e., range, path-loss characteristics) with a larger number of nodes, a series of simulations utilizing the LoRaWAN-SIM simulator were performed [165]. A quantity of 100 to 500 nodes were used and each node was capable of sending 1 confirmed packet every 20 minutes for 1 day. The packets were received by 4 gateways which were placed remotely from the 30 m × 30 m storage area.

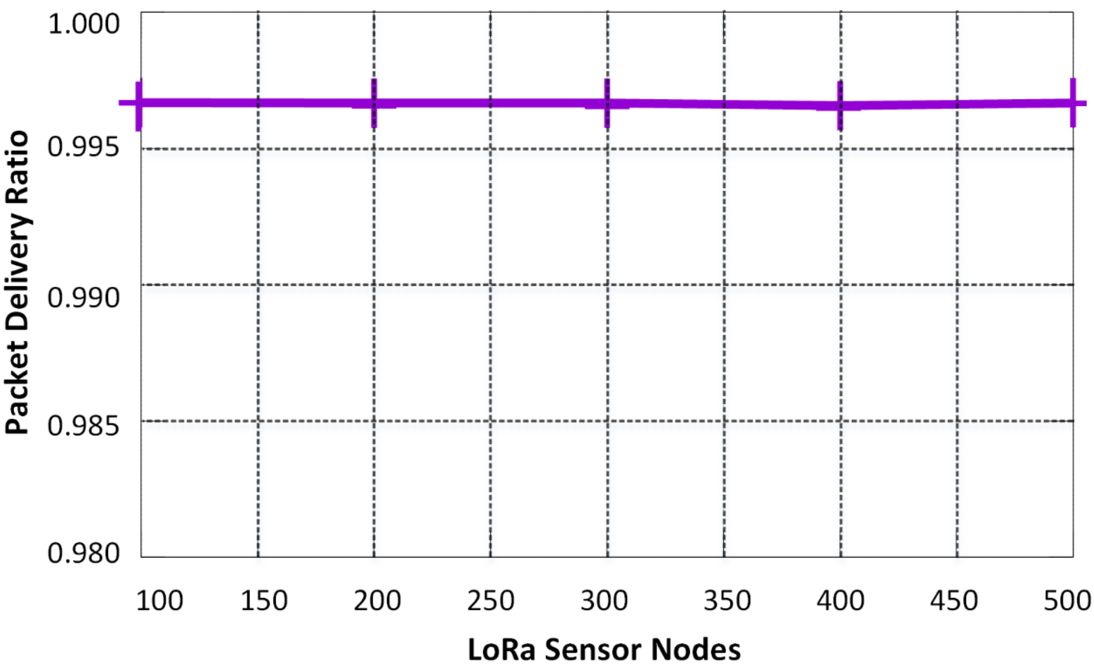

Figure 5.2: LoRaWAN packet delivery ratio for 100 to 500 nodes (Fig. 3 of [4]).

The results are depicted in Figure 5.2, showing an acceptable packet delivery ratio (PDR) of greater than 0.995 even for a high number of devices and demonstrates that wireless communication is reliable [166]. The theoretical and experimental validation of the wireless technology shows that LoRaWAN is the most suitable candidate for museum artefact monitoring applications for numerous reasons discussed earlier. Importantly, LoRaWAN also provides a cost-effective solution with low infrastructure costs, a high network reliability (PDR > 0.995) and a power consumption of less than 105 mW DC.

5.4 Development and Testing of a LoRaWAN Testbed Network

This section discusses the development and performance evaluation of the LoRaWAN testbed network for museum artefact monitoring stored in museum storage area facilities. This section also explains the deployment and performance analysis of the LoRaWAN testbed network.

5.4.1 Development of LoRa sensor node and network

In order to develop a sensor node, open-source hardware platform of LoRaWAN (LSN50-V2) from Dragino Technology Co. Limited was used [167]. In addition, to integrate the temperature and relative humidity SHT31 sensor from Sensirion AG [148], an Inter-Integrated Circuit (I2C) communication protocol was used to interface the sensor with the LoRaWAN hardware platform. The developed LoRaWAN sensor node was powered using a 4 Ah Lithium-Thionyl Chloride (Li-SoCl2) battery. The LoRaWAN sensor nodes were configured to use an adaptive data rate (i.e., Spreading Factor = SF7 to SF12), Coding Rate (CR) = 4/5, Channel bandwidth (BW) = 125 kHz and confirmed (also referred as acknowledgment based) data transmission. The commercial LoRaWAN gateways (Model No = TTN-GW-868) from The Things Network (TTN), the Netherlands was used to receive the measured temperature and relative humidity readings from the sensor node [168]. The gateways were mains-powered and registered with the TTN network server stack, which was used as a LoRaWAN network server. The network server manages the network and performs several activities, including security checks, schedule acknowledgements through the optimal gateway and adaptive data rate changes. Further, the network server forwards data packets to the application server, which is responsible for securely handling, managing, and interpreting sensor data and delivering it to specific Hypertext Transfer Protocol (HTTP) endpoints (e.g., Ubidots, DATACAKE and Thingspeak). In order to forward data packets to such endpoints, the TTN application server also hosts an MQ Telemetry Transport (MQTT) server for streaming application data and supports HTTP webhooks[12].

[12] The TTN webhooks feature allows the application server to send application-related messages to specific HTTP endpoints (IoT platform). Typical use cases of webhooks are for visualizing or acting on uplink data from another IoT platform and scheduling downlinks from such IoT platforms.

The TTN webhook builds integrations between the application server and the commercial IoT platform "DATACAKE[13]." The TTN application server sends a webhook i.e., temperature and humidity data to the DATACAKE platform whenever data is received from a sensor node. The data is then visualized in the custom-developed dashboard on the DATACAKE platform, as shown in Figure 5.3. The measured temperature and relative humidity data is then stored on the DATACAKE server and can be accessed remotely using a laptop and computer with the help of a WiFi or Local area network (LAN) connection.

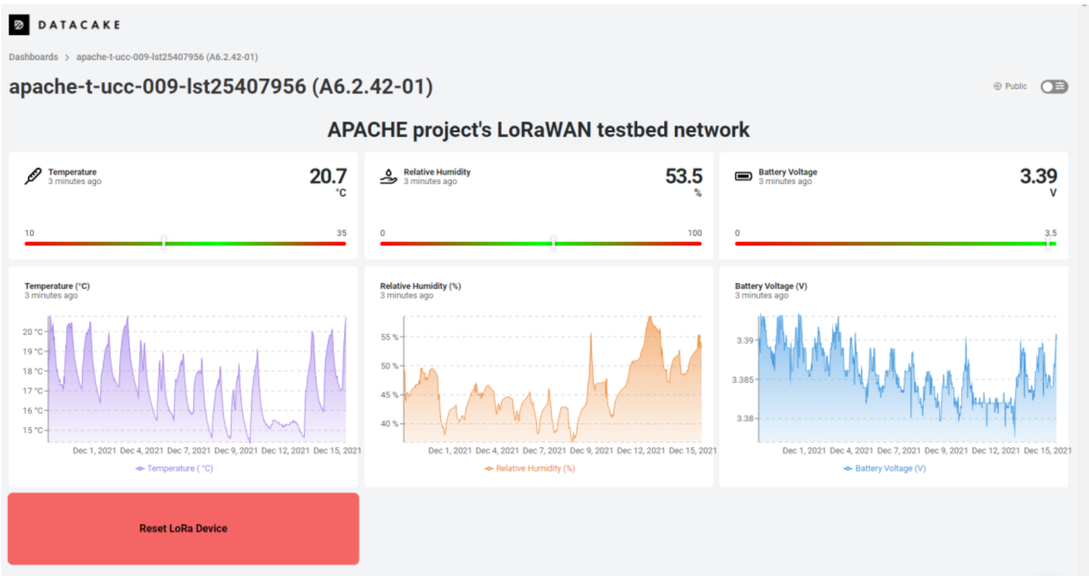

Figure 5.3: User dashboard of the LoRaWAN network.

[13] Datacake is a commercial IoT platform that is used to develop user data portals in the research work outlined in this chapter.

5.4.2 Performance evaluation of the LoRaWAN testbed network

This subsection summarizes the experimental setup and method used to evaluate the performance of the developed LoRaWAN sensor network. In order to evaluate the wireless communications performance of the developed testbed network, the testbed was deployed in a protected building structure similar to a typical museum storage facility, i.e., inside Tyndall National Institute office building, Block A. The Block A building was constructed in 1812 and has thick concrete walls. Figure 5.4 shows the deployment map of the LoRaWAN gateways and sensor nodes. The total area of the deployment site is approximately 80 m × 20 m, which is larger than the typical size of a museum storage area i.e., 40 m x 10 m x 5 m.

In Figure 5.4, the circular ring symbols (in red, yellow, and blue) represent the location of the sensor node, and the multicolour diamond ring symbols denote the location of the gateways. The deployed LoRaWAN platform consists of 20 LoRaWAN sensor nodes and 3 LoRaWAN gateways. Figure 5.4 (a) shows 2 and 3 sensor nodes deployed on the ground and the 1st floor, respectively. Similarly, a total of 6 sensor nodes and 1 gateway were deployed on the 2nd floor, and 9 sensor nodes and 2 gateways were positioned on the 3rd floor, as shown in Figure 5.4 (b).

Furthermore, as discussed in section 5.3.2, the packet delivery ratio (PDR) metric was used to evaluate the wireless communication performance of the testbed network in a protected building structure. The PDR is the ratio of the number of packets received by the LoRaWAN server to the total number of packets sent by the sensor node. In order to measure PDR, each LoRaWAN sensor node was configured with the following parameters: Duty cycle = 1 confirmed packet transmission every 20 minutes, adaptive data rate = enabled, CR = 4/5 and channel bandwidth = 125 kHz, and experiment duration = 1 week, i.e., approximately 504 data packet transmission. A developed user data portal i.e., *DATACAKE* was used to store data packets for the entire experiment duration. Finally, the PDR of the developed LoRaWAN testbed network was measured, and a detailed measurement-based PDR calculation is presented in the Section 5.5.

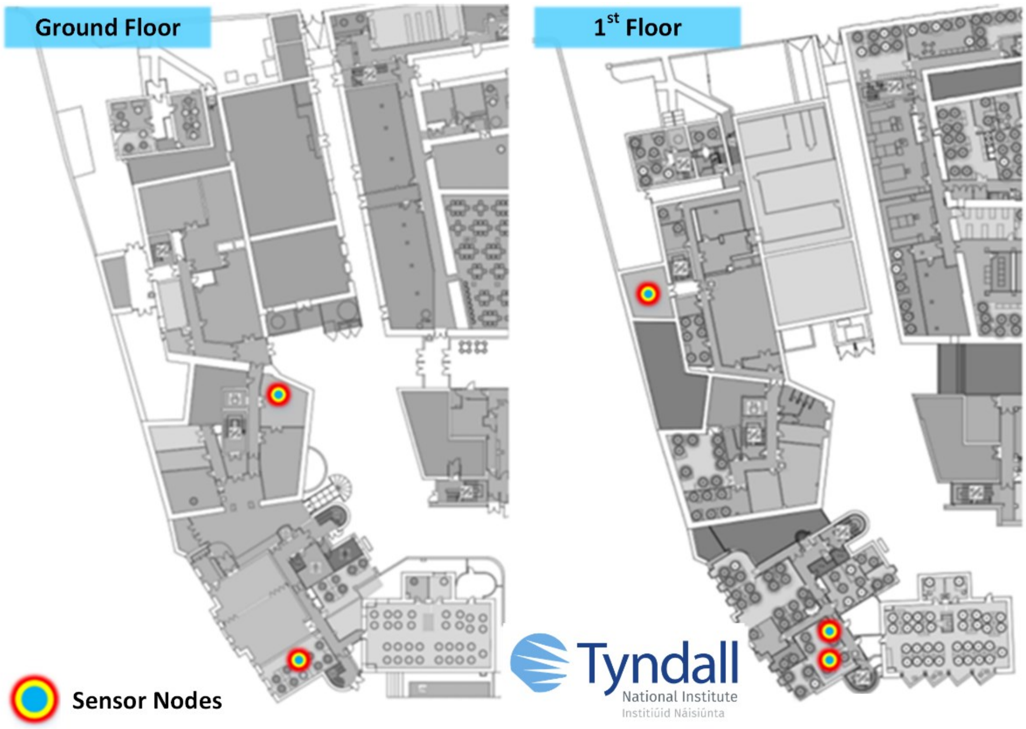

(a)

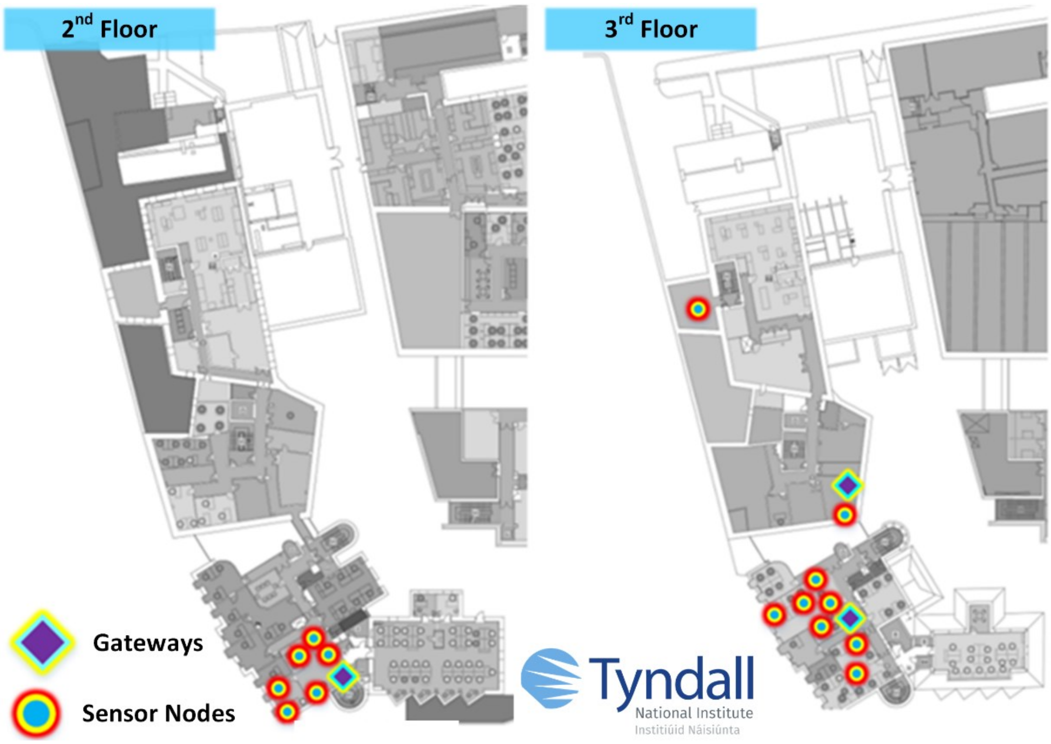

(b)

Figure 5.4: Deployment (a) Ground and 1st floor (b) 2nd and 3rd floor.

5.5 Results and Discussion

This section presents the measured wireless communication performance, i.e., packet delivery ratio of the developed LoRaWAN testbed network in a protected building structure. This section also illustrates the measurement-based results of the current consumption measurements that were performed during various sensor node activities such as data transmission, data reception and sleep and estimation of the battery lifetime.

5.5.1 Packet delivery ratio

This subsection describes the packet delivery ratio (PDR) of the LoRaWAN testbed network, which was deployed in the Tyndall National Institute building (see Figure 5.4). In this study, a total number of 20 sensor nodes were deployed, and each node was configured to send 1 confirmed packet every 20 minutes for a period of 1 week. The packets were received by 3 gateways (see section 0 for additional details). The results are depicted in Figure 5.5, showing a high PDR of 0.994.

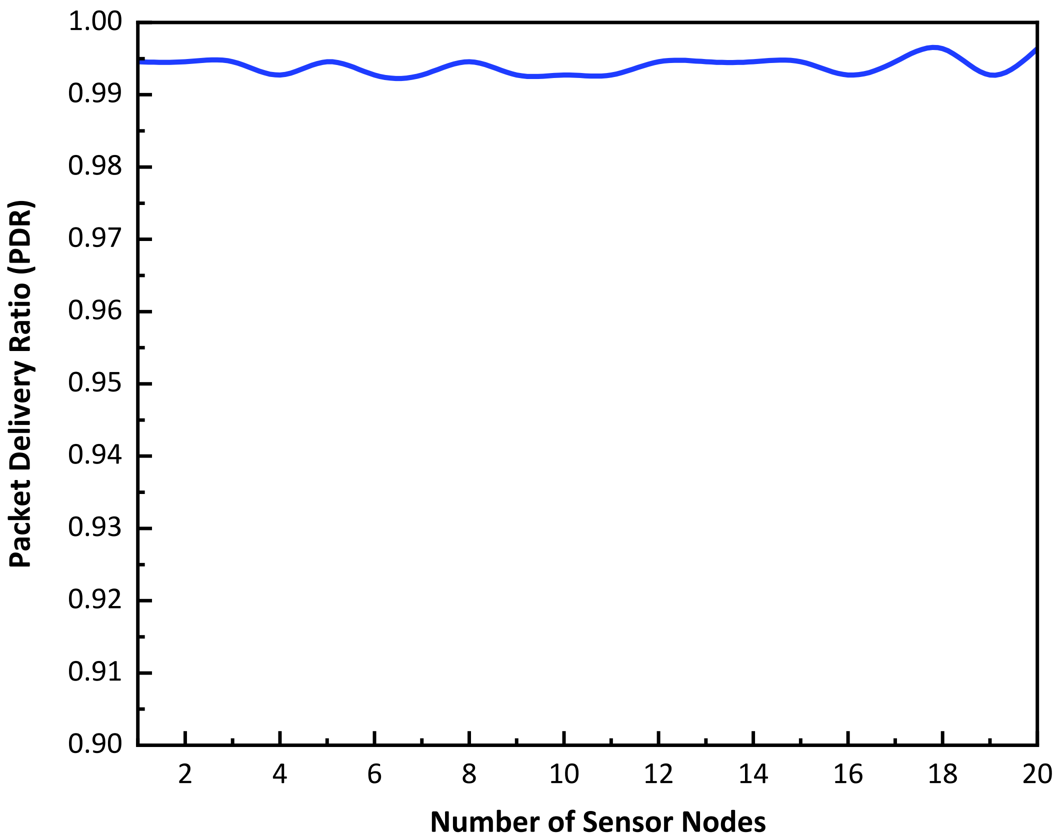

Figure 5.5: LoRaWAN packet delivery ratio for 20 nodes network.

The PDR of 0.994 demonstrates that wireless communication is reliable [166]. The measured PDR result is in agreement with simulated PDR that discussed in section 5.3.2.

5.5.2 Power consumption and battery lifetime estimation

This subsection summarizes the power consumption results for the LoRa sensor node and provides an estimate of the expected battery life. To measure the transmit (T_X) current consumption, the LoRa sensor node was programmed to transmit data packets at 5 minutes intervals with an adaptive data rate (ADR) setting. Figure 5.6 shows the current consumption of the LoRa sensor node over a period of approximately 140 minutes. From Figure 5.6, it can be seen that the maximum current consumption observed was 71.96 mA DC.

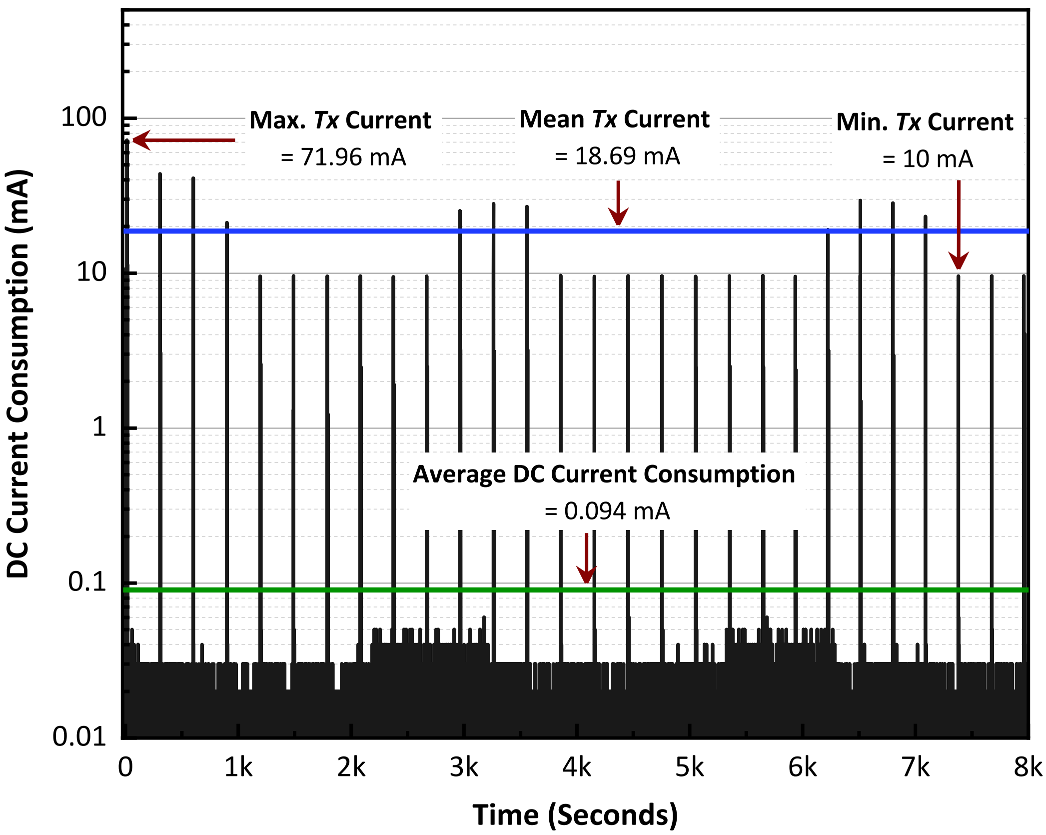

Figure 5.6: DC current consumption of the LoRaWAN sensor during transmission.

This current consumption value was recorded during the network joining and authentication period with a spreading factor value of SF12. In contrast, a minimum current consumption of 10 mA DC was recorded using a spreading factor of SF7. It means that the LoRa sensor node requires a mean current of 18.69 mA DC for data transmission. The mean receive (R_X) current of approximately 7.6 mA DC was measured during this experiment. The sleep current for the LoRa sensor node is shown in the Figure 5.7 and it can be seen that LoRa module requires a mean current of 12.69 μA DC during sleep mode. Finally, the average DC current consumption of 0.094 mA was calculated from the measured data (see Figure 5.6).

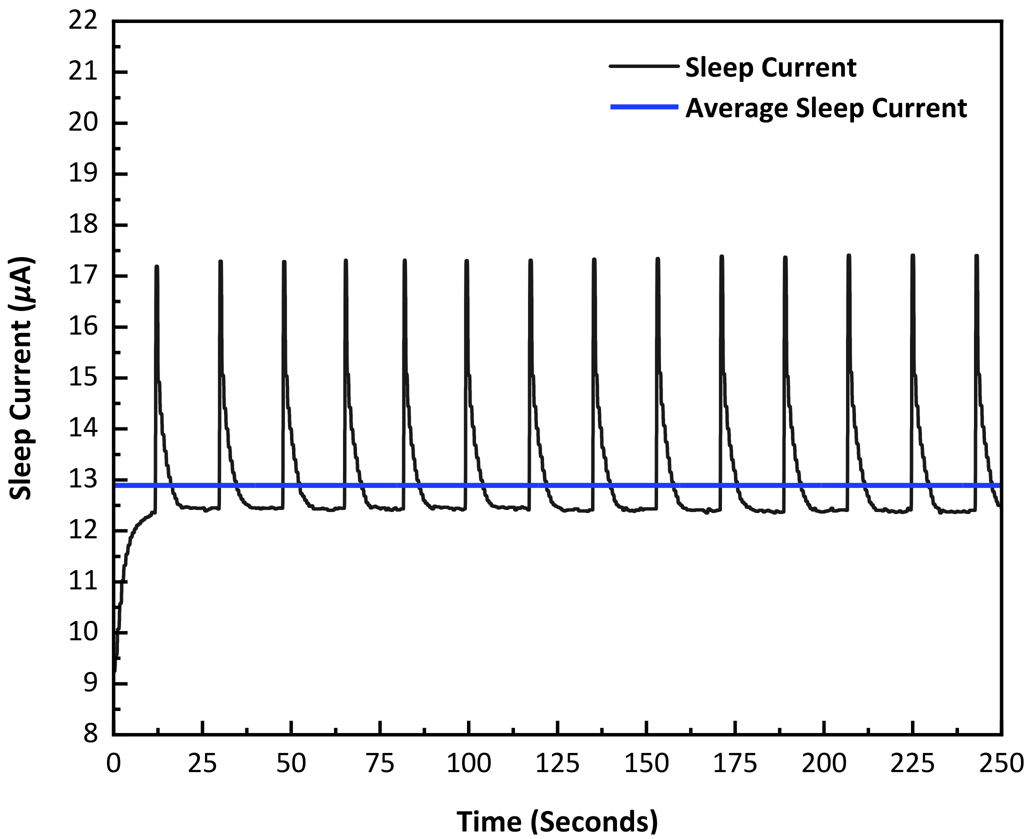

Figure 5.7: Current consumption profile of LoRaWAN sensor device during sleep.

Finally, the battery capacity of the LoRa sensor node was estimated with the help of the experimentally-measured current consumption figures. In order to estimate the total battery life, the power consumption and airtime of the sensor node was analysed in two scenarios, i.e., best case (scenario-A) and worst-case (scenario-B), as shown in Table 5.3. In scenario-A the following parameters were considered: Adaptive data rate = enabled, Mean T_X current = 18.69 mA DC, Mean Rx current = 7.6 mA DC and Sleep current consumption = 12.69 μA. Similarly, in (scenario-B) current consumption during higher spreading factor i.e., SF = 12 was investigated considering the following measured current consumption profile: Peak T_X current = 71.96 mA DC, R_X current = 10 mA DC and Sleep current = 12.69 μA DC. In addition, the current consumption of 9.6 mA DC was also considered for other electronics, such as a microcontroller (MCU) and temperature and humidity sensor. Finally, a system efficiency of 90 % was assumed to compensate self-discharging rate of the Li-SOCl2 battery, which is 1 % per year [169].

In order to achieve a 10-year battery life, assuming 1 data transmission per day, then a maximum battery capacity of 1.38 Ah is estimated. The developed LoRaWAN sensor node consists of a 4 Ah Li-SOCl2 batteries, which is almost three times the minimum estimated battery capacity. The developed LoRa sensor node has satisfies the battery lifetime requirement of this implementation, which is intended to be 10 years.

Table 5.3: Battery lifetime estimation of LoRa sensor node.

Scenarios	Scenario A (Best Case)	Scenario B (Worst Case)
Sensor node activities per day		
Data transmission cycle (per day)	1	1
Approximate sleep (hr)	24	24
Sampling time (ms)	838	838
Transmit time (ms)	61.7	1482.8
Receive time (ms)	100	2179
ADR settings	Enabled (SF = SF7 to SF12) BW = 125 kHz Max Tx power = 14 dBm	SF = SF12, BW = 125 kHz Max Tx power = 14 dBm
Payload (Bytes)	11	11
Current consumption during various activities		
Sleep current (mA)	0.013	0.013
Sampling current (mA)	9.6	9.6
Transmit current (mA)	18.69 (average)	71.96
Receive current (mA)	7.6	10
Power usage comparison in percentage		
Sleep (%)	99.10	88.93
Sampling (%)	0.73	0.65
Transmit (%)	0.10	8.65
Receive (%)	0.07	1.77
Design Goals		
System efficiency (%)	90	90
Target battery (Year) life	10	10
Estimated battery capacity (Ah)	**1.24**	**1.38**

5.6 Deployment of LoRaWAN Network in a Museum Environment

This subsection describes the deployment of the LoRaWAN network in the Public Museum in Cork, Ireland which was established in 1910 and which currently houses more than 40,000 artefacts. The total area of the museum site is approximately 60 m × 36 m. A total number of 7 sensor nodes were deployed in the Cork Public Museum, in which 3 sensor nodes were deployed on the ground floor in artefact display facilities, and the remaining 4 nodes were deployed on the first floor, where artefacts were conserved within the storage facilities. The LoRa sensor nodes were configured to use ADR (i.e., Spreading Factor = SF7 to SF12), Coding Rate = 4/5, Channel bandwidth = 125 kHz and acknowledgment-based data transmission. Figure 5.8 shows the photograph of one of the deployed sensor node within the storage crate that was developed during the APACHE project. In addition, Figure 5.9 (a) and (b) show measured temperature and relative humidity over 1 week using deployed LoRa sensor nodes in Cork Public Museum. During this 1 week period, the wireless communication performance of the deployed sensor network was measured (i.e., PDR) and a PDR figure of 0.997 was achieved. The achieved PDR value of 0.997 demonstrated that robust wireless communications between the sensor nodes and the LoRa gateway was achieved [166].

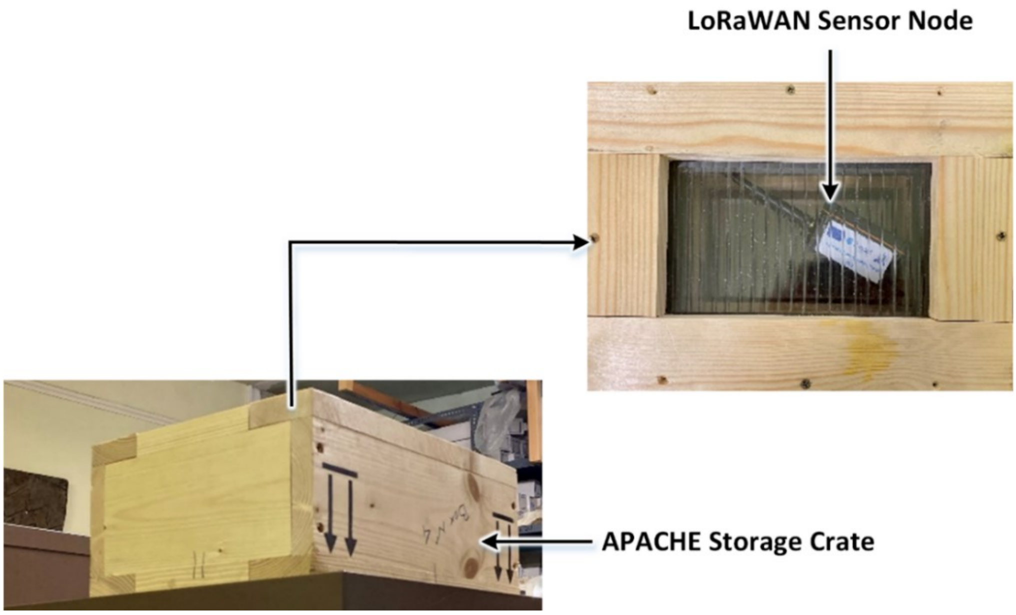

Figure 5.8: Deployed LoRa sensor node in Cork Public Museum, Ireland.

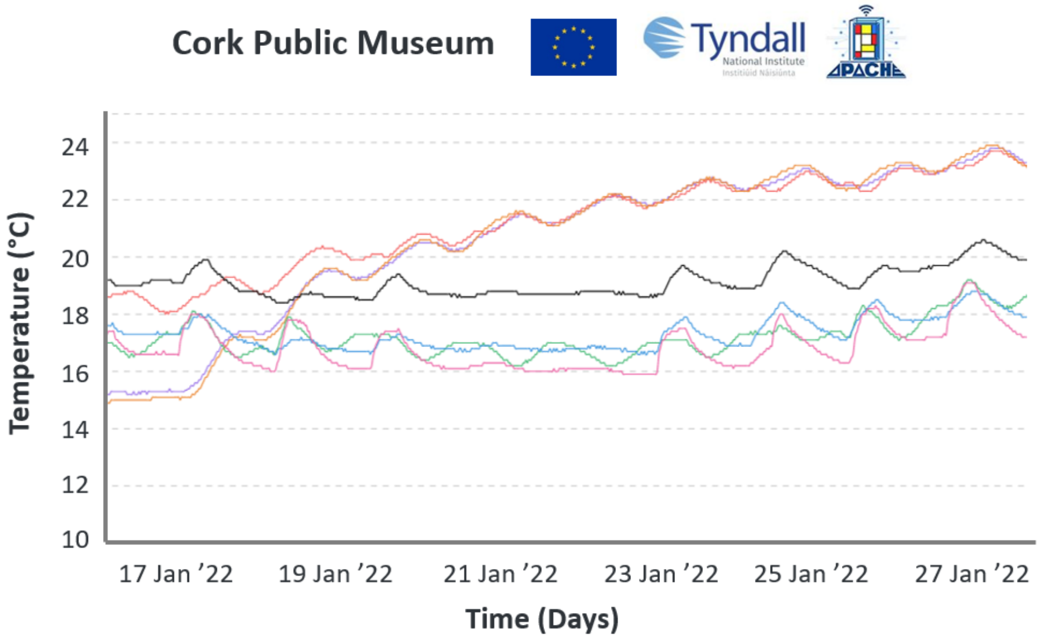

(a)

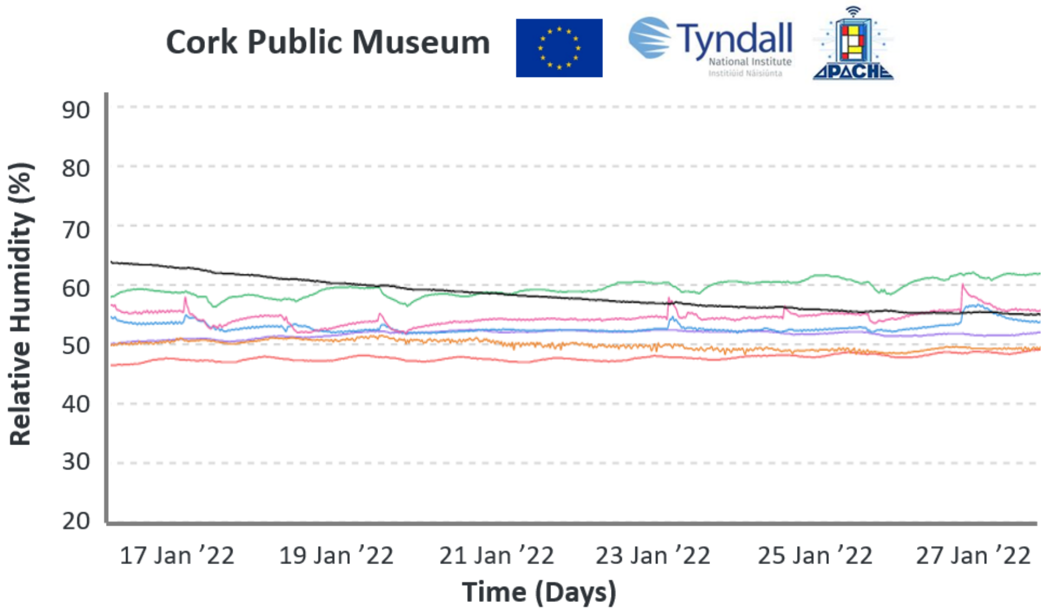

(b)

Figure 5.9: Measured parameters (a) temperature, (b) relative humidity.

5.7 Conclusions

This chapter presented the evaluation and selection of the optimum feasible wireless technology for museum artefact monitoring stored in museum storage facilities. In order to select a feasible wireless technology for this application, eight wireless technologies were studied in detail, and key wireless performance parameters were compared with user requirements. In addition, a testbed network of two potential technologies, i.e., LoRaWAN and BLE, was developed and deployed inside a 5600 m^2 space in both a protected (stone wall construction) and modern building structure to evaluate the wireless communication performance by way of measurements. Moreover, a LoRaWAN scalability approach was also used to simulate the packet delivery ratio for a 500-node network.

Furthermore, the LoRaWAN testbed network was successfully developed and deployed using a commercial LoRaWAN gateway and open-source hardware platform for sensor nodes. The user data portal was also successfully developed using a commercial IoT platform to visualize the time-varying temperature and relative humidity data. The developed testbed included 20 sensor nodes and 3 gateways. The testbed was deployed in a protected building structure in Tyndall National Institute, Cork, for performance validation. The result shows that LoRaWAN technology is a cost-effective solution with low infrastructure costs and high network reliability, i.e., PDR > 0.994 for museum artefact monitoring stored in museum storage facilities. The tested LoRaWAN sensor nodes also demonstrated a power consumption of less than 69 mW DC and an estimated battery lifetime of 10 years with a 1.38 Ah Li-SOCl2 battery.

Finally, the developed LoRaWAN platform was deployed in the Public Museum in Cork, Ireland. Deployment results demonstrated a packet delivery ratio (PDR) of greater than 0.997, indicating that wireless communication between the sensor nodes and the LoRa gateway is reliable. All deployed seven sensor nodes in Cork Public Museum are currently functioning in a real-time deployment as of 5th December 2022.

Chapter 6: Conclusions and Future Work

This chapter summarizes the research work conducted and described in this thesis. The key focus of this thesis was to design a new low-cost, battery-less NFC sensor transponder for monitoring museum artefact with enhanced wireless communication range compared to the state-of-the-art. In addition, this thesis also had a goal to develop, for the first time, a smart museum archive box featuring a fully integrated wireless powered temperature and humidity sensor.

In the last 5 years, battery-less NFC sensor transponders have witnessed significant advancement due to the increasing number of Internet of Things (IoT) applications and especially with the incorporation of NFC reader technology within smartphones [5]. In addition, advancement in low to ultra-low power electronics and sensors has steered the rapid growth of battery-less sensing devices such as NFC sensor transponders. The use of battery-less NFC sensor transponders for museum artefact monitoring (as opposed to battery-powered sensors) is advantageous because *no* additional wireless infrastructure other than a smart phone is required. Instead, the transponder can wirelessly powered via the smartphone, and measured sensor data can be read conveniently. In addition, after integrating the NFC sensor transponder within an archive box, the box does not need to be opened in the time [131]period between or during measurements, so the internal environment is undisturbed.

However, the design of battery-less NFC sensor transponders is challenging for museum artefact monitoring applications because the DC power consumption of the electronics (particularly the microcontroller) is finite and this sets limits on how much power DC can be harvested as well as setting limits on the maximum the wireless communication range. Another key challenge of the developed smart archive box is realization of a box assembly that does not require glue or adhesive. This avoids possible contamination of the atmosphere inside the box from the packaging itself.

In Chapter 2 of this thesis, several gaps and challenges in the current state-of-the-art relating to museum artefact monitoring were identified and the possibility for battery-less NFC sensing was highlighted. Based on the literature review, a hypothesis was formulated that focused on optimizing the overall harvested DC power consumption of the NFC sensor to enhance the wireless communication range. In addition, this research also focused on integrating the NFC sensor transponder within an archive box without the need for adhesive in the packaging.

6.1 Contribution to State-of-the-Art

This thesis aimed to address the aforementioned challenges by developing a low power, battery-less NFC sensor transponder.

The key contributions of this thesis are as follows:

- This thesis, for the first time, reports a smart museum archive box that features a fully integrated wireless powered temperature and humidity sensor. The smart archive box has been developed explicitly for microclimate environmental monitoring of stored museum artefacts in cultural heritage applications.
- The NFC sensor transponder has been optimized for low power operation with a measured peak harvested DC power consumption of 597 μW while yielding a 5 cm wireless communication range with the smartphone used as a reader. The DC power consumption of the NFC sensor transponder is approximately 33.6 % lower when compared with the state-of-the-art.
- A multi-nodal energy harvesting approach was also presented, i.e., vibration energy harvester assisted operation, a wireless communication range of 11 cm was achieved, which is 120 % greater than similar NFC sensors reported in the literature.
- A long-range wireless sensor was also implemented using the LoRaWAN standard. The wireless communication performance of LoRaWAN is shown to offer the optimal solution for long-range (several hundred metres) wireless monitoring of museum storage crates and displays with a measured packet delivery ratio (PDR) of 0.994.

In Chapter 3 [1-3], the hardware and firmware design for the NFC sensor transponder was presented. For this design, both voltage and frequency scaling techniques were used to minimize the DC power consumption of the sensor. In addition, a fully integrated archive box that features wirelessly powered temperature and humidity sensing capabilities for monitoring museum artefacts was presented. Furthermore, this chapter also explored the feasibility of wireless communication range enhancement of the NFC sensor transponder by assisting the transponder with an energy harvester powered by vibrational energy to power the sensor electronics. Finally, in this chapter, the integration of a custom laser induced graphene (LIG) based humidity sensor with the NFC sensor transponder was also presented.

In Chapter 4 [1-3], performance measurement and characterization of the battery-less NFC sensor transponders described in Chapter 3 was presented. The developed NFC sensor transponder was optimized for low power operation, resulting in a measured peak DC power consumption of 597 μW in free space, which is the lowest reported when compared with the state-of-the-art in the literature. Wireless communications performance testing was carried out on the prototype sensor and yielded a maximum range of 5 cm using a Samsung Galaxy S20 smartphone and 16.4 cm using a Voyantic Tagformance pro measurement system with a +25 dBm RF transmit power level. In addition, the minimum RF receiver sensitivity of the developed NFC sensor transponder was measured to be 67.8 mA/m and 87.6 mA/m at a resonant frequency of 13.74 MHz and 13.59 MHz in the free space case and after integration within the archive box, respectively. In this chapter, the key performance parameters of the developed NFC sensor were compared with the ISO/IEC 15693 air interface specification and are in good agreement with it as summarized in Table 4.1 in Chapter 4. With a measured mean error of ± 0.34 $^\circ$C in temperature from 6.8 $^\circ$C to 50.6 $^\circ$C, the proposed NFC sensor qualifies for accurate temperature measurements for monitoring museum artefact. A low-cost prototype NFC sensor transponder (i.e., € 4.91 in volumes of 10,000 units, see Table 3.4 in Chapter 3) was developed and characterized in this thesis and was successfully *demonstrated* to the project stakeholders across Europe during three public training events in Paris, Turin and Budapest.

Furthermore, the NFC sensor transponders were *deployed* in the Cork Public Museum, Cork, Ireland and the Guggenheim Museum, Venice, Italy.

Finally, the feasibility of wireless communication range enhancement of the NFC sensor transponder by powering the NFC sensor electronics using energy harvested from a vibrational energy harvester (VEH) was also explored. The maximum wireless communication range of 11 cm in free space was achieved, which is *120 %* greater than that reported in the literature [26, 82]. The mechanical energy harvesting capability of the VEH to assist in powering the NFC sensor would open wider fields of wireless sensing applications.

Finally in Chapter 5, the development and assessment of a LoRaWAN testbed for monitoring museum artefacts stored in museum storage facilities was presented [4]. In order to select feasible wireless technology for the intended application, eight individual wireless technologies were studied in detail, and key wireless performance parameters were compared with user requirements. Furthermore, the testbed network of LoRaWAN technology was successfully developed, which consists of 3 commercial LoRaWAN gateways and 20 sensor nodes. The developed LoRaWAN platform was *deployed* in the public museum in Cork, Ireland, as a proof of concept. Deployment results demonstrated that wireless communications between the sensor nodes and the LoRa gateway was robust with a packet delivery ratio (PDR) of greater than 0.997 [166]. The main finding of this study is that LoRaWAN is the most suitable wireless technology for museum artefact monitoring applications. LoRaWAN also provides a cost-effective implementation with low infrastructure costs, high network reliability (PDR > 0.994) and an estimated battery lifetime of 10 years with a 1.38 Ah Li-SOCl2 battery.

The battery-less NFC sensor prototype developed, tested and demonstrated in this work is especially *beneficial* for small and middle-size museums with limited or inappropriate storage climates and budget constraints that preclude the use of expensive air conditioning systems.

For the first time, the developed solution enables accurate microclimate environmental monitoring without the need for movement or opening of the archive box with no battery replacements. This feature is especially advantageous for museum conservators to readily monitor and reduce the risk of degradation of valuable cultural heritage artefacts in storage.

6.2 Future Work

The work presented in this thesis suggests following potential areas for further research and investigation.

- For the battery-less NFC sensor temperature and humidity sensor transponder presented in Chapter 3, fully characterization of the accuracy of relative humidity measurements of the transponder would be advantageous using an environmental chamber test system. In addition, future work could also focus on investigating methods for automatic sensor data collection solutions from the deployed smart archive boxes to improve user convenience.
- For the battery-less NFC-enabled LIG/GO humidity sensor presented in Chapter 3, the characterization of the humidity sensor after integration with the NFC sensor over a wide range of relative humidity, i.e., 0 % to 97 % [3] was not performed in this thesis work but would also be a valuable addition for the future work.
- The LoRaWAN testbed network presented in chapter 5 of this thesis uses a sensor node based on an open-source hardware platform (LSN50-V2) from Dragino Technology Co. Limited [167]. Developing a dedicated LoRaWAN sensor node with optimized DC power consumption for monitoring museum artefacts would be a valuable addition to future work.

Bibliography

[1] Dinesh R. Gawade, Steffen Ziemann, Sanjeev Kumar, Daniela Iacopino, Marco Belcastro, Davide Alfieri, Katharina Schuhmann, Manfred Anders, Melusine Pigeon, and John Barton, "A smart archive box for museum artifact monitoring using battery-less temperature and humidity sensing," *Sensors,* vol. 21, no. 14, p. 4903, 2021.

[2] Kankana Paul, Dinesh R. Gawade, Roy B. V. B. Simorangkir, Brendan O'Flynn, John L. Buckley, Andreas Amann, and Saibal Roy, "Concertina−Shaped Vibration Energy Harvester−Assisted NFC Sensor With Improved Wireless Communication Range," *IEEE Internet of Things Journal,* pp. 1-1, 2022.

[3] George Paterakis, Eoghan Vaughan, Dinesh R. Gawade, Richard Murray, George Gorgolis, Stefanos Matsalis, George Anagnostopoulos, John L. Buckley, Brendan O'Flynn, Aidan J. Quinn, Daniela Iacopino, and Costas Galiotis, "Highly Sensitive and Ultra-Responsive Humidity Sensors Based on Graphene Oxide Active Layers and High Surface Area Laser-Induced Graphene Electrodes," *Nanomaterials,* vol. 12, no. 15, p. 2684, 2022.

[4] Dinesh R. Gawade, Roy BVB Simorangkir, Dimitrios Zorbas, Sanjeev Kumar, Steffen Ziemann, Daniela Iacopino, John Barton, Katharina Schuhmann, Manfred Anders, and Brendan O'Flynn, "A museum artefact monitoring testbed using LoRaWAN," in *2021 IEEE Symposium on Computers and Communications (ISCC)*, 2021, pp. 1-3: IEEE.

[5] Chandrasekar and Ashudeb Dutta, "Recent Developments in Near Field Communication: A Study," *Wireless Personal Communications,* pp. 1-20, 2020.

[6] Irene Cappelli, Ada Fort, Marco Mugnaini, Enza Panzardi, Alessandro Pozzebon, Marco Tani, and Valerio Vignoli, "Battery-less HF RFID sensor tag for soil moisture measurements," *IEEE Transactions on Instrumentation and Measurement,* 2020.

[7] Martí Boada, Antonio Lazaro, Ramon Villarino, and David Girbau, "Battery-less soil moisture measurement system based on a NFC device with energy harvesting capability," *IEEE Sensors Journal,* vol. 18, no. 13, pp. 5541-5549, 2018.

[8] Marti Boada, Antonio Lazaro, Ramon Villarino, E Gil, and David Girbau, "Near-field soil moisture sensor with energy harvesting capability," in *2018 48th European Microwave Conference (EuMC)*, 2018, pp. 235-238: IEEE.

[9] Antonio Lazaro, Marti Boada, Ramon Villarino, and David Girbau, "Color measurement and analysis of fruit with a battery-less NFC sensor," *Sensors,* vol. 19, no. 7, p. 1741, 2019.

[10] Martí Boada, Antonio Lázaro, Ramón Villarino, and David Girbau, "NFC Battery-Less Colour Sensor and its Applications," in *2020 Global Congress on Electrical Engineering (GC-ElecEng)*, 2020, pp. 46-50: IEEE.

[11] Christoph Strangfeld, Sergej Johann, and Matthias Bartholmai, "Smart RFID Sensors Embedded in Building Structures for Early Damage Detection and Long-Term Monitoring," *Sensors,* vol. 19, no. 24, p. 5514, 2019.

[12] Thomas Bigler, Gábor Kovács, Albert Treytl, and Roman Windl, "NFC for Powering Sensors in Concrete," in *2020 25th IEEE International Conference on Emerging Technologies and Factory Automation (ETFA)*, 2020, vol. 1, pp. 1355-1358: IEEE.

[13] Pablo Escobedo, MM Erenas, N Lopez-Ruiz, MA Carvajal, S Gonzalez-Chocano, I de Orbe-Paya, LF Capitan-Valley, AJ Palma, and A Martinez-Olmos, "Flexible passive near field communication tag for multigas sensing," *Analytical chemistry,* vol. 89, no. 3, pp. 1697-1703, 2017.

[14] Cappelli Irene, Fort Ada, Mugnaini Marco, Panzardi Enza, Pozzebon Alessandro, Tani Marco, and Vignoli Valerio, "Battery-less HF RFID sensor tag for humidity measurements based on TiO 2 nanoparticles," in *2020 IEEE International Instrumentation and Measurement Technology Conference (I2MTC)*, 2020, pp. 1-6: IEEE.

[15] Amro Eldebiky, Mourad Elsobky, Harald Richter, and Joachim N Burghartz, "Humidity and temperature sensor system demonstrator with NFC tag for HySiF applications," *Advances in Radio Science: ARS,* vol. 16, pp. 109-116, 2018.

[16] Jonathan Ashley-Smith, Andreas Burmester, and Melanie Eibl, *Climate for Collections-Standards and Uncertainties. Postprints of the Munich Climate Conference 7 to 9 November 2012*. Doerner Institut, 2013.

[17] Rouchon-Quillet, Céline Remazeilles, Jacky Bernard, Alain Wattiaux, and Léopold Fournès, "The impact of gallic acid on iron gall ink corrosion," *Applied Physics A,* vol. 79, no. 2, pp. 389-392, 2004.

[18] Jana Kolar, Andrej Štolfa, Matija Strlič, Matevž Pompe, Boris Pihlar, Miloš Budnar, Jure Simčič, and Birgit Reissland, "Historical iron gall ink containing documents—properties affecting their condition," *Analytica chimica acta,* vol. 555, no. 1, pp. 167-174, 2006.

[19] British Standards Institution, *Specification for Managing Environmental Conditions for Cultural Collections: PAS 198: 2012*. British Standards Limited, 2012.

[20] Cecily M Grzywacz, *Monitoring for gaseous pollutants in museum environments*. Getty Publications, 2006.

[21] Testo. *testo 160 TH - WiFi data logger with integrated temperature and humidity sensor*. [Online available]: https://www.testo.com/en-UK/testo-160-th/p/0572-2021 (Accessed on: 06 December 2022).

[22] Marti Boada, Antonio Lazaro, Ramon Villarino, Ernest Gil-Dolcet, and David Girbau, "Battery-less NFC bicycle tire pressure sensor based on a force-sensing resistor," *IEEE Access,* vol. 9, pp. 103975-103987, 2021.

[23] Syed Muhammad Ali, Thanh-Binh Nguyen, and Wan-Young Chung, "New Directions for Skincare Monitoring: An NFC-Based Battery-Free Approach Combined With Deep Learning Techniques," *IEEE Access,* vol. 10, pp. 27368-27380, 2022.

[24] Bruno Miguel Gil Rosa, Salzitsa Anastasova-Ivanova, and Guang Zhong Yang, "NFC-Powered flexible chest patch for fast assessment of cardiac, hemodynamic, and endocrine parameters," *IEEE transactions on biomedical circuits and systems,* vol. 13, no. 6, pp. 1603-1614, 2019.

[25] Marti Boada, Antonio Lazaro, Ramon Villarino, and David Girbau, "Battery-less NFC sensor for pH monitoring," *IEEE Access,* vol. 7, pp. 33226-33239, 2019.

[26] Pablo Escobedo, MD Fernández-Ramos, N López-Ruiz, O Moyano-Rodríguez, A Martínez-Olmos, IM Pérez de Vargas-Sansalvador, MA Carvajal, LF Capitán-Vallvey, and AJ Palma, "Smart facemask for wireless CO2 monitoring," *Nature communications,* vol. 13, no. 1, pp. 1-12, 2022.

[27] Xueqing Qian, Zhen Li, Zhaozong Meng, Nan Gao, and Zonghua Zhang, "Flexible RFID tag for sensing the total minerals in drinking water via smartphone tapping," *IEEE Sensors Journal,* vol. 21, no. 21, pp. 24749-24758, 2021.

[28] Bruno Miguel Gil Rosa, Salzitsa Anastasova, and Guang Z Yang, "NFC-powered implantable device for on-body parameters monitoring with secure data exchange link to a medical blockchain type of network," *IEEE Transactions on Cybernetics,* 2021.

[29] Antonio Lazaro, Marti Boada, Ramon Villarino, and David Girbau, "Battery-Less Smart Diaper Based on NFC Technology," *IEEE Sensors Journal,* vol. 19, no. 22, pp. 10848-10858, 2019.

[30] Karnpimon Krorakai, Supannika Klangphukhiew, Sirinan Kulchat, and Rina Patramanon, "Smartphone-based NFC potentiostat for wireless electrochemical sensing," *Applied Sciences,* vol. 11, no. 1, p. 392, 2021.

[31] Wenting Dang, Libu Manjakkal, William Taube Navaraj, Leandro Lorenzelli, Vincenzo Vinciguerra, and Ravinder Dahiya, "Stretchable wireless system for sweat pH monitoring," *Biosensors and Bioelectronics,* vol. 107, pp. 192-202, 2018.

[32] Microsensys. *TELID 332-th product datasheet*. [Online available]: https://www.microsensys.de/fileadmin/user_upload/pdf-dateien/ds_sensor-transpond/TELID332-05.pdf (Accessed on: 06 December 2022).

[33] Gosense. *Gosense wireless ltd Product Index- NFC and RFID Mobile Sensors* [Online available]: http://www.gosense-wireless.com/GoSense%20TH-StatID%20DS%20Rev1.pdf (Accessed on: 06 December 2022).

[34] Microsensys. *Product datasheet- TELID 232.nfc* [Online available]: https://www.microsensys.de/fileadmin/user_upload/pdf-dateien/datasheets/TELID232nfc-01.pdf (Accessed on: 06 December 2022).

[35] Monarch Instrument. *Track-It RFID Temp or Temp/Humidity Data Logger* [Online available]: https://monarchinstrument.com/products/track-it-rfid-temp-temp-humidity-data-logger?variant=30756070984 (Accessed on: 06 December 2022).

[36] Intellilog. *End-to-End Cold Chain Monitoring*. [Online available]: https://intellilog.io/, (Accessed on: 06 December 2022).

[37] Mario Cardullo and William Parks, "Transponder apparatus and system," Patent US3713148A, 23/01/19973, 1970. Available: https://patents.google.com/patent/US3713148A/en.

[38] Martí Boada Navarro, "PhD Thesis: Battery-less near field communications (nfc) sensors for internet of things (iot) applications," PhD, Department of Electronic, Electrical and Automatic Engineering, Universitat Rovira i Virgili, 2020.

[39] Caroline Peres, Melusine Pigeon, Nadeem Rather, Dinesh R. Gawade, John Buckley, Hamed Jafarzadeh, and Brendan O'Flynn, "Theoretical models for underwater RFID and the impact of water salinity on the design of wireless systems," *International Journal on Advances in Networks and Services,* vol. 13, no. 34, pp. 45-59, 2020.

[40] Dinesh R. Gawade, John Buckley, Nadeem N Rather, Steffen Ziemann, Alex Zabeo, John Barton, Daniela Iacopino, Katharina Schuhmann, Manfred Anders, and Micheal Burke, "A battery-less NFC sensor transponder for museum artefact monitoring-a review of NFC sensor technology and a proposed solution," presented at the The Thirteenth International Conference on Sensor Technologies and Applications SENSORCOMM 2019, Nice, France, October 27, 2019 to October 31, 2019, 2019.

[41] Peter Haigh, Michael Hayes, Dinesh R. Gawade, and Brendan O'Flynn, "Towards Autonomous Smart Sensing Systems," in *2020 IEEE International Instrumentation and Measurement Technology Conference (I2MTC)*, 2020, pp. 1-6.

[42] Caroline Peres, Melusine Pigeon, Nadeem Rather, Dinesh Gawade, John Buckley, Hamed Jafarzadeh, and Brendan O'Flynn, "Theoretical models for underwater RFID and the impact of water salinity on the design of wireless systems," *International Journal on Advances in Networks and Services,* vol. 13, no. 34, pp. 45-59, 2020.

[43] Roland Minihold. *Near Field Communication (NFC) technology and measurements white paper*. [Online available]: https://scdn.rohde-schwarz.com/ur/pws/dl_downloads/dl_application/application_notes/1ma182/1MA182_5E_NFC_WHITE_PAPER.pdf 2011 (Accessed on: 06 December 2022).

[44] Caroline Peres da Silva, "Smart marine sensing systems for integrated multi-trophic aquaculture (IMTA)," 2021.

[45] Farsens. *Rocky100 Powered EPC C1G2 Batteryless Sensor Development Platform Featuring TI MSP430FR2433 MCU", EVAL01-MEDUSA-RM-V01*. [Online available]: http://www.farsens.com/wp-content/uploads/2018/01/DS-EVAL01-MEDUSA-RM-V01.pdf 2018, (Accessed on: 06 December 2022).

[46] EPC Global, "Specification for RFID air interface," *EPC Radio-Frequency Identity Protocols Class-1 Generation-2 UHF RFID Protocol for Communications at,* vol. 860, pp. 1-94, 2005.

[47] Zhonglin Cao, Ping Chen, Zhong Ma, Sheng Li, Xingxun Gao, Rui-xin Wu, Lijia Pan, and Yi Shi, "Near-field communication sensors," *Sensors,* vol. 19, no. 18, p. 3947, 2019.

[48] Vedat Coskun, Busra Ozdenizci, and Kerem Ok, "A survey on near field communication (NFC) technology," *Wireless personal communications,* vol. 71, no. 3, pp. 2259-2294, 2013.

[49] STMicroelectronics. *TN1216 Technical note ST25 NFC guide*. [Online available]: https://www.stmicroelectronics.com.cn/content/ccc/resource/technical/document/technical_note/f9/a8/5a/0f/61/bf/42/29/DM00190233.pdf/files/DM00190233.pdf/jcr:content/translations/en.DM00190233.pdf (Accessed on: 06 December 2022).

[50] Tom Igoe, Don Coleman, and Brian Jepson, *Beginning NFC: near field communication with Arduino, Android, and Phonegap*. " O'Reilly Media, Inc.", 2014.

[51] Klaus Finkenzeller, *RFID handbook: fundamentals and applications in contactless smart cards, radio frequency identification and near-field communication*. John Wiley & Sons, 2010.

[52] International Organization for Standardization/International Electrotechnical Commission, "ISO/IEC 18092 Information technology—Telecommunications and information exchange between systems—Near Field Communication—Interface and Protocol (NFCIP-1)," *ISO/IEC,* vol. 18092, 2004.

[53] *ISO/IEC 21481:2012 Information technology — Telecommunications and information exchange between systems — Near Field Communication Interface and Protocol -2 (NFCIP-2)*, 2012.

[54] *Near Field Communication Interface and Protocol (NFCIP-1), ETSI*, 2013.

[55] NFC Forum, "New NFC Forum Technical Specifications Broaden Tag Support and Enhance Interoperability," ed, 2015.

[56] STMicroelectronics. *NFC / RFID ST25 product overview*. [Online available]: https://www.st.com/content/ccc/resource/sales_and_marketing/presentation/product_presentation/group1/a9/5d/77/96/be/9a/48/7e/ST25_NFC_RFID_product_overview/files/ST25_product_overview.pdf/jcr:content/translations/en.ST25_product_overview.pdf 2020, (Accessed on: 06 December 2022).

[57] NFC Forum. *NFC Forum Releases Wireless Charging Specification 2.0*. [Online available]: https://www.businesswire.com/news/home/20211020005036/en/NFC-Forum-Releases-Wireless-Charging-Specification-2.0 2021, (Accessed on: 06 December 2022).

[58] NFC_Forum, "NFC Forum Issues Specifications For Four Tag Types," ed, 2007.

[59] Jian Yang, Christian Poellabauer, Pramita Mitra, and Cynthia Neubecker, "Beyond beaconing: Emerging applications and challenges of BLE," *Ad Hoc Networks,* vol. 97, p. 102015, 2020.

[60] NFC_Forum, "New NFC Forum Technical Specifications Broaden Tag Support and Enhance Interoperability," in *New and Candidate Specifications Bring Additional Flexibility and Range of Communications to NFC Interactions*, ed, 2015.

[61] GS1, "EPC Radio-Frequency Identity Protocols Generation-2 UHF RFID," 2013, Available: https://www.gs1.org/sites/default/files/docs/epc/uhfc1g2_2_0_0_standard_20131101.pdf (Accessed on: 06 December 2022).

[62] NFC_Forum, "Certified NFC Forum Type 5 Chips from STMicroelectronics Bring Tamper-Detect Capability to Smaller, More Convenient Tags," ed, 2018.

[63] NFC Forum, "NFC Forum – ISO/IEC 14443 Analog Parameter Comparison and Alignment Methodology, Procedures and Results," 2019, Available: https://nfc-forum.org/wp-content/uploads/2017/02/NFC_Forum-Analog_Parameter_Comparison_and_Alignment.pdf (Accessed on: 06 December 2022).

[64] Powercast. *PCT200 Powercast High-Function RFID Sensor Datalogger- Datasheet*. [Online available]: http://www.powercastco.com/wp-content/uploads/2017/06/PCT200-Datasheet-Rev-1.pdf (Accessed on: 06 December 2022).

[65] *ISO/IEC 14443-1:2018 Contactless proximity objects — Part 1: Physical characteristics*, 2018.

[66] *ISO/IEC 15693-1:2018(en) Cards and security devices for personal identification — Contactless vicinity objects — Part 1: Physical characteristics*, 2018.

[67] Texas_Instrument. ISO / NFC Standards and Specifications-Overview.

[68] Antonio Lazaro, Ramon Villarino, and David Girbau, "A survey of NFC sensors based on energy harvesting for IoT applications," *Sensors,* vol. 18, no. 11, p. 3746, 2018.

[69] Zebra-logiscenter. *Zebra RFD8500 RFID READERS*. [Online available]: https://www.logiscenter.ie/rfd8500-5000100-eu-zebra-rfd8500-rfid-readers (Accessed on: 06 December 2022).

[70] Polaris. *Battery-free Sensors Market Size Worth $284.69 Million by 2030*. [Online available]: https://www.polarismarketresearch.com/press-releases/battery-free-sensor-market 2021, (Accessed on: 06 December 2022).

[71] Sanjay Kumar, Dhananjay Singh, Rahul Singh, Gagan Gupta, and SK Singh, "An IoT based secure transaction system using Micro field communication," in *IOP Conference Series: Materials Science and Engineering*, 2020, vol. 748, no. 1, p. 012014: IOP Publishing.

[72] Avery Dennison. *TT Sensor Plus Product Datasheet* [Online available]: https://label.averydennison.com/content/dam/averydennison/lpm-responsive/europe/english/documents/data-sheet/product/intelligent-labels/time-and-temp-tracking/ds-eu-tt-sensor-plus-en.pdf (Accessed on: 06 December 2022).

[73] Identiv. *uTrust Sense Temperature Tracker*. [Online available]: https://www.identiv.com/products/rfid-nfc-inlays/sensors (06 December 2022).

[74] Esko Strömmer, Mika Hillukkala, and Arto Ylisaukko-oja, "Ultra-low power sensors with near field communication for mobile applications," in *IFIP Conference on Wireless Sensor and Actor Networks*, 2007, pp. 131-142: Springer.

[75] Hillukkala Mika, Heiskanen Mikko, and Ylisaukko-oja Arto, "Practical implementations of passive and semi-passive nfc enabled sensors," in *2009 First International Workshop on Near Field Communication*, 2009, pp. 69-74: IEEE.

[76] Johan Sidén, Vincent Skerved, Jinlan Gao, Stefan Forsström, Hans-Erik Nilsson, Theo Kanter, and Mikael Gulliksson, "Home care with nfc sensors and a smart phone," in *Proceedings of the 4th International Symposium on Applied Sciences in Biomedical and Communication Technologies*, 2011, pp. 1-5.

[77] Syed Muhammad Ali and Wan-Young Chung, "Monitoring transepidermal water loss and skin wettedness factor with battery-free NFC sensor," *Sensors,* vol. 20, no. 19, p. 5549, 2020.

[78] Gang Xu, Chen Cheng, Zhaoyang Liu, Wei Yuan, Xinzhou Wu, Yanli Lu, Sze Shin Low, Jinglong Liu, Lihang Zhu, and Daizong Ji, "Battery-free and wireless epidermal electrochemical system with all-printed stretchable electrode array for multiplexed In situ sweat analysis," *Advanced Materials Technologies,* vol. 4, no. 7, p. 1800658, 2019.

[79] Syed Muhammad Ali and Wan-Young Chung, "Detection of skin RGB color with a battery-free NFC skincare device," in *2021 IEEE Sensors*, 2021, pp. 1-4: IEEE.

[80] Gang Xu, Chen Cheng, Wei Yuan, Zhaoyang Liu, Lihang Zhu, Xintong Li, Yanli Lu, Zetao Chen, Jinglong Liu, and Zheng Cui, "Smartphone-based battery-free and flexible electrochemical patch for calcium and chloride ions detections in biofluids," *Sensors and Actuators B: Chemical,* vol. 297, p. 126743, 2019.

[81] Mengyao Yuan, Rami Ghannam, Petros Karadimas, and Hadi Heidari, "Flexible RFID Patch for Food Spoilage Monitoring," in *2018 IEEE Asia Pacific Conference on Postgraduate Research in Microelectronics and Electronics (PrimeAsia)* 2018, pp. 68-71: IEEE.

[82] Pablo Escobedo, M. Bhattacharjee, F. Nikbakhtnasrabadi, and R. Dahiya, "Smart Bandage With Wireless Strain and Temperature Sensors and Batteryless NFC Tag," *IEEE Internet of Things Journal,* vol. 8, no. 6, pp. 5093-5100, 2021.

[83] Rahim Rahimi, Uriel Brener, Shirisha Chittiboyina, Tahereh Soleimani, David A Detwiler, Sophie A Lelièvre, and Babak Ziaie, "Laser-enabled fabrication of flexible and transparent pH sensor with near-field communication for in-situ monitoring of wound infection," *Sensors and Actuators B: Chemical,* vol. 267, pp. 198-207, 2018.

[84] Bernhard Vennemann, Dominik Obrist, and Thomas Rösgen, "A smartphone-enabled wireless and batteryless implantable blood flow sensor for remote monitoring of prosthetic heart valve function," *PLoS One,* vol. 15, no. 1, p. e0227372, 2020.

[85] Austria Microsystems AG. *Discontinuation of SL13A (former "SAL") – to be substituted by AS39513* [Online available]: https://ams.com/documents/20143/304123/EOL_SL13A.pdf 2015, (Accessed on: 06 December 2022).

[86] Austria Microsystems AG. *End of Life (EOL) Notification* [Online available]: https://ams.com/documents/20143/4351465/AS39513_EN001001_1-00.pdf, 2020, (Accessed on: 06 December 2022).

[87] Irene Cappelli, Ada Fort, Marco Mugnaini, Enza Panzardi, Alessandro Pozzebon, Marco Tani, and Valerio Vignoli, "Battery-less HF RFID sensor tag for soil moisture measurements," *IEEE Transactions on Instrumentation and Measurement,* vol. 70, pp. 1-13, 2020.

[88] Matthew D Steinberg, Christine Slottved Kimbriel, and Lieve S d'Hont, "Autonomous near-field communication (NFC) sensors for long-term preventive care of fine art objects," *Sensors and Actuators A: Physical,* vol. 285, pp. 456-467, 2019.

[89] Changjiang Xiao, Nengcheng Chen, Dandan Li, You Lv, and Jianya Gong, "SCRMS: An RFID and sensor web-enabled smart cultural relics management system," *Sensors,* vol. 17, no. 1, p. 60, 2017.

[90] Jonathan Tse, "Development of a new environmental monitoring system for museums and galleries using RFID-enabled technology," *Studies in Conservation,* vol. 61, no. sup2, pp. 334-336, 2016.

[91] Rajpreet Kaur Gulati, Amitangshu Pal, and Krishna Kant, "Experimental evaluation of a near-field magnetic induction based communication system," in *2019 IEEE Wireless Communications and Networking Conference (WCNC)*, 2019, pp. 1-6: IEEE.

[92] Eric Freudenthal, David Herrera, Frederick Kautz, Carlos Natividad, Alexandria Ogrey, Justin Sipla, Abimael Sosa, Carlos Betancourt, and Leonardo Estevez, "Suitability of nfc for medical device communication and power delivery," in *2007 IEEE Dallas Engineering in Medicine and Biology Workshop*, 2007, pp. 51-54: IEEE.

[93] Qiu Jun, Hu Chao, Yang Yunhan, and Qiu Jizui, "Application of modern communication technology in smart home system," in *2018 IEEE International Conference on Information and Automation (ICIA)*, 2018, pp. 1577-1581: IEEE.

[94] Karel Sima, Tomas Syrovy, Silvan Pretl, Jaroslav Freisleben, David Cesek, and Ales Hamacek, "Flexible smart tag for cold chain temperature monitoring," in *2017 40th International Spring Seminar on Electronics Technology (ISSE)*, 2017, pp. 1-5: IEEE.

[95] Robin Raju, Greg E Bridges, and Sharmistha Bhadra, "Wireless Passive Sensors for Food Quality Monitoring: Improving the Safety of Food Products," *IEEE Antennas and Propagation Magazine,* vol. 62, no. 5, pp. 76-89, 2020.

[96] Thanh-Binh Nguyen, Viet-Thang Tran, and Wan-Young Chung, "Pressure Measurement-Based Method for Battery-Free Food Monitoring Powered by NFC Energy Harvesting," *Scientific Reports,* vol. 9, no. 1, p. 17556, 2019/11/26 2019.

[97] Tharindu Athauda and Nemai Chandra Karmakar, "Review of RFID-based sensing in monitoring physical stimuli in smart packaging for food-freshness applications," (in English), *Wireless Power Transfer,* vol. 6, no. 2, pp. 161-174, Sep 2019.

[98] Gabriela Simone Lorite, Tuula Selkälä, Teemu Sipola, Jesús Palenzuela, Elena Jubete, Ana Viñuales, Germán Cabañero, Hans J Grande, Jarkko Tuominen, and Sanna Uusitalo, "Novel, smart and RFID assisted critical temperature indicator for supply chain monitoring," *Journal of Food Engineering,* vol. 193, pp. 20-28, 2017.

[99] Mitradip Bhattacharjee, Pablo Escobedo, Fatemeh Nikbakhtnasrabadi, and Ravinder Dahiya, "NFC based Polymer Strain Sensor for Smart Packaging," in *2020 XXXIIIrd General Assembly and Scientific Symposium of the International Union of Radio Science*, 2020, pp. 1-4: IEEE.

[100] Xuan-Tu Cao and Wan-Young Chung, "An enhanced multiplication of RF energy harvesting efficiency using relay resonator for food monitoring," *Sensors,* vol. 19, no. 9, p. 1963, 2019.

[101] Wan-Young Chung, Giang Truong Le, Thang Viet Tran, and Nam Hoang Nguyen, "Novel proximal fish freshness monitoring using batteryless smart sensor tag," *Sensors and Actuators B: Chemical,* vol. 248, pp. 910-916, 2017.

[102] Nam Hoang Nguyen and Wan-Young Chung, "Battery-less pork freshness real-time monitoring system with high efficient RF energy scavenging," in *2017 International Conference on Applied System Innovation (ICASI)*, 2017, pp. 235-238: IEEE.

[103] Milad Eyvazi Hesar, Dibyendu Khan, Niloofar Sadat Seyedsadrkhani, and Sven Ingebrandt, "Contactless, Battery-free, and Stretchable Wearable for Continuous Recording of Seismocardiograms," *ACS Applied Electronic Materials,* 2020.

[104] Akihito Noda, "Wearable NFC Reader and Sensor Tag for Health Monitoring," in *2019 IEEE Biomedical Circuits and Systems Conference (BioCAS)*, 2019, pp. 1-4.

[105] Han-Won Cho, Jo Hee Yoon, Sang-Sun Yoo, Bong Gill Choi, and Hyung-Joun Yoo, "A Batteryless Chronic Wound Monitoring System with NFC," in *2019 IEEE Eurasia Conference on Biomedical Engineering, Healthcare and Sustainability (ECBIOS)*, 2019, pp. 31-34: IEEE.

[106] Rahim Rahimi, Uriel Brener, Manuel Ochoa, and Babak Ziaie, "Flexible and transparent pH monitoring system with NFC communication for wound monitoring applications," in *2017 IEEE 30th International Conference on Micro Electro Mechanical Systems (MEMS)*, 2017, pp. 125-128.

[107] Thanh-Binh Nguyen, Trung-Hau Nguyen, and Wan-Young Chung, "Battery-Free and Noninvasive Estimation of Food pH and CO2 Concentration for Food Monitoring Based on Pressure Measurement," *Sensors,* vol. 20, no. 20, p. 5853, 2020.

[108] Sanjeev Kumar, John Buckley, John Barton, and Brendan O'Flynn, "Performance analysis of a novel flexible NFC Tag for IoT applications," in *12th Smart Systems Integration Conference 2018*, 2018, pp. 432-435.

[109] STMicroelectronics. *ST25DV16K- Datasheet*. [Online available]: https://www.st.com/resource/en/datasheet/st25dv04k.pdf 2018, (Accessed on: 06 December 2022).

[110] STMicroelectronics. *Datasheet of STM32L031x4 STM32L031x6*. [Online available]: https://www.st.com/resource/en/datasheet/stm32l031k6.pdf 2018, (Accessed on: 06 December 2022).

[111] STMicroelectronics. *Datasheet - STLQ015*. [Online available]: https://www.st.com/resource/en/datasheet/stlq015.pdf/ 2020, (Accessed on: 06 December 2022).

[112] Sensirion. *Datasheet- SHTC3 Humidity and Temperature Sensor IC*. [Online available]: https://www.sensirion.com/fileadmin/user_upload/customers/sensirion/Dokumente/2_Humidity_Sensors/Datasheets/Sensirion_Humidity_Sensors_SHTC3_Datasheet.pdf/ (Accessed on: 06 December 2022).

[113] STMicroelectronics. *TA0342 Technical article: Accurate power consumption estimation for STM32L1 series of ultra-low-power microcontrollers*. [Online available]: https://www.st.com/resource/en/technical_article/dm00024152-accurate-power-consumption-estimation-for-stm32l1-series-of-ultra-low-power-microcontrollers-stmicroelectronics.pdf/ 2013, (Accessed on: 06 December 2022).

[114] STMicroelectronics. *STEVAL-SMARTAG1 Data brief*. [Online available]: https://www.st.com/resource/en/data_brief/steval-smartag1.pdf/ 2018, (Accessed on: 06 December 2022).

[115] Texas Instrument. *RF430FRL152HEVM User's Guide*. [Online available]: https://www.ti.com/lit/ug/slau607c/slau607c.pdf?ts=1611854593411 2018, (Accessed on: 06 December 2022).

[116] NXP. *NHS3152TEMOADK: NHS3152 General Starter Kit*. [Online available]: https://www.nxp.com/products/rfid-nfc/nfc-hf/ntag-smartsensor/nhs3152-general-starter-kit:NHS3152TEMOADK (Accessed on: 06 December 2022).

[117] STMicroelectronics. *AN4913 Application note: Energy harvesting delivery impact on ST25DVxxx behavior during RF communication*. [Online available]: https://www.st.com/resource/en/application_note/dm00329035-energy-harvesting-delivery-impact-on-st25dvxxx-behavior-during-rf-communication-stmicroelectronics.pdf 2017, (Accessed on: 06 December 2022).

[118] STMicroelectronics. *User manual of X-NUCLEO-NFC04A1 NFC/RFID*. [Online available]: https://www.st.com/resource/en/user_manual/dm00402774-getting-started-with-the-xnucleonfc04a1-nfcrfid-tag-ic-expansion-board-based-on-st25dv04k-for-stm32-nucleo-stmicroelectronics.pdf 2018, (Accessed on: 06 December 2022).

[119] STMicroelectronics. *UM1956 User manual STM32 Nucleo-32 boards*. [Online available]: https://www.st.com/resource/en/user_manual/dm00231744-stm32-nucleo32-boards-mb1180-stmicroelectronics.pdf 2018, (Accessed on: 06 December 2022).

[120] Mikroe. *TEMP&HUM 9 CLICK*. [Online available]: https://www.mikroe.com/temphum-9-click, (Accessed on: 06 December 2022).

[121] NXP. *UM10204 I2C-bus specification and user manual*. [Online available]: https://www.nxp.com/docs/en/user-guide/UM10204.pdf (Accessed on: 06 December 2022).

[122] *Cards and security devices for personal identification — Contactless vicinity objects —Part 2: Air interface and initialization* 2019.

[123] STMicroelectronics. *AN4911 - Application note - NDEF management with ST25DVxxx and ST25TVxxx products*. [Online available]: https://www.st.com/resource/en/application_note/dm00328901-ndef-management-with-st25dvxxx-and-st25tvxxx-products-stmicroelectronics.pdf 2018, (Accessed on: 06 December 2022).

[124] Tim WC Brown, Thomas Diakos, and Johann A Briffa, "Evaluating the eavesdropping range of varying magnetic field strengths in NFC standards," in *2013 7th European Conference on Antennas and Propagation (EuCAP)*, 2013, pp. 3525-3528: IEEE.

[125] Anantha P Chandrakasan and Robert W Brodersen, "Minimizing power consumption in digital CMOS circuits," *Proceedings of the IEEE,* vol. 83, no. 4, pp. 498-523, 1995.

[126] Advanced RISC Machine. *ARMv8-A Power Management*. [Online available]: https://developer.arm.com/documentation/100960/0100/Dynamic-Voltage-and-Frequency-Scaling?lang=en/ 2017, (Accessed on: 06 December 2022).

[127] STMicroelectronics. *eDesignSuite*. [Online available]: https://www.st.com/content/st_com/en/support/resources/edesign.html (Accessed on: 06 December 2022).

[128] PCBway. *PCB Prototype Instant Quote*. [Online available]: https://www.pcbway.com/?gw1&campaignid=172480651&adgroupid=8787904531&feeditemid=&targetid=aud-453960202066:kwd-338664447536&loc_physical_ms=1007835&matchtype=b&network=g&device=c&devicemodel=&creative=377957049820&keyword=prototype%20pcb&placement=&target=&adposition=&gclid=Cj0KCQjwpdqDBhCSARIsAEUJ0hPq7NZRIyi6wo49Jn1IoH8--k99xXQyRapO4Dpfzt-rnbElHOX1v-kaAi7MEALw_wcB (Accessed on: 06 December 2022).

[129] Eoghan Vaughan, Cathal Larrigy, Micheal Burke, Labrini Sygellou, Aidan J. Quinn, Costas Galiotis, and Daniela Iacopino, "Visible Laser Scribing Fabrication of Porous Graphitic Carbon Electrodes: Morphologies, Electrochemical Properties, and Applications as Disposable Sensor Platforms," *ACS Applied Electronic Materials,* vol. 2, no. 10, pp. 3279-3288, 2020/10/27 2020.

[130] Box Shop. *Telescope boxes*. [Online available]: https://www.boxshop24.com/en/Telescope-boxes.html (Accessed on: 06 December 2022).

[131] Voyantic. *Tagformance Pro Measurement System Manual*. [Online available]: https://voyantic.com/lab/tagformance-pro/ 2020, (Accessed on: 06 December 2022).

[132] Thomas H Lee, *The design of CMOS radio-frequency integrated circuits*. Cambridge university press, 2003.

[133] Antonio Lazaro, Marti. Boada, Ramón Villarino, and David Girbau, "Study on the Reading of Energy-Harvested Implanted NFC Tags Using Mobile Phones," *IEEE Access,* vol. 8, pp. 2200-2221, 2020.

[134] Fluke. *Fluke 971 Temperature Humidity Meter Technical datasheet*. [Online available]: https://www.fluke-direct.com/pdfs/cache/www.fluke-direct.com/971/datasheet/971-datasheet.pdf (Accessed on: 06 December 2022).

[135] Jean Tétreault, "Products used in Preventive Conservation–Technical Bulletin 32," *Canadian Conservation Institute, Canadá,* 2018.

[136] *Multiwall Polycarbonate Panels Offer Better Insulation*. [Online available]: https://www.tuflite.com/blog/multiwall-polycarbonate-panels-offer-better-insulation (Accessed on: 06 December 2022).

[137] APACHE Project. *First Public Training*. [Online available]: https://www.apacheproject.eu/the-first-public-training/ 2021, (Accessed on: 06 December 2022).

[138] APACHE Project. *Second Public Training*. [Online available]: https://www.apacheproject.eu/the-second-public-training/ 2021, (Accessed on: 06 December 2022).

[139] APACHE Project. *Final Public Training*. [Online available]: https://www.apacheproject.eu/final-public-training/ 2022, (Accessed on: 06 December 2022.

[140] Cork Public Museum. *About Cork Public Museum*. [Online available]: https://www.corkcity.ie/en/cork-public-museum/explore/about-us/ 2022, (Accessed on: 06 December 2022).

[141] ICCROM. *International Centre for the Study of the Preservation and Restoration of Cultural Property*. [Online available]: https://www.iccrom.org/publication/re-org-method-reorganize-museum-storage (Accessed on: 06 December 2022).

[142] Lina M Pestana Leão de Brito, Laura M Rodríguez Peralta, Filipe E Sousa Santos, and Roberto P Ramos Fernandes, "Wireless sensor networks applied to museums' environmental monitoring," in *2008 The Fourth International Conference on Wireless and Mobile Communications*, 2008, pp. 364-369: IEEE.

[143] Monica Maceli, "Internet of things in the archives: novel tools for environmental monitoring of archival collections," *Records Management Journal,* 2020.

[144] Stéphane Rioual, Benoit Lescop, Julien Pellé, Gerusa De Alkmim Radicchi, Gilles Chaumat, Marie Dominique Bruni, Johan Becker, and Dominique Thierry, "Monitoring of the environmental corrosivity in museums by rfid sensors: Application to pollution emitted by archeological woods," *Sustainability,* vol. 13, no. 11, p. 6158, 2021.

[145] Sanjeev Kumar, John L Buckley, John Barton, Melusine Pigeon, Robert Newberry, Matthew Rodencal, Adhurim Hajzeraj, Tim Hannon, Ken Rogers, and Declan Casey, "A wristwatch-based wireless sensor platform for IoT health monitoring applications," *Sensors,* vol. 20, no. 6, p. 1675, 2020.

[146] Elizabeth M Astorga González, Esteban Municio, Maikel Noriega Alemán, and Johann M Marquez-Barja, "Cultural heritage and internet of things," in *Proceedings of the 6th EAI International Conference on Smart Objects and Technologies for Social Good*, 2020, pp. 248-251.

[147] Alexandru Lavric, Adrian I. Petrariu, and Valentin Popa, "Long Range SigFox Communication Protocol Scalability Analysis Under Large-Scale, High-Density Conditions," *IEEE Access,* vol. 7, pp. 35816-35825, 2019.

[148] Sensirion. *Digital Humidity Sensor SHT3x*. [Online available]: https://www.sensirion.com/en/environmental-sensors/humidity-sensors/digital-humidity-sensors-for-various-applications/ (Accessed on: 06 December 2022).

[149] Kais Mekki, Eddy Bajic, Frederic Chaxel, and Fernand Meyer, "A comparative study of LPWAN technologies for large-scale IoT deployment," *ICT express,* vol. 5, no. 1, pp. 1-7, 2019.

[150] Rashmi Sharan Sinha, Yiqiao Wei, and Seung-Hoon Hwang, "A survey on LPWA technology: LoRa and NB-IoT," *Ict Express,* vol. 3, no. 1, pp. 14-21, 2017.

[151] Sakshi Popli, Rakesh Kumar Jha, and Sanjeev Jain, "A survey on energy efficient narrowband internet of things (NBIoT): architecture, application and challenges," *IEEE Access,* vol. 7, pp. 16739-16776, 2018.

[152] STMicroelectronics. *S2-LP Ultra-low power, high performance, sub-1 GHz transceiver*. [Online available]: https://www.st.com/en/wireless-connectivity/s2-lp.html/ 2021, (Accessed on: 06 December 2022).

[153] Zolertia. *Zolertia re-mote platform*. [Online available]: https://raw.githubusercontent.com/Zolertia/Resources/master/RE-Mote/Hardware/Revision\%20B/Datasheets/ZOL-RM0x-B\%20-\%20RE-Mote\%20revision\%20B\%20Datasheet\%20v.1.0.0.pdf/ 2017, (Accessed on: 06 December 2022).

[154] Texas Instrument. *CC3200 SimpleLink Wi-Fi and Internet-of-Things Solution, a Single-Chip Wireless MCU*. [Online available]: https://www.ti.com/lit/ds/symlink/cc3200.pdf?ts=1627332781604&ref_url=https%253A%252F%252Fwww.ti.com%252Fproduct%252FCC3200, 2015, (Accessed on: 06 December 2022).

[155] Nordic Semiconductor. *nRF52840, Product Specification."* [Online available]: https:// infocenter.nordicsemi.com/pdf/nRF52840 PS v1.2.pdf (Accessed on: 06 December 2022).

[156] Zhu Jianyong, Luo Haiyong, Chen Zili, and Li Zhaohui, "RSSI based Bluetooth low energy indoor positioning," in *2014 International Conference on Indoor Positioning and Indoor Navigation (IPIN)*, 2014, pp. 526-533: IEEE.

[157] Austria Microsystems AG. *SL900A EPC Class 3 Sensory Tag*. [Online available]: https://ams.com/documents/20143/36005/SL900A_DS000294_5-00.pdf/d399f354-b0b6-146f-6e98-b124826bd737/ 2018, (Accessed on: 06 December 2022).

[158] Farsens, "Rocky100 Powered EPC C1G2 Batteryless Sensor Development Platform Featuring TI MSP430FR2433 MCU", EVAL01-MEDUSA-RM-V01," 2018, Available: http://www.farsens.com/wp-content/uploads/2018/01/DS-EVAL01-MEDUSA-RM-V01.pdf.

[159] Sakshi Popli, Rakesh Kumar Jha, and Sanjeev Jain, "A Survey on Energy Efficient Narrowband Internet of Things (NBIoT): Architecture, Application and Challenges," *IEEE Access,* vol. 7, pp. 16739-16776, 2019.

[160] 1NCE. *1NCE Princing the IoT Flat Rate*. [Online available]: https://1nce.com/wp-content/1NCE-Pricing.pdf (Accessed on: 06 December 2022).

[161] Pycom. *Datasheet Sigfox/LoRa Antenna Kit* [Online available]: http://www.farnell.com/datasheets/2574252.pdf (Accessed on: 06 December 2022).

[162] Roy B. V. B. Simorangkir, Dinesh R. Gawade, Sanjeev Kumar, Brendan O'Flynn, John L. Buckley, Tim Hannon, Paul Donovan, and Robert Newberry, "Screen Printed Epidermal Antenna for IoT Health Monitoring," in *2021 IEEE Asia-Pacific Microwave Conference (APMC)*, 2021, pp. 395-397.

[163] Pai Chet Ng and James She, "A novel overlay mesh with bluetooth low energy network," in *2019 IEEE Wireless Communications and Networking Conference (WCNC)*, 2019, pp. 1-6: IEEE.

[164] DigiKey. *NRF52840-DK Price*. [Online available]: https://www.digikey.ie/products/en?keywords=nrf52840-dk (Accessed on: 06 December 2022).

[165] Dimitrios Zorbas, Christelle Caillouet, Khaled Abdelfadeel Hassan, and Dirk Pesch, "Optimal data collection time in LoRa networks—A time-slotted approach," *Sensors,* vol. 21, no. 4, p. 1193, 2021.

[166] Gyeongheon Lee and Joosang Youn, "Group-based transmission scheduling scheme for building LoRa-based massive IoT," in *2020 International Conference on Artificial Intelligence in Information and Communication (ICAIIC)*, 2020, pp. 583-586: IEEE.

[167] Dragino. *Dragion LoRaST IoT module*. [Online available]: https://www.dragino.com/products/lora/item/127-lora-st.html (Accessed on: 06 December 2022).

[168] The Things. *Getting Started With The Things Gateway*. [Online available]: http://www.farnell.com/datasheets/2552236.pdf (Accessed on: 06 December 2022).

[169] Esma Kökten, Bahadır Can Çalışkan, Saeid Karamzadeh, and Ece Gelal Soyak, "Low-Power Agriculture IoT System with LoRa: Open Field Storage Observation," *Electrical, Control and Communication Engineering,* vol. 16, no. 2, pp. 88-94, 2020.